9-15-2011

Analysis of Transient Electromagnetic Scattering from an Overfilled Cavity Embedded in an Impedance Ground Plane

Robert S. Callihan

ANALYSIS OF TRANSIENT ELECTROMAGNETIC SCATTERING FROM AN OVERFILLED CAVITY EMBEDDED IN AN IMPEDANCE GROUND PLANE

DISSERTATION

Robert S. Callihan, Lieutenant Colonel, USAF

AFIT/DAM/ENC/11-01

DEPARTMENT OF THE AIR FORCE
AIR UNIVERSITY

AIR FORCE INSTITUTE OF TECHNOLOGY

Wright-Patterson Air Force Base, Ohio

AFIT/DAM/ENC/11-01

ANALYSIS OF TRANSIENT ELECTROMAGNETIC SCATTERING FROM AN OVERFILLED CAVITY EMBEDDED IN AN IMPEDANCE GROUND PLANE

DISSERTATION

Presented to the Faculty

Graduate School of Engineering and Management

Air Force Institute of Technology

Air University

Air Education and Training Command

in Partial Fulfillment of the Requirements for the

Degree of Doctor of Philosophy in Applied Mathematics

Robert S. Callihan, B.S.M.S., M.B.A.

Lieutenant Colonel, USAF

September 2011

AFIT/DAM/ENC/11-01

ANALYSIS OF TRANSIENT ELECTROMAGNETIC SCATTERING FROM AN OVERFILLED CAVITY EMBEDDED IN AN IMPEDANCE GROUND PLANE

Robert S. Callihan, B.S.M.S., M.B.A.
Lieutenant Colonel, USAF

Approved:

//signed//	September 2011
Dr. Aihua W. Wood Chairman	Date
//signed//	September 2011
Dr. Alan V. Lair Member	Date
//signed//	September 2011
Dr. Michael J. Havrilla Member	Date
//signed//	September 2011
Capt Kevin R. Pond Member	Date

Accepted:

//signed//	September 2011
M. U. Thomas Dean, Graduate School of Engineering and Management	Date

AFIT/DAM/ENC/11-01

Abstract

In this research, we consider the transient, or time-domain, scattering problem of an overfilled cavity embedded in an impedance ground plane. This problem is a significant advancement from previous work where more simplified boundary conditions were used, which can limit the number of applications. This research supports a wide range of military applications such as the study of cavity-like structures on aircraft and vehicles. More importantly, this research helps detect the biggest threat on today's battlefield: improvised explosive devices.

An important step in solving the problem is introducing an artificial boundary condition on a semicircle enclosing the cavity; this couples the fields from the infinite exterior domain to those fields inside. The problem is first discretized in time using the Newmark scheme, and at each time step, we derive the variational formulation and establish well-posedness of the problem. This sets the foundation for the finite element method used in the numerical analysis. Using both planar and overfilled cavity models, we provide numerical results through the depictions of the electric field and radar cross section of the cavities.

Acknowledgments

I am very thankful to many people here at AFIT during the course of my research. I am very grateful to my research advisor, Dr. Aihua Wood, for accepting me as a student and showing faith in my abilities early in this journey. That was very important, and I appreciated her wisdom, guidance, and support for me and my family, especially during the difficult moments. I would also like to thank the rest of my research committee: Dr. Alan Lair, for his support and accepting me into this program; Dr. Michael Havrilla, for his thorough and enlightening discussions about the mathematics and the physical happenings; and Captain Kevin Pond, for his support and insight into the numerical phase of the research. I have benefitted tremendously from all of you and I thank you each very much.

I would also like to thank our sponsor, Dr. John Roadcap from the Air Force Research Laboratory, for his support and interest in my efforts.

I would like to collectively thank the following individuals, who took time with me to answer questions and offer insights into various aspects of the research: Dr. Matthew Fickus, Dr. William Baker, Dr. Jeff McGuirk, Dr. Tri Van, and Dr. Kyle Novak. I would also like to thank Mr. Dwight Wilson and CDR Neal Kraft for their help and support when I needed it.

Finally, to my family: my wife, Kristy; my children, Cole and Carras; my mother, Pam, and my father, Bob; my brother, Derek; my mother-in-law, Martie, and my father-in-law, Tony. Your support throughout my research made all of the difference and I certainly would not have completed this without you.

Robert S. Callihan

Table of Contents

Page

Abstract iv

Acknowledgments v

List of Figures viii

List of Abbreviations ix

I. Introduction 1

1.1 Motivation 1
1.2 General Problem Statement 4
1.3 Function Spaces and Requirements 7
1.4 Time versus Frequency Domain 9

II. Related and Previous Work / Literature Review 11

2.1 Solving the Electromagnetic Scattering Problem 11
2.2 History of Impedance Boundary Conditions 13
2.3 Impedance Boundary Conditions in the Time Domain 13
2.4 Research on Overfilled Cavities and Similar Geometries 15

III. Mathematical Formulation 21

3.1 Approach to Solution and Semidiscrete Problem 21
3.2 Integral Representation of Solution 26
3.3 Green's Function Development 30
3.4 Steklov-Poincaré Operator Analysis 38
3.5 Green's Function Analysis: Derivative and Singularity Evaluation 51

IV. Variational Formulation 57

4.1 Recasting the Boundary Value Problem 57
4.2 Variational Formulation 59

V. Finite Element Analysis 69

5.1 Construction of the Discrete Problem 69
5.2 Error Analysis 72
5.3 Stability Analysis 78

Page

VI. Numerical Simulation 86

6.1 Finite Element Approximation 86
6.2 Numerical Results 97

VII. Conclusions and Future Work 113

7.1 Conclusions 113
7.2 Future Work 114

Appendix A. Derivations 117

Bibliography 118

List of Figures

Figure		Page
1.	IED Depiction [53]	3
2.	Problem Geometry - TM polarization depicted	5
3.	Durán's Exterior Problem Geometry [29]	17
4.	Durán's Interior Problem Geometry [29]	17
5.	Jin and Riley Conformal Antenna [56]	19
6.	Sub-Domains of Problem	22
7.	Exterior Domain	28
8.	Shallow Planar Cavity (1 meter by 0.25 meters)	99
9.	Shallow Cavity - TM Solution at (0,0) - Eta Point Eight	100
10.	Shallow Cavity - TM Solution at (0,0) - Eta Point Two	101
11.	Radar Cross Section at 289.5 MHz	102
12.	Radar Cross Section at 480.45 MHz	104
13.	Overfilled Cavity (1 meter deep; 0.5 meter radius of protrusion)	105
14.	Interior Domain Mesh - Overfilled Cavity	106
15.	Exterior Domain Mesh - Overfilled Cavity	107
16.	Overfilled Cavity - TM Solution - Eta Point Eight	108
17.	Overfilled Cavity - TM Solution - Eta Point Two	110
18.	Overfilled Radar Cross Section at 289.5 MHz	111
19.	Overfilled Radar Cross Section at 480.45 MHz	112

List of Abbreviations

Abbreviation		Page
RCS	radar cross section	1
IEDs	improvised explosive devices	2
PEC	perfect electric conductor	3
IBC	impedance boundary condition	3
AFOSR	Air Force Office of Scientific Research	4
AFRL	Air Force Research Laboratory	4
FLTC	Focused Long Term Challenges	4
TM	transverse magnetic	6
TE	transverse electric	6
FEM	finite element method	8
BEM	boundary element method	9
FE/BI	finite element / boundary integral	9
MoM	method of moments	11
FDTD	finite difference time domain	11
CAA	computational aeroacoustics	14
DtN	Dirichlet-to-Neumann	17
SOV	separation of variables	18
PMC	perfect magnetic conductor	19
PDE	partial differential equation	21

ANALYSIS OF TRANSIENT ELECTROMAGNETIC SCATTERING FROM AN OVERFILLED CAVITY
EMBEDDED IN AN IMPEDANCE GROUND PLANE

I. Introduction

1.1 Motivation

The study of electromagnetic scattering of plane waves has long been an area of great interest in the scientific community. Many analytical and computational methods have been explored, and the various approaches to the study of scattering problems are matched by the wide variety of applications. These include acoustics, optics, and microwave technology, but it is particularly appropriate to the military regarding radar applications.

At the essence of any scattering problem is the concept of the computation of radar cross section (RCS). RCS is defined as a measure of power scattered in a given direction when a target is illuminated by an incident wave, which helps reveal the signature of a target [62]. This leads to efforts not only to measure and predict RCS, but also to enhance or minimize RCS. More demands and complexities in modern design and integration of systems require that a solid foundation exist for all types of problems involving RCS measurements.

Intense research in this area is motivated in part by the fact that of all the contributors to RCS, cavities have a significant impact on a structure's overall signature [5]. Many scattering geometries have been studied in the context of military applications. A common one is the cavity, and examples of cavity-like structures on aircraft

and vehicles are engine inlets, cracks, gaps, and cavity-backed antennas [47]. Planar cavities representing these objects have been studied in detail, but the overfilled cavity is important because it may more accurately model surfaces that include defects and perturbations [111]. For example, this geometry is exhibited in aperture and conformal antennas, which are designed to operate in the presence of a ground plane [56].

For the military, though, the battlefield has evolved significantly. For example, in today's conflicts and engagements in Afghanistan, precision is critical not only in identifying the enemy in challenging terrain, but also in expediting the decision making process through positive identification of threats. One of the biggest threats today are improvised explosive devices (IEDs). These devices are concealed or partially buried in the ground and are detonated by an electronic or pressure-activated trigger (See Figure 1). Information on IEDs is often gathered from drones and sensors, which have the capability to detect ground that has been dug up and disturbed to plant IEDs. In addition, jammers can be used to interfere and stop electronic detonation of IEDs [74]. Consider the following facts:

> The number of IED attacks that killed or wounded coalition forces increased to 60 in December (2009) from 32 in December 2008. The total number of IEDs, including those that were found before they detonated, increased to 8,690 last year (in 2009) from 3,783 in 2008. [74]

The military has improved its ability to detect and eradicate IEDs in 2010 through the expanding use of foot patrols, planes, drones, and balloons. This is evidenced by a 37% decrease in troops wounded or killed by IEDs [106]. However, there still will be a need to locate these devices in challenging terrain. Clearly, then, IEDs exhibit the characteristics of an overfilled cavity, and their detection gives rise to a scattering problem. In this context, it is critical to the military to understand the

mathematical foundation of this scattering problem that is applicable in a wide range of environments.

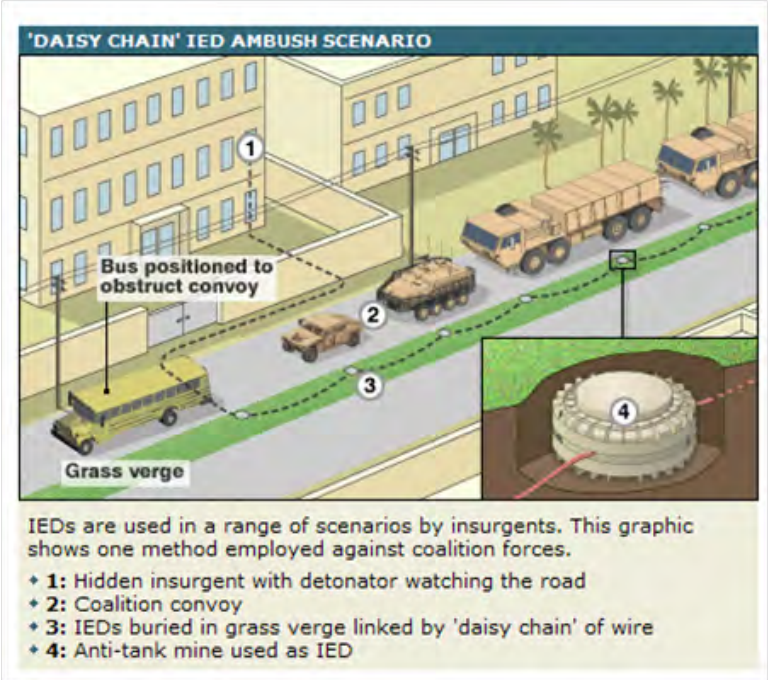

Figure 1. IED Depiction [53]

Most of the published research and mathematical development for cavity-type problems generally assumes the ground plane is a perfect electric conductor (PEC). However, for this problem it makes sense that an imperfect conductor is more physically realistic when the surface in question is the ground, which can be represented with an impedance boundary condition (IBC). The impedance at the surface is a measurable quantity dependent on the material defined on the surface, and one would expect this idea would give rise to more complicated expressions mathematically as opposed to perfectly conducting surfaces [95]. An IBC might be evident on a painted or coated surface on a plane or vehicle. It is also used to model a honeycomb or perforated material [16]. Moreover, it is also used in approximating the ground and objects lying on the ground (See, for example, [100]). Thus, an IBC is most appro-

priate to model IED detection. It is the goal, then, to provide a solid mathematical foundation for this geometry with IBCs.

Furthermore, it is critical to note that this study ties directly to the Air Force Office of Scientific Research (AFOSR) mission statement in the research area of electromagnetics, which is to "Conduct research in electromagnetics to ... evaluate methods to recognize ... and track targets (including Improvised Explosive Devices) ..." [2]. Also, it falls in line with Air Force Research Laboratory (AFRL) Focused Long Term Challenges (FLTC), specifically FLTC 3, which is "Dominant Difficult Surface Target Engagement and Defeat," which "is focused on the ability to deliver selectable and scalable non-lethal or lethal effects against adversaries and/or their support activities, IEDs ... in an urban warfare environment" [3].

1.2 General Problem Statement

Let $\Omega \subset \mathbb{R}^2$ be the cross-section (cavity interior) of a z-invariant cavity in the infinite ground plane. That is, Ω has the same definition for all values of z. We will assume that the cavity fillings, with material of relative permittivity ($\varepsilon_r \geq 1$), protrude above the ground plane. We denote S as the cavity wall and Γ the cavity aperture so that $\partial\Omega = S \cup \Gamma$. The infinite ground plane excluding the cavity opening is denoted as Γ_{ext}, and the infinite homogenous, isotropic region above the cavity as $\mathcal{U} = \mathbb{R}^2_+ \backslash \Omega$. Furthermore, let $\mathcal{B}_R$ be a semicircle of radius R, centered at the origin and surrounded by free space, large enough to completely enclose the overfilled portion of the cavity. We denote the region bounded by $\mathcal{B}_R$ and the cavity wall S as Ω_R, so that Ω_R consists of the cavity itself and the homogeneous part between $\mathcal{B}_R$ and Γ. Let $\mathcal{U}_R$ be the homogeneous region outside of Ω_R; that is, $\mathcal{U}_R = \{(r, \theta) : r > R, 0 < \theta < \pi\}$. Refer to Figure 2 for the complete problem geometry.

The problem statement is given the incident electromagnetic wave $(\boldsymbol{E}^{\text{i}}, \boldsymbol{H}^{\text{i}})$ im-

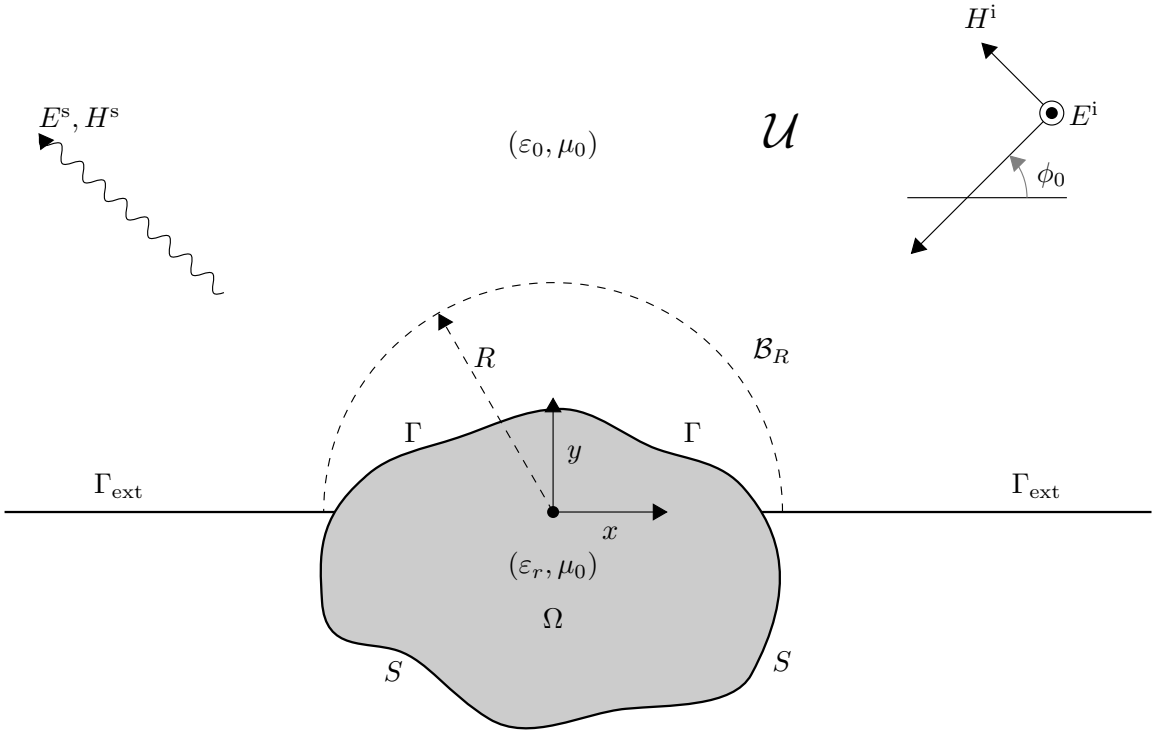

Figure 2. Problem Geometry - TM polarization depicted

pinging on the overfilled cavity, we wish to determine the resulting scattered fields $(\boldsymbol{E}^{\mathrm{s}}, \boldsymbol{H}^{\mathrm{s}})$. This is a two-dimensional problem, and due to the uniformity in the z-axis, it can be decomposed into two fundamental polarizations: transverse magnetic (TM) and transverse electric (TE). Its solution then can be expressed as a linear combination of the solutions to TM and TE problems.

We first consider the TM polarization problem, and the following formulation is modeled after Van and Wood (See [105]). In this case, the magnetic field $\boldsymbol{H}$ is transverse to the z-axis so that $\boldsymbol{E}$ and $\boldsymbol{H}$ are of the form

$$\boldsymbol{E} = (0, 0, E_z), \quad \boldsymbol{H} = (H_x, H_y, 0).$$

In this case, the nonzero component of the total electric field E_z satisfies Maxwell's equations and the following boundary value problem (see Appendix A for derivation of impedance boundary conditions in the time domain):

$$\text{(TM)} \quad \begin{cases} -\Delta E_z + \varepsilon_r \dfrac{\partial^2 E_z}{\partial t^2} = 0 & \text{in } \Omega \cup \mathcal{U} \times (0, \infty), \\ \dfrac{\partial E_z}{\partial t} = -\dfrac{\eta}{\mu} \dfrac{\partial E_z}{\partial \boldsymbol{n}} & \text{on } S \cup \Gamma_{\text{ext}} \times (0, \infty), \\ E_z|_{t=0} = E_0, \quad \left.\dfrac{\partial E_z}{\partial t}\right|_{t=0} = E_{t,0} & \text{in } \Omega \cup \mathcal{U} \end{cases}$$

where $\varepsilon_r = \varepsilon/\varepsilon_0$ is the relative electric permittivity, E_0 and $E_{t,0}$ are the given initial conditions and $\eta = \sqrt{\mu_r/\varepsilon_r}$ is the normalized intrinsic impedance of the infinite ground plane. We define the normal derivative $\dfrac{\partial E_z}{\partial \boldsymbol{n}} = \nabla E_z \cdot \hat{n}$, where $\hat{n}$ is the outward unit normal. We are assuming that we have a non-dispersive material in the cavity, i.e. $\dfrac{\partial \varepsilon_r}{\partial \omega} = 0$, or that the permittivity is not a function of frequency, but could vary with respect to position.

We observe the scattered field E_z^s solves

$$\begin{cases} -\Delta E_z^s + \dfrac{\partial^2 E_z^s}{\partial t^2} &= 0 & \text{in } \mathcal{U} \times (0,\infty), \\ \dfrac{\partial E_z^s}{\partial t} + \dfrac{\eta}{\mu}\dfrac{\partial E_z^s}{\partial \boldsymbol{n}} &= -(\dfrac{\partial E_z^i}{\partial t} + \dfrac{\eta}{\mu}\dfrac{\partial E_z^i}{\partial \boldsymbol{n}}) & \text{on } \Gamma_{\text{ext}} \cup \Gamma \times (0,\infty), \end{cases}$$

and also satisfies the radiation condition at infinity

$$\lim_{r\to\infty} \sqrt{r}\left(\frac{\partial E_z^s}{\partial r} + \frac{1}{c}\frac{\partial E_z^s}{\partial t}\right) = 0, \quad t > 0. \tag{1.2.1}$$

The homogeneous region $\mathcal{U}$ above the protruding cavity is assumed to be air and hence its permittivity is $\varepsilon_r = 1$. In $\mathcal{U}$, the total field can be decomposed as $E_z = E_z^i + E_z^s$ where E_z^i is the incident field, and E_z^s the scattered field.

1.3 Function Spaces and Requirements

The appropriate and relevant theorems and propositions used and cited in this work will appear at the appropriate points in the manuscript. Nevertheless, the goal here is to briefly discuss the motivation for the appropriate functional spaces and numerical methods that will be used. We will use the Lebesgue scalar product,

$$\langle u, v\rangle = \int_T u\bar{v}dT,$$

with $\|u\| = \Big(\int_T |u|^2\, dT\Big)^{1/2} < \infty$, where T is a bounded subset of $\mathbb{R}^2$. We refer to these as square integrable functions.

We note that Hilbert spaces, or complete inner product spaces, are most applicable to real-world computational schemes [107]. We will also need to deal with "function spaces that are larger than the classes of continuous and continuously differentiable functions" [10]. The reason is that when dealing with the differential equation in a

numerical framework, finite element subspaces are piecewise continuous at best. Thus, we require a less restrictive way in which to define boundedness through the space of square integrable functions, or $L^2(\Omega_R)$. As previously defined, $L^2(\Omega_R)$ contains sets of piecewise continuous functions used in the finite element method (FEM). To ensure boundedness of the differential operator over the domain of square integrable functions, the derivatives must also be square integrable, which leads to the idea of Sobolev spaces [107]. Thus, the framework established here lends itself to numerical methods, but more importantly, this function space will be needed for any weak formulation of the boundary value problem [97].

We first define the Sobolev space $H^1(\Omega_R)$ for the bounded domain Ω_R with norm:

$$\|u\|_{H^1(\Omega_R)} = \Big[\int_{\Omega_R} \big(\|u\|^2 + \|\nabla u\|^2 \big) \Big]^{1/2},$$

where $u \in L^2(\Omega_R)$ [10].

This can be expressed alternatively, as it is in [54], as:

$$H^1(\Omega_R) = \Big\{ u \in L^2(\Omega_R) \quad | \quad \|\nabla u\|_{L^2}^2 + \|u\|_{L^2}^2 < \infty \Big\}.$$

Therefore, the Sobolev space $H^1(\Omega_R)$ is the space of functions in $L^2(\Omega_R)$ whose derivatives are also in $L^2(\Omega_R)$. These derivatives are defined in a weak sense, and this space does include continuous piecewise linear functions [35]. Another perspective is that in order for the test functions to be well-defined, we require that the partial derivatives be defined globally in nature, and "tolerant of certain kinds of singularities" [35]. Derivatives in the classical sense are local in nature, so we want a more global definition where we can incorporate singularities.

We will also need to extend the idea of Sobolev spaces to the boundary. This will be apparent when working with the coupling of the problem on the artificial

boundary, $\mathcal{B}_R$. We define the trace of a function as the value of a function on its boundary. For our problem this is a linear mapping from the Sobolev space on the domain Ω_R to the Sobolev space on the boundary $\mathcal{B}_R$ [54]. Furthermore, the trace theorem (see Theorem 4.2.2) states that the trace of functions in $H^1(\Omega_R)$ as mapped to $H^{1/2}(\mathcal{B}_R)$ is well-defined and bounded [10]. We are particularly interested in the spaces $H^1(\Omega_R)$, its trace $H^{1/2}(\mathcal{B}_R)$, and the dual space of $H^{1/2}(\mathcal{B}_R)$, $H^{-1/2}(\mathcal{B}_R)$. The dual space is simply the set of bounded linear functionals on the space $H^{1/2}(\mathcal{B}_R)$.

All of this will help lay the framework for numerical applications. It is important to note that the methods we will discuss, the FEM and the boundary element method (BEM) "belong to the most used numerical discretization methods for the approximate solution of elliptic boundary value problems" [97]. We will ultimately see that a combination of these methods will be required, and is referred to in the literature as a hybrid finite element / boundary integral (FE/BI) method.

1.4 Time versus Frequency Domain

Any scattering problem starts with Maxwell's equations which describe the propagation of electromagnetic waves, and the resulting problem can be analyzed in either the time domain or frequency domain. Quite often, scattering problems are posed in the frequency domain due to its convenience in a mathematical sense, and time harmonic behavior is assumed. Field quantities that are harmonically oscillating with a single frequency constitute time-harmonic behavior [55]. Frequency domain analysis is "ideally suited for scattering analysis" from plane waves in arbitrary directions or when the scattering source is localized [56]. One possible motivation for studying in the frequency domain is that in optics, most applications deal with narrow bands of radiation, making studying fixed-frequency problems relevant [9].

Nevertheless, with increases in computing power in the digital age, time domain

methods have increased in popularity [88]. It is especially important to the military in many strategic areas involving short-pulse communication and radar systems [31]. It is also important to understand and predict behavior in the time domain because of the potential to simulate transient phenomena, perform broadband characterization, and model nonlinear devices [55]. The time domain "is ideally suited for antenna analysis, where one is often interested in a solution over a broad frequency band for one or a few excitations" [56]. It is also better suited for "visual representations of understanding field interactions" [88]. Therefore, research in the time domain offers many advantages, yet will be more mathematically challenging. Furthermore, a study from a mathematical perspective will provide a new foundation in the literature, since most mathematical approaches are from the frequency domain.

II. Related and Previous Work / Literature Review

2.1 Solving the Electromagnetic Scattering Problem

Electromagnetic scattering from cavities with varying geometries has been studied extensively in computational electromagnetics over the years. Anastassiu did a thorough review all methods used for modeling electromagnetic scattering from cavities, with a specific focus on engine inlets and open ducts from aircraft. He claimed this was "One of the most challenging problems in modern applied electromagnetics" [5]. This could be due in part to the "appearance of spurious modes caused by interior resonances" [105].

Anastassiu divided the approaches into exact or modal methods (such as Wiener-Hopf and mode matching), high frequency and spectral methods, integral equation methods (boundary integral approach, method of moments (MoM)), and differential-equation methods (FEM, FE/BI, finite difference time domain (FDTD)). The majority of these applications, however, are generally done on perfectly conducting surfaces, which may be sufficient and appropriate for most applications [5]. Nevertheless, the major numerical techniques in electromagnetics remain the MoM, FDTD, and FEM. It is worth noting that hybrid methods, involving a combination of integral equation and differential equation methods, have gained popularity, particulary if it is possible to use a certain method where it is most computationally efficient [107]. From our perspective, the FEM and BEM will be most important, as we will seek a hybrid FE/BI approach. It is worth noting that the BEM was developed in the 1950s, and has shown to be a powerful tool in the study of physical phenomena in an unbounded domain, such as scattering [89].

From a mathematical perspective, differential equation methods and integral equation methods interest us the most. Purely mathematical treatments of scattering,

however, appear to be more limited in scope than the numerical and computational electromagnetic applications. It is clearly important to establish the mathematical framework and well-posedness (existence and uniqueness) in a general setting before one can implement these methods for specific settings and geometries. Colton, Kress, and Cakoni have done extensive mathematical work in the area of scattering theory over the years, and have used results to transition to a growing area of interest, inverse scattering, which is the reconstruction of the object given a scattered field (see [10] and [19]). Monk provides a thorough treatment for the underlying mathematics of the FEM, and discusses inverse problems as well [75]. It is important to note that the study of inverse scattering problems in the context of IEDs would also be a significant contribution, as particular shapes could be identified as IEDs. Nédélec has also contributed significantly in the context of integral equations and integral representation of solutions [77]. Angell and Kirsch studied optimization methods in the context of antennas, but still showed the need of direct scattering solutions as a foundation, using a problem with IBCs as an example [6]. Chandler-Wilde has also done extensive research over the years, focusing on scattering with IBCs and rough surfaces (see, for example, [12]).

However, all of these authors' analysis is primarily in the frequency domain. All have contributed extensively in this regard, with many common threads, such as developing cases involving IBCs at the surface. All use variational formulation methods to establish well-posedness, which provides a natural foundation for computational methods such as FEM. Yet the complications involving an overfilled cavity geometry are not addressed by these authors. Therefore, before we consider the related work in this specific area, we first consider the details of the IBC and its development over the years.

2.2 History of Impedance Boundary Conditions

The impedance concept was first mentioned in 1938 for time harmonic field theory by Schelkunoff [109]. However, Shchukin is first credited with developing the IBC by 1940. Leontovich also later derived surface impedance boundary conditions in 1948, so they all can be considered the first major contributors to the development of the impedance boundary condition [81]. These impedance boundary conditions were further developed by Senior in 1960, and they were almost exclusively used in the frequency domain until the early 1990s [66]. It was then that these boundary conditions in the time domain received more attention, particularly in the area of numerical implementation. Therefore, the IBC in the time domain is still a relatively recent and evolving area of research.

2.3 Impedance Boundary Conditions in the Time Domain

Because the impedance boundary condition is inherently a frequency-domain topic, its conversion and implementation in the time domain is difficult and remains an ongoing area of research. There are two general approaches to this conversion: assuming no frequency dependence of the material (i.e. constant parameter materials), or assuming the material is dispersive and frequency-dependent. Clearly, using a dispersive impedance boundary condition enjoys the advantage of being applicable over a larger frequency bandwidth, but it is more complex to implement [66].

Impedance boundary conditions have been used extensively in integral equation formulations, the FDTD, and the frequency-domain FEM. In Jin and Riley's book, their formulations for incorporating the IBCs are initially done in the frequency domain, and then inverse Fourier transformed [56]. In fact, most of the computational approaches in this area seek to accurately model frequency dependence.

Lee, Shin, and Kong modeled the impedance boundary condition in the time do-

main, discretized using a centered-difference method, and used the resulting expressions in the FDTD method. They approximate the impedance boundary condition as a rational function of frequency, accounting for the dispersiveness of the condition, and then transform into a time domain equation [69].

Ida and Yufrevev have done extensive research into the area of impedance boundary conditions for transient scattering problems. Most of their research involves formulating integral equations for use with methods with the FDTD or BEM methods. They also investigate higher orders of approximation of impedance boundary conditions, to include derivation of the boundary conditions in time domain. Most of their work revolves around implementation of the IBCs into the time domain for some numerical solver (See, for example, [52],[115],[114],[116],[113]).

Chen, Lu, and Michielssen studied a coupled set of time domain integral equations with an impedance boundary condition. According to their work, the method never develops internally resonant fields and is validated by numerical examples [84].

This concept not only is applicable in electromagnetics, but also is a popular area in computational aeroacoustics (CAA), in which computation of sound propagation through an engine inlet is important. Ozyoruk and Long develop a time domain IBC using a Z-transform, and they model it as a rational function. They incorporate a time discretized IBC into a Runge-Kutta scheme [80]. Bin, Hussaini, and Lee develop a broadband time domain IBC [58]. Maloney and Smith ([72]) and Schutt-Aine and Oh ([79]) also researched implementation of the IBC into the FDTD.

Therefore, the IBC has been studied quite extensively from a computational perspective in the time domain, but is lacking from a purely mathematical perspective. Our goal, then, is to provide a foundation for this process, keeping in mind we are interested more in the effects of a general Robin boundary condition (i.e. $\frac{\partial u}{\partial n} + ku = f$) on the structure of the problem, rather than the explicit conversion of the IBC into

the time domain.

As a result, we will start with the idea that there are two general approaches to conversion. If we assume constant parameter materials, we end up with a straightforward conversion where we can substitute $\frac{\partial}{\partial t}$ for $\imath\omega$, which resembles a first-order absorbing boundary condition [55].

There is also another possible mathematical justification of this approach. If we consider the expression for surface impedance as in [8] as:

$$\eta = (1 + \imath)\sqrt{\frac{\omega\mu}{2\sigma}},$$

where σ is the conductivity of the surface, we note a dependence of η on frequency (ω). However, if we were dealing with a situation where σ was proportional to some multiple of frequency, we could state that the frequency dependence is suppressed. As a result, our assumption would closely resemble the IBC.

Finally, we mention that Wang in [108] studied transient scattering with a curved absorbing boundary. The numerical examples depicting the scattered field in this work will be important to us during the validation phase because FEM will be used with the Newmark method. Thus, we can use this study as a baseline to ensure our results compare favorably.

2.4 Research on Overfilled Cavities and Similar Geometries

The geometry of a cavity closely resembles structures involving defects, perturbations, grooves, cracks, or rough or grated surfaces, while an overfilled cavity can represent partially buried or embedded objects in a plane. For example, Hamid and Hamid studied scattering by a partially buried dielectric sphere in the infinite PEC plane. They arrive at an analytic solution based on the method of images, and present

numerical results for a variety of conditions [40]. Also, Wang and Li studied a partially embedded cylinder in a random dielectric rough surface. They used the MoM technique and provided numerical results. Tsaur and Chang investigated a dielectric cylinder buried in a shallow circular trough in the two-dimensional ground plane, and derived a series solution as well as numerical results in the frequency domain, using a mode-matching (or region-matching) method for both the TE and TM cases (see [102] and [103]).

The study of impedance boundary conditions with objects or protrusions from the surface can be traced back to the late 1960s. Goshin considered the problem of an impedance cylinder resting on an impedance plane, citing the effects of surface waves and expresses an exact solution [37]. Glisson studied an arbitrarily shaped surface with impedance boundary conditions [34]. More recently, Swearingen studied acoustic scattering from an impedance cylinder placed normal to an impedance plane, modeling scattering from trees in a forest [101].

Chandler-Wilde has done a significant amount of mathematical research in the area of impedance boundary value problems of the Helmholtz equation in the half-plane (see [13], [11], and [67]), as well as with scattering from unbounded rough surfaces [14]. His work has been restricted primarily to the frequency domain. Lines and Chandler-Wilde, however, did study an inverse scattering problem in the context of the time domain with a rough scattering surface [70].

Mathematical research involving overfilled cavities in the infinite ground plane has primarily been limited to the frequency domain with both an impedance boundary condition as well as a PEC ground plane. Durán, et al., established existence and uniqueness of "outgoing solutions for the Helmholtz equation in a locally perturbed half-plane" with impedance boundary conditions [29]. They developed a Green's function solution for the impedance half-plane. In addition, they establish an expres-

sion for the radiation condition due to surface waves from the boundary. Their study of the perturbation of the boundary resembles the geometry of an overfilled cavity, as they studied it in the context of outdoor sound propagation or perturbed water waves in a sea harbor.

They also separate the domain into two sub-domains connected through an artificial semicircular boundary, coupled through a Dirichlet-to-Neumann (DtN) operator (See Figures 3 and 4), which maps the values of the scattered field on the artifical boundary to its normal derivative. They establish results for both the two-dimensional and three-dimensional cases in the frequency domain (see [29] and [30]). Their problem closely resembles our problem geometry, and we will use that approach as a framework, particularly for the exterior problem.

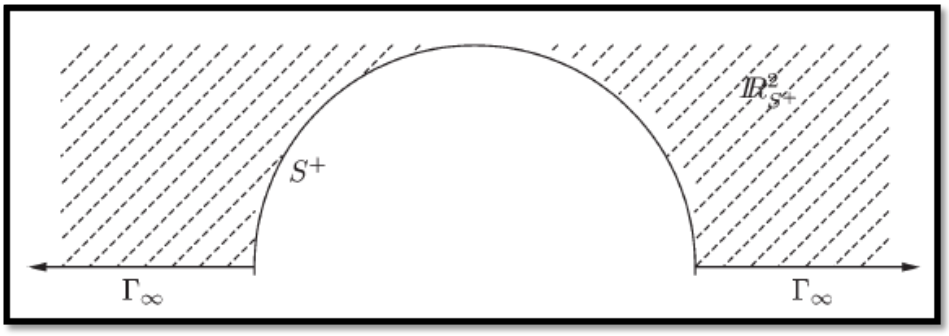

Figure 3. Durán's Exterior Problem Geometry [29]

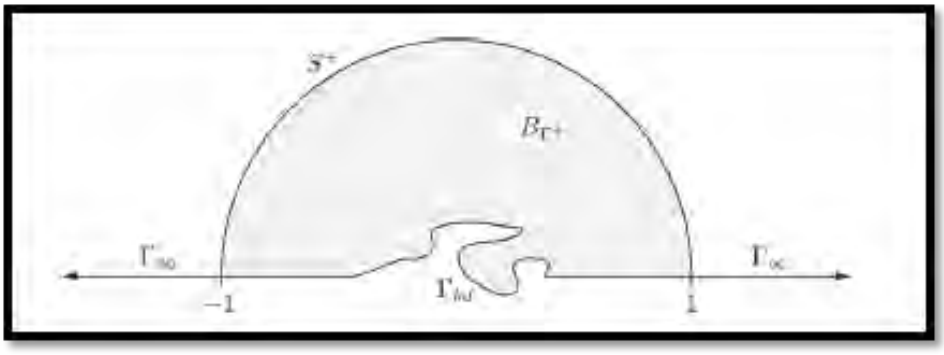

Figure 4. Durán's Interior Problem Geometry [29]

Wood considered the scattering of a time-harmonic plane wave by an overfilled cavity in the two-dimensional PEC ground plane [111]. She also uses an artificial boundary condition on a semicircle enclosing the overfilled portion of the cavity; this boundary couples the exterior fields to those inside the cavity. She solves for the fields exactly via a separation of variables (SOV) technique, and then establishes existence and uniqueness of the interior problem through a variational formulation using the properties of the DtN operator on the artificial boundary. Huang and Wood extend this work by implementing a finite element method to numerically simulate the results of this problem geometry [51].

Also, D. U. Kui also studied overfilled cavities in his dissertation entitled, " Numerical Computation of Electromagnetic Scattering From Large Cavities" [65]. Kui cites Wood's previously discussed work and methods in this area, and studies the case for multiple overfilled cavities, where the artificial boundary enclosing all of the overfilled cavities takes the form of a semiellipse instead of a semicircle. Kui uses the elliptic coordinate system to prove uniqueness and existence for the TM and TE cases using SOV and the same techniques Wood uses in [111] for the semicircular artificial boundary. Kui notes one advantage of this semielliptical artificial boundary for multiple overfilled cavities is that it increases accuracy and efficiency due to the smaller size of the computational domain [65].

Jin and Riley propose the use of the FE/BI method to analyze an antenna structure embedded in a ground plane that partly protrudes above the surface (refer to Figure 5). They introduce a "truncation surface" and employ image theory to formulate the exterior fields via integral equations. These boundary integral equations take into account the effect of the ground plane on the radiated scattered fields. This also eliminates internal resonance problems [56].

The overfilled cavity geometry has also been studied from a mathematical per-

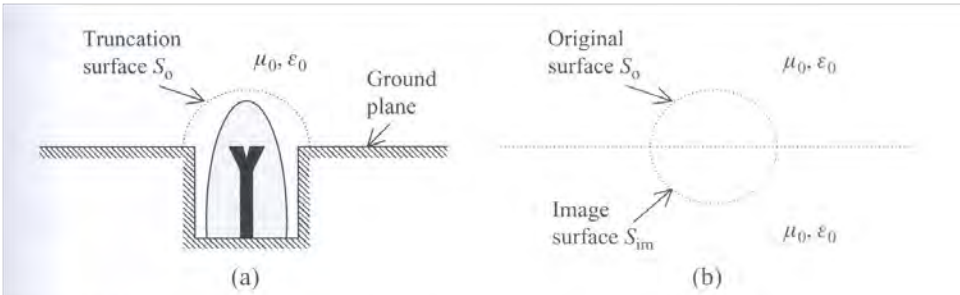

Figure 3.14 Antenna structure partially residing in a cavity and protruding above a ground plane. (a) Original problem. (b) Equivalent image problem for the truncation surface.

Figure 5. Jin and Riley Conformal Antenna [56]

spective in the time domain. Van and Wood studied the overfilled cavity in the PEC ground plane in the time domain. They first discretized the problem in time, and then used the coupling technique and DtN operator to help establish existence and uniqueness of the variational forms. In addition, they perform finite element error analysis and stability analysis for the time stepping scheme [105]. Huang and Wood extended this work by implementing a hybrid finite element and Fourier transform method to provide an analytical and numerical solution. Again, they solve for the fields in the exterior region analytically, and use the FEM to solve for the interior fields. The results are finally inverted back into the time domain [49].

Huang, Wood, and Havrilla use a hybrid finite element-Laplace transform method to analyze the scattering problem of an overfilled cavity in the PEC ground plane in the time domain. Their approach is generally similar to Van and Wood in [105]; however, they employ a domain decomposition technique integrated into the FE/BI method. Here, an overlapping zone is created between the interior and exterior domains where the Laplace transform is used as an analytic link condition. They also provide numerical validation as well as an error analysis [50].

It is also important to note that the previous results assuming a PEC ground plane can also be extended to a perfect magnetic conductor (PMC) ground plane. The PMC

case is in essence the dual of the PEC case. That is, for the TM case, instead of a homogeneous Dirichlet condition for the tangential component of the electric field ($E_z = 0$), it would be a homogeneous Neumann condition ($\frac{\partial E_z}{\partial n} = 0$). Similarly, for the TE case, instead of the Neumann condition for the tangential component of the magnetic field, we would have a Dirichlet condition [94]. Even though pure PMC materials are not known to exist, these results would be an important application to the study of metamaterials which could closely model this boundary condition. Applications in the study of metamaterials include smaller antennas and cloaking research [71].

III. Mathematical Formulation

3.1 Approach to Solution and Semidiscrete Problem

In order to solve a partial differential equation (PDE), the primary analytic approaches we can use are SOV, developing a Green's function, and variational formulation [39]. It has been shown that the separation of variables method is appropriate for this problem geometry for a PEC or PMC surface. For an IBC, however, there are more complications involved with this method. Hanson and Yakovlev address the impedance plane problem through SOV by solving two one-dimensional problems, and combining the results to get an expression for the Green's function as well as for the generated field [41]. As mentioned previously, Durán et al. and Chandler-Wilde also obtained expressions for the Green's function of an impedance half-plane. In addition, Politis et al. develops several representations of the Green's function for a modified Helmholtz equation with IBCs on the surface [82]. Therefore, a generalized Green's function method will be the most appropriate method to solve the problem. That is, we can derive a Green's function for an infinite planar surface with an IBC, and for the exterior problem, get an integral expression for the scattered field that contains the Green's function. Finally, we will use a variational formulation to solve the interior problem. Thus, having explored all of these primary analytic methods in order to show existence and uniqueness, we will use both the generalized Green's function method as well as variational formulation to obtain a solution.

Furthermore, these analytic methods will provide the foundation for both the finite and boundary element methods, implemented as a hybrid FE/BI method. That is, the variational formulation is a framework for the FEM, which has "almost universal applicability" [97]. In addition, "the use of BEM requires the explicit knowledge of a fundamental solution", or Green's function, "which allows the transformation of

the PDE to a boundary integral equation to be solved" [97]. Furthermore, "BEM are often used . . . to find solutions of boundary value problems in exterior unbounded domains" [97]. Clearly, then, these techniques are the most appropriate to solve our problem. According to Costabel in [23], we will also find that the use of boundary integral equations has two important uses for us: "as a theoretical tool for proving the existence of solutions and as a practical tool for the construction of solutions." The integral representation formula is a critical starting point for these applications.

To formulate and solve this problem, we will first decompose the entire solution domain to two sub-domains via an artificial semicircle, $\mathcal{B}_R$, which entirely encloses the overfilled cavity. These two sub-domains consist of the infinite upper half plane over the impedance plane exterior to the semicircle, denoted $\mathcal{U}_R$, and the cavity plus the interior region of the semicircle, denoted Ω_R. Refer to Figure 6 for a depiction of the two sub-domains.

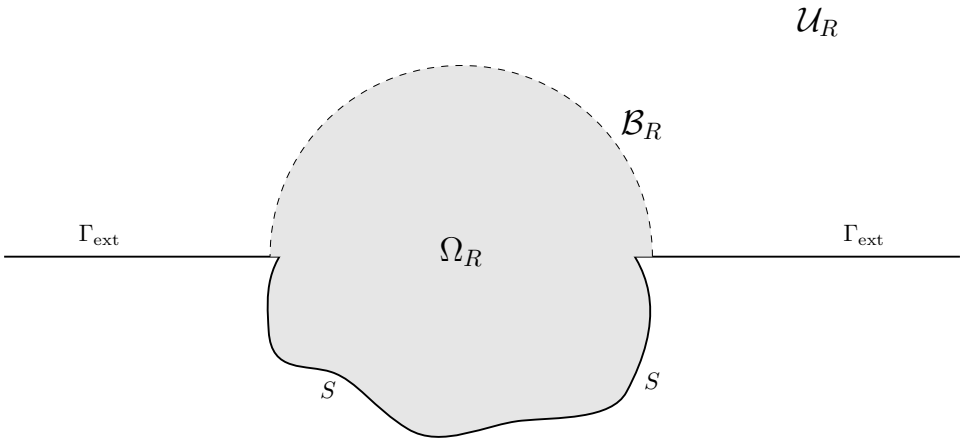

Figure 6. Sub-Domains of Problem

The two regions are coupled over the artificial semicircle through the use of this DtN operator, thus exploiting the electromagnetic field continuity over the artificial boundary. The variational formulation used for the interior problem will allow us to establish well-posedness. In turn, the hybrid approach will come into play as we use

the solution obtained from the FEM on the interior as the solution on the artificial boundary. This will allow us to get an expression for the scattered field in the exterior domain, as desired. This technique of using a semicircular artificial boundary with a DtN mapping has been used by Givoli and Vigdergauz in [33], Lin and Grosh in [112], and Zhao and Liu in [17]. However, they assumed more simplified boundary conditions on the planar surface allowing a SOV approach involving explicit series representation.

It is important to first address the possibilities for incorporating the time dependence into the problem. We would expect additional difficulties due to this added dimension, where concerns regarding stability of the method used become a factor [22]. The literature mentions three general approaches to transient problems when working towards formulating boundary integral methods: space-time integral equations, Laplace-transform methods, and general time-stepping methods [22].

For this problem, following Van and Wood in [105], we will choose to use the Newmark scheme, an implicit time-stepping method that offers the advantage of stability. This concept of applying the time discretization directly to the PDE was first suggested by Rothe in 1930 [15]. This results in a sequence of boundary value problems for inhomogeneous elliptic equations, where the inhomogeneities are simply the solutions at the previous time steps [15]. One advantage is that once the procedure is established for the solution at one time step, we can "march arbitrarily far in time by simply repeating this procedure" [22]. It is worth noting that the Newmark scheme is primarily used in time-domain studies of dynamic analysis of structures, though it does have some use in electromagnetic scattering problems.

Therefore, we will discretize the TM equations in time by using the Newmark time-marching scheme. When compared to a forward, backward, or central difference scheme, some advantages of the Newmark method are that it can be made uncondi-

tionally stable and it has the "best truncation error" for a choice of parameters [88]. This method is a two-step finite difference method in which there is a prediction of the answer followed by a correction of the predicted value. At each time step, we construct a nonlocal boundary condition on the semicircle $\mathcal{B}_R$ to couple the solution in the infinite domain exterior to $\mathcal{B}_R$ and the solution in the bounded domain inside $\mathcal{B}_R$.

The Newmark scheme is defined by the following: Let N be a positive integer, T be the time interval, $\delta t = T/N$ be the temporal step size, and $t_{n+1} = (n+1)\delta t$ for $n = 0, 1, 2, ..., N-1$. Denote the following as approximations at $t = t_{n+1}$:

$$\begin{aligned} u^{n+1} &\approx u, \\ \dot{u}^{n+1} &\approx \frac{\partial u}{\partial t}, \\ \ddot{u}^{n+1} &\approx \frac{\partial^2 u}{\partial t^2}. \end{aligned}$$

These approximations are related by

$$u^{n+1} = u^n + \delta t \dot{u}^n + \frac{(\delta t)^2}{2}\big[2\beta\ddot{u}^{n+1} + (1-2\beta)\ddot{u}^n\big],\ 0 \le n \le N-1, \tag{3.1.1}$$

$$\dot{u}^{n+1} = \dot{u}^n + \delta t\big[\gamma\ddot{u}^{n+1} + (1-\gamma)\ddot{u}^n\big],\ 0 \le n \le N-1, \tag{3.1.2}$$

where γ and β are parameters to be determined to guarantee stability of the time-marching scheme [105].

We will denote u^i as the incident field E_z^i, u the total field E_z, and u^s the scattered field E_z^s. The semidiscrete problem is to find $u^{n+1}, n = 0, 1, ..., N$, such that we have the following:

Prediction

$$\tilde{u}^{n+1} = u^n + \delta t \dot{u}^n + \frac{(\delta t)^2}{2}(1-2\beta)\ddot{u}^n, \tag{3.1.3}$$

$$\tilde{\dot{u}}^{n+1} = \dot{u}^n + \delta t(1-\gamma)\ddot{u}^n, \tag{3.1.4}$$

Solution

$$\begin{cases} -\Delta u^{n+1} + \alpha^2 \varepsilon_r u^{n+1} &= \alpha^2 \varepsilon_r \tilde{u}^{n+1} & \text{in } \Omega_R, \\ \dot{u}^{n+1} &= -\dfrac{\eta}{\mu}\dfrac{\partial u^{n+1}}{\partial n} & \text{on } S, \\ u^{n+1} &= u^{s,n+1} + u^{i,n+1} & \text{on } \mathcal{B}_R, \end{cases} \tag{3.1.5}$$

Correction

$$\ddot{u}^{n+1} = \alpha^2(u^{n+1} - \tilde{u}^{n+1}), \tag{3.1.6}$$

$$\dot{u}^{n+1} = \tilde{\dot{u}}^{n+1} + \delta t \gamma \ddot{u}^{n+1}, \tag{3.1.7}$$

where $\alpha^2 = \dfrac{1}{(\delta t)^2 \beta}$.

The IBC on Γ_{ext} and S (See Appendix A for the derivation of these conditions) becomes:

$$\dot{u}^{n+1} = -\frac{\eta}{\mu}\frac{\partial u^{n+1}}{\partial n}. \tag{3.1.8}$$

Using the correction factor described above for $\ddot{u}^{n+1}$ and $\dot{u}^{n+1}$, we can express the IBC in (3.1.8) for the total field as:

$$\delta t \gamma \alpha^2 u^{n+1} + \frac{\eta}{\mu}\frac{\partial u^{n+1}}{\partial n} = \delta t \gamma \alpha^2 \tilde{u}^{n+1} - \tilde{\dot{u}}^{n+1}. \tag{3.1.9}$$

Therefore, the scattered field $u^{s,n+1}$ satisfies the following *exterior problem*:

$$\begin{cases} -\Delta u^{s,n+1} + \alpha^2 u^{s,n+1} &= \alpha^2 \tilde{u}^{s,n+1} & \text{in } \mathcal{U}_R, \\ u^{s,n+1}(R,\theta) &= g(R,\theta) & \text{on } \mathcal{B}_R, \\ \delta t \gamma \alpha^2 u^{s,n+1} + \dfrac{\eta}{\mu}\dfrac{\partial u^{s,n+1}}{\partial n} &= \delta t \gamma \alpha^2 \tilde{u}^{s,n+1} - \tilde{\dot{u}}^{s,n+1} + K & \text{on } \Gamma_{\text{ext}}, \end{cases} \tag{3.1.10}$$

where $g \stackrel{def}{=} u^{n+1} - u^{i,n+1}$ and

$$K = -\delta t \gamma \alpha^2 u^{i,n+1} - \frac{\eta}{\mu}\frac{\partial u^{i,n+1}}{\partial n} + \delta t \gamma \alpha^2 \tilde{u}^{i,n+1} - \tilde{\dot{u}}^{i,n+1},$$

and the radiation condition is satisfied:

$$\lim_{r\to\infty} \sqrt{r}\left(\frac{\partial u^{s,n+1}}{\partial r} + \frac{1}{c}\dot{u}^{s,n+1}\right) = 0. \tag{3.1.11}$$

We note that in considering the value of K above, since the incident wave is known, the prediction will equal the actual value. Therefore, $K = 0$.

3.2 Integral Representation of Solution

In what follows, we suppress the $n+1$ superscript from (3.1.10). We seek the solution for the nonhomogeneous modified Helmholtz equation:

$$-\Delta u(\boldsymbol{r}) + \alpha^2 u(\boldsymbol{r}) = f(\boldsymbol{r}) \quad \text{in } \mathcal{U}_R, \tag{3.2.1}$$

where $\boldsymbol{r}$ denotes position, $f(\boldsymbol{r}) = \alpha^2 \tilde{u}^{s,n+1}$, subject to nonhomogeneous boundary conditions of the form:

$$Au(\boldsymbol{r}_s) + B\frac{\partial u(\boldsymbol{r}_s)}{\partial \boldsymbol{n}} = h(\boldsymbol{r}_s) \quad \text{on } \Gamma_{\text{ext}}\ . \tag{3.2.2}$$

Here, $\boldsymbol{r}_s$ is on the surface, and A and B are constants defined as $A = \delta t\gamma\alpha^2$ and $B = \dfrac{\eta}{\mu}$, and $h(\boldsymbol{r}_s) = \delta t\gamma\alpha^2\tilde{u}^{s,n+1} - \tilde{\dot{u}}^{s,n+1}$.

We require that the associated Green's function satisfy (where $\boldsymbol{r'}$ denotes source location):

$$-\Delta G(\boldsymbol{r}|\boldsymbol{r'}) + \alpha^2 G(\boldsymbol{r}|\boldsymbol{r'}) = \delta(\boldsymbol{r} - \boldsymbol{r'}) \quad \text{in } \mathcal{U}, \tag{3.2.3}$$

$$AG(\boldsymbol{r}|\boldsymbol{r'}) + B\frac{\partial G(\boldsymbol{r}|\boldsymbol{r'})}{\partial n} = 0 \qquad \text{on } \Gamma_{\text{ext}}\ . \tag{3.2.4}$$

Using a generalized Green's function method, we multiply (3.2.1) by $G(\boldsymbol{r}|\boldsymbol{r'})$ and (3.2.3) by $u(\boldsymbol{r})$ to get

$$-\Delta u(\boldsymbol{r})G(\boldsymbol{r}|\boldsymbol{r'}) + \alpha^2 u(\boldsymbol{r})G(\boldsymbol{r}|\boldsymbol{r'}) = f(\boldsymbol{r})G(\boldsymbol{r}|\boldsymbol{r'}) \tag{3.2.5}$$

$$-\Delta G(\boldsymbol{r}|\boldsymbol{r'})u(\boldsymbol{r}) + \alpha^2 G(\boldsymbol{r}|\boldsymbol{r'})u(\boldsymbol{r}) = \delta(\boldsymbol{r} - \boldsymbol{r'})u(\boldsymbol{r}). \tag{3.2.6}$$

Next we subtract (3.2.5) from (3.2.6) and integrate over the enclosed surface $\mathcal{U}_R$ (see Figure 7) to get:

$$\begin{aligned}\iint_{\mathcal{U}_R} \big(- \Delta G(\boldsymbol{r}|\boldsymbol{r'})u(\boldsymbol{r}) + \Delta u(\boldsymbol{r})G(\boldsymbol{r}|\boldsymbol{r'})\big) \cdot \boldsymbol{n}dS &= \iint_{\mathcal{U}_R} \delta(\boldsymbol{r} - \boldsymbol{r'})u(\boldsymbol{r})dS \\ &\quad - \iint_{\mathcal{U}_R} f(\boldsymbol{r})G(\boldsymbol{r}|\boldsymbol{r'})dS \\ &= u(\boldsymbol{r'}) - \iint_{\mathcal{U}_R} f(\boldsymbol{r})G(\boldsymbol{r}|\boldsymbol{r'})dS.\end{aligned} \tag{3.2.7}$$

We apply Green's second identity in two dimensions to the left-hand side of (3.2.7)

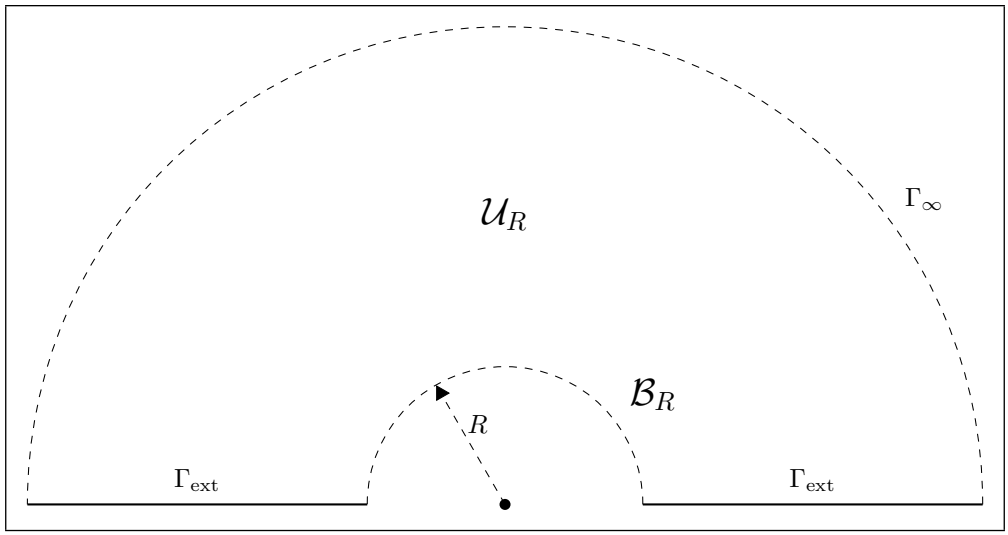

Figure 7. Exterior Domain

to get:

$$\int_C \left(G(\boldsymbol{r}|\boldsymbol{r'})\nabla u(\boldsymbol{r}) - u(\boldsymbol{r})\nabla G(\boldsymbol{r}|\boldsymbol{r'})\right) \cdot \boldsymbol{n} d\ell = u(\boldsymbol{r'}) - \iint_{\mathcal{U}_R} f(\boldsymbol{r}) G(\boldsymbol{r}|\boldsymbol{r'}) dS, \text{ or}$$

$$u(\boldsymbol{r'}) = \iint_{\mathcal{U}_R} f(\boldsymbol{r}) G(\boldsymbol{r}|\boldsymbol{r'}) dS + \int_C \left(G(\boldsymbol{r}|\boldsymbol{r'})\nabla u(\boldsymbol{r}) - u(\boldsymbol{r})\nabla G(\boldsymbol{r}|\boldsymbol{r'})\right) \cdot \boldsymbol{n} d\ell, \quad (3.2.8)$$

where C is defined as the contour enclosing the surface, $\mathcal{U}_R$, in Figure 7, and $C = \Gamma_{\text{ext}} + \mathcal{B}_R + \Gamma_\infty$. This is a common development and expected result in the literature (See, for example, [8] or [55]).

Thus, our solution depends on the sources inside the enclosed region as well as the values of u and ∇u on the contour [27]. The Green's function, which will be developed separately, depends on the boundary conditions and radiation condition. Therefore, we seek to simplify the expression on the boundary, attempting to incorporate the impedance boundary condition.

Following [26], we will add and subtract the terms $\dfrac{B}{A}\dfrac{\partial u(\boldsymbol{r})}{\partial n}\dfrac{\partial G(\boldsymbol{r}|\boldsymbol{r'})}{\partial n}$ from the

boundary integral expression in (3.2.8) on Γ_{ext} to get:

$$\begin{aligned}
&\int_{\Gamma_{\text{ext}}} \Big[G(\boldsymbol{r}|\boldsymbol{r'}) \frac{\partial u(\boldsymbol{r})}{\partial n} - u(\boldsymbol{r}) \frac{\partial G(\boldsymbol{r}|\boldsymbol{r'})}{\partial n} + \frac{B}{A} \frac{\partial u(\boldsymbol{r})}{\partial n} \frac{\partial G(\boldsymbol{r}|\boldsymbol{r'})}{\partial n} - \frac{B}{A} \frac{\partial u(\boldsymbol{r})}{\partial n} \frac{\partial G(\boldsymbol{r}|\boldsymbol{r'})}{\partial n} \Big] d\ell \\
&= \int_{\Gamma_{\text{ext}}} \frac{1}{A} \Big[(AG(\boldsymbol{r}|\boldsymbol{r'}) \frac{\partial u(\boldsymbol{r})}{\partial n} - Au(\boldsymbol{r}) \frac{\partial G(\boldsymbol{r}|\boldsymbol{r'})}{\partial n} + B \frac{\partial u(\boldsymbol{r})}{\partial n} \frac{\partial G(\boldsymbol{r}|\boldsymbol{r'})}{\partial n} \\
&- B \frac{\partial u(\boldsymbol{r})}{\partial n} \frac{\partial G(\boldsymbol{r}|\boldsymbol{r'})}{\partial n} \Big] d\ell \\
&= \int_{\Gamma_{\text{ext}}} \frac{1}{A} \Bigg[AG(\boldsymbol{r}|\boldsymbol{r'} \frac{\partial u(\boldsymbol{r})}{\partial n} + B \frac{\partial u(\boldsymbol{r})}{\partial n} \frac{\partial G(\boldsymbol{r}|\boldsymbol{r'})}{\partial n} - Au(\boldsymbol{r}) \frac{\partial G(\boldsymbol{r}|\boldsymbol{r'})}{\partial n} \\
&- B \frac{\partial u(\boldsymbol{r})}{\partial n} \frac{\partial G(\boldsymbol{r}|\boldsymbol{r'})}{\partial n} \Bigg] d\ell \\
&= \int_{\Gamma_{\text{ext}}} \frac{1}{A} \Bigg[\Bigg(AG(\boldsymbol{r}|\boldsymbol{r'}) + B \frac{\partial G(\boldsymbol{r}|\boldsymbol{r'})}{\partial n} \Bigg) \frac{\partial u(\boldsymbol{r})}{\partial n} - \Bigg(Au(\boldsymbol{r}) + B \frac{\partial u(\boldsymbol{r})}{\partial n} \Bigg) \frac{\partial G(\boldsymbol{r}|\boldsymbol{r'})}{\partial n} \Bigg] d\ell.
\end{aligned}$$

Now we use the values of (3.2.2) and (3.2.4) to get:

$$\begin{aligned}
&= \int_{\Gamma_{\text{ext}}} \frac{1}{A} \Bigg[\big(0\big) \frac{\partial u(\boldsymbol{r})}{\partial n} - \big(h(\boldsymbol{r})\big) \frac{\partial G(\boldsymbol{r}|\boldsymbol{r'})}{\partial n} \Bigg] d\ell \\
&= \int_{\Gamma_{\text{ext}}} \frac{1}{A} \big(- h(\boldsymbol{r})\big) \big[\frac{\partial G(\boldsymbol{r}|\boldsymbol{r'})}{\partial n} \big] d\ell.
\end{aligned}$$

We recognize that at Γ_∞, the radiation condition will cause the corresponding contour integral to vanish, so (3.2.8) further reduces to:

$$\begin{aligned}
u(\boldsymbol{r'}) = &\iint_{\mathcal{U}_R} f(\boldsymbol{r}) G(\boldsymbol{r}|\boldsymbol{r'}) dS + \int_{\mathcal{B}_R} \big(G(\boldsymbol{r}|\boldsymbol{r'}) \nabla u(\boldsymbol{r}) - u(\boldsymbol{r}) \nabla G(\boldsymbol{r}|\boldsymbol{r'}) \big) \cdot \boldsymbol{n} d\ell \\
&- \frac{1}{A} \int_{\Gamma_{\text{ext}}} h(\boldsymbol{r}) \big[\frac{\partial G(\boldsymbol{r}|\boldsymbol{r'})}{\partial n'} \big] d\ell. \qquad (3.2.9)
\end{aligned}$$

Since $\boldsymbol{r}$ and $\boldsymbol{r'}$ are arbitrary, and because the Green's function is symmetric (see

(3.3.7)), we interchange $\boldsymbol{r}$ and $\boldsymbol{r'}$ to get:

$$u(\boldsymbol{r}) = \iint_{\mathcal{U}_R} f(\boldsymbol{r'})G(\boldsymbol{r}|\boldsymbol{r'})dS' + \int_{\mathcal{B}_R} \big(G(\boldsymbol{r}|\boldsymbol{r'}))\frac{\partial u(\boldsymbol{r})}{\partial n'} - u(\boldsymbol{r'})\frac{\partial G(\boldsymbol{r}|\boldsymbol{r'})}{\partial n'}\big)d\ell' - \frac{1}{A}\int_{\Gamma_{\text{ext}}} h(\boldsymbol{r'})\big[\frac{\partial G(\boldsymbol{r}|\boldsymbol{r'})}{\partial n'}\big]d\ell', \tag{3.2.10}$$

where the normal derivative is taken with respect to the primed (or source) coordinates.

3.3 Green's Function Development

The integral representation of the solution found previously depends on finding the associated Green's function. The geometry depicted in Figure 7 for the exterior solution is an annular sector, which accounts for the overfilled portion of the cavity. However, as in Durán et al., we first will develop the explicit Green's function for an impedance half-plane and apply it to the modified problem geometry. We will note that the Green's function for an impedance plane has been studied in great detail by several authors such as Politis in [82], Ochmann and Brick in [78], and most recently Hein in [42]. In fact, Hein's dissertation significantly expands the work of Durán et al. in [28], so this is an ongoing area of research. Nevertheless, we will still follow and expand the development of the Green's function in Durán et al. and apply it to the modified Helmholtz equation (See [29] and [28]).

We fix a source point $\boldsymbol{r'} = (x', y') \in \mathcal{U} = \mathbb{R}^2_+ \setminus \Omega$. Thus, the Green's function must solve the boundary value problem:

$$\begin{cases} -\Delta G(\boldsymbol{r}|\boldsymbol{r'}) + \alpha^2 G(\boldsymbol{r}|\boldsymbol{r'}) &= \delta(\boldsymbol{r} - \boldsymbol{r'}) & \text{in } \mathcal{U}, \\ AG(\boldsymbol{r}|\boldsymbol{r'}) + B\dfrac{\partial G(\boldsymbol{r}|\boldsymbol{r'})}{\partial y} &= 0 & \text{on } \{y = 0\}. \end{cases} \tag{3.3.1}$$

Following Durán in [28], since no horizontal variation exists in the strict half-plane

problem, we can assume without loss of generality that $x' = 0$. In order to reduce the PDE in (3.3.1) to an ODE, we take a Fourier transform in the horizontal direction x, and denote the Fourier variable ξ:

$$
\begin{aligned}
&F[G] = \widehat{G}(\xi, y) = \int_{-\infty}^{\infty} G(\boldsymbol{r}|\boldsymbol{r'}) e^{-i\xi x} dx, \\
&\frac{\partial \widehat{G}(\xi, y)}{\partial x} = (-i\xi) \int_{-\infty}^{\infty} G(\boldsymbol{r}|\boldsymbol{r'}) e^{-i\xi x} dx = (-i\xi) F[G], \\
&\frac{\partial^2 \widehat{G}(\xi, y)}{\partial x^2} = (-i\xi)(-i\xi) F[G] = -\xi^2 F[G], \\
&F[\delta(\boldsymbol{r} - \boldsymbol{r'})] = F[\delta(x - x')\delta(y - y')] = \frac{1}{\sqrt{2\pi}} \delta(y - y'), \\
&-\left[\frac{\partial^2 \widehat{G}(\xi, y)}{\partial x^2} + \frac{\partial^2 \widehat{G}(\xi, y)}{\partial y^2} \right] + \alpha^2 \widehat{G}(\xi, y) = \frac{1}{\sqrt{2\pi}} \delta(y - y').
\end{aligned}
$$

Thus, we obtain the equation in the vertical variable y:

$$
\begin{cases}
-\dfrac{\partial^2 \widehat{G}(\xi, y)}{\partial y^2} + \left(\xi^2 + \alpha^2\right) \widehat{G}(\xi, y) = \dfrac{1}{\sqrt{2\pi}} \delta(y - y') \text{ for } y > 0 \\
\qquad\qquad A\widehat{G}(\xi, y) + B \dfrac{\partial \widehat{G}(\xi, y)}{\partial y} = 0 \text{ for } y = 0, \text{ or } \Gamma_{\text{ext}}
\end{cases}
\tag{3.3.2}
$$

We will solve this via scattering superposition (See [41]), where we seek a solution of the form

$$\widehat{G} = G^p + G^h,$$

where G^p represents the principal Green's function that satisfies the jump and continuity conditions, and G^h when added to G^p will satisfy the radiation and boundary condition for our particular problem.

First, we solve for G^p, away from $y = y'$:

$$-\frac{\partial^2 G^p(\xi, y)}{\partial y^2} + \left(\xi^2 + \alpha^2\right) G^p(\xi, y) = 0 \implies$$
$$\frac{\partial^2 G^p(\xi, y)}{\partial y^2} - \left(\xi^2 + \alpha^2\right) G^p(\xi, y) = 0.$$

The general solutions will be of the form:

$$G^p(\xi, y) = \begin{cases} C_1 e^{\sqrt{\xi^2+\alpha^2}y} + C_2 e^{-\sqrt{\xi^2+\alpha^2}y} & \text{for } y < y' \\ C_3 e^{\sqrt{\xi^2+\alpha^2}y} + C_4 e^{-\sqrt{\xi^2+\alpha^2}y} & \text{for } y > y'. \end{cases}$$

We require that $G^p(\xi, y) \in L^2(-\infty, \infty)$, further reducing to:

$$G^p(\xi, y) = \begin{cases} C_1 e^{\sqrt{\xi^2+\alpha^2}y} & \text{for } y < y' \\ C_4 e^{-\sqrt{\xi^2+\alpha^2}y} & \text{for } y > y'. \end{cases}$$

Enforcing the continuity conditions at $y = y'$ yields:

$$C_1 e^{\sqrt{\xi^2+\alpha^2}y'} = C_4 e^{-\sqrt{\xi^2+\alpha^2}y'} \implies C_1 = C_4 e^{-2\sqrt{\xi^2+\alpha^2}y'}.$$

Finally, applying the jump conditions :

$$\lim_{\varepsilon \to 0} \frac{\partial G^p(\xi, y)}{\partial y}\bigg|_{y=y'-\varepsilon}^{y=y'+\varepsilon} = -1 \implies$$
$$-C_4\sqrt{\xi^2+\alpha^2}e^{-\sqrt{\xi^2+\alpha^2}(y'+\varepsilon)} - C_1\sqrt{\xi^2+\alpha^2}e^{\sqrt{\xi^2+\alpha^2}(y'-\varepsilon)} = -1 \implies$$
$$-C_4 e^{-\sqrt{\xi^2+\alpha^2}y'} - C_1 e^{\sqrt{\xi^2+\alpha^2}y'} = -\frac{1}{\sqrt{\xi^2+\alpha^2}}.$$

Substituting for C_1 yields:

$$\begin{aligned} -C_4 e^{-\sqrt{\xi^2+\alpha^2}y'} - (C_4 e^{-2\sqrt{\xi^2+\alpha^2}y'})e^{\sqrt{\xi^2+\alpha^2}y'} &= -\frac{1}{\sqrt{\xi^2+\alpha^2}} \\ -2C_4 e^{-\sqrt{\xi^2+\alpha^2}y'} &= -\frac{1}{\sqrt{\xi^2+\alpha^2}} \implies \\ C_4 &= \frac{e^{\sqrt{\xi^2+\alpha^2}y'}}{2\sqrt{\xi^2+\alpha^2}}, \\ C_1 &= \frac{e^{-\sqrt{\xi^2+\alpha^2}y'}}{2\sqrt{\xi^2+\alpha^2}}. \end{aligned}$$

Therefore, we can express the principal Green's function for the impedance half-plane as

$$\begin{aligned} G^p(\xi, y) &= \begin{cases} \dfrac{e^{-\sqrt{\xi^2+\alpha^2}y'}}{2\sqrt{\xi^2+\alpha^2}} e^{\sqrt{\xi^2+\alpha^2}y} ... y < y' \\ \dfrac{e^{\sqrt{\xi^2+\alpha^2}y'}}{2\sqrt{\xi^2+\alpha^2}} e^{-\sqrt{\xi^2+\alpha^2}y} ... y > y' \end{cases} \\ &= \begin{cases} \dfrac{e^{\sqrt{\xi^2+\alpha^2}(y-y')}}{2\sqrt{\xi^2+\alpha^2}} ... y < y' \\ \dfrac{e^{-\sqrt{\xi^2+\alpha^2}(y-y')}}{2\sqrt{\xi^2+\alpha^2}} ... y > y' \end{cases} \end{aligned}$$

which simplifies to

$$G^p(\xi, y) = \frac{e^{-\sqrt{\xi^2+\alpha^2}|y'-y|}}{2\sqrt{\xi^2+\alpha^2}}. \tag{3.3.3}$$

Now, to determine G^h, we first determine the homogeneous solution of:

$$\frac{\partial^2 G^h(\xi, y)}{\partial y^2} - \left(\xi^2 + \alpha^2\right) G^h(\xi, y) = 0,$$

which is

$$G^h(\xi, y) = C_5 e^{\sqrt{\xi^2+\alpha^2}y} + C_6 e^{-\sqrt{\xi^2+\alpha^2}y},$$

and $C_5 = 0$ due to the radiation condition. Therefore, we have our Green's function

representation as:

$$\widehat{G}(\xi,y)=G^p(\xi,y)+G^h(\xi,y)=\frac{e^{-\sqrt{\xi^2+\alpha^2}|y'-y|}}{2\sqrt{\xi^2+\alpha^2}}+C_6e^{-\sqrt{\xi^2+\alpha^2}y}.$$

Applying the IBC to $\widehat{G}$ above yields:

$$\begin{aligned}
&A\widehat{G}(\xi,y)+B\frac{\partial\widehat{G}(\xi,y)}{\partial y}\bigg|_{y=0}=0 \implies\\
&A\bigg(\frac{e^{-\sqrt{\xi^2+\alpha^2}|y'-y|}}{2\sqrt{\xi^2+\alpha^2}}+C_6e^{-\sqrt{\xi^2+\alpha^2}y}\bigg)+\\
&B\bigg(\frac{\sqrt{\xi^2+\alpha^2}e^{-\sqrt{\xi^2+\alpha^2}|y'-y|}}{2\sqrt{\xi^2+\alpha^2}}-C_6\sqrt{\xi^2+\alpha^2}e^{-\sqrt{\xi^2+\alpha^2}y}\bigg)\bigg|_{y=0}=0.
\end{aligned}$$

At $y=0$ we have:

$$\begin{aligned}
A\bigg(\frac{e^{-\sqrt{\xi^2+\alpha^2}|y'|}}{2\sqrt{\xi^2+\alpha^2}}+C_6\bigg)+B\bigg(\frac{\sqrt{\xi^2+\alpha^2}e^{-\sqrt{\xi^2+\alpha^2}|y'|}}{2\sqrt{\xi^2+\alpha^2}}-C_6\sqrt{\xi^2+\alpha^2}\bigg)&=0\\
A\frac{e^{-\sqrt{\xi^2+\alpha^2}|y'|}}{2\sqrt{\xi^2+\alpha^2}}+AC_6+B\frac{\sqrt{\xi^2+\alpha^2}e^{-\sqrt{\xi^2+\alpha^2}|y'|}}{2\sqrt{\xi^2+\alpha^2}}-BC_6\sqrt{\xi^2+\alpha^2}&=0\\
C_6\big(A-B\sqrt{\xi^2+\alpha^2}\big)=-\frac{(A+B\sqrt{\xi^2+\alpha^2})e^{-\sqrt{\xi^2+\alpha^2}y'}}{2\sqrt{\xi^2+\alpha^2}}&\\
C_6=-\frac{(A+B\sqrt{\xi^2+\alpha^2})}{(A-B\sqrt{\xi^2+\alpha^2})}\frac{e^{-\sqrt{\xi^2+\alpha^2}y'}}{2\sqrt{\xi^2+\alpha^2}}.&
\end{aligned}$$

Now we are able to write our final Green's function representation as :

$$\begin{aligned}
\widehat{G}(\xi,y)&=G^p(\xi,y)+G^h(\xi,y)\\
&=\frac{e^{-\sqrt{\xi^2+\alpha^2}|y'-y|}}{2\sqrt{\xi^2+\alpha^2}}-\frac{(A+B\sqrt{\xi^2+\alpha^2})}{(A-B\sqrt{\xi^2+\alpha^2})}\frac{e^{-\sqrt{\xi^2+\alpha^2}y'}}{2\sqrt{\xi^2+\alpha^2}}e^{-\sqrt{\xi^2+\alpha^2}y}.
\end{aligned}$$

Factoring out $\frac{1}{2}$ and multiplying by a scale of $\frac{1}{\sqrt{2\pi}}$ yields:

$$\widehat{G}(\xi, y) = \frac{1}{\sqrt{8\pi}}\left(\frac{e^{-\sqrt{\xi^2+\alpha^2}|y'-y|}}{\sqrt{\xi^2+\alpha^2}} - \frac{(A+B\sqrt{\xi^2+\alpha^2})}{(A-B\sqrt{\xi^2+\alpha^2})}\frac{e^{-\sqrt{\xi^2+\alpha^2}y'}}{\sqrt{\xi^2+\alpha^2}}e^{-\sqrt{\xi^2+\alpha^2}y}\right) \quad (3.3.4)$$

Now we take the inverse Fourier transform of the previous expression to get the desired spatial expression:

$$\begin{aligned} G(\boldsymbol{r}|\boldsymbol{r'}) = &\frac{1}{4\pi}\int_{-\infty}^{\infty}\frac{e^{-\sqrt{\xi^2+\alpha^2}|y'-y|}}{\sqrt{\xi^2+\alpha^2}}e^{i(x'-x)\xi}d\xi \\ &- \frac{1}{4\pi}\int_{-\infty}^{\infty}\left(\frac{(A+B\sqrt{\xi^2+\alpha^2})}{(A-B\sqrt{\xi^2+\alpha^2})}\right)\frac{e^{-\sqrt{\xi^2+\alpha^2}(y'+y)}}{\sqrt{\xi^2+\alpha^2}}e^{i(x'-x)\xi}d\xi. \end{aligned} \quad (3.3.5)$$

Recognizing that the second term in the spatial expression above may be rewritten as

$$-\frac{1}{4\pi}\int_{-\infty}^{\infty}\left(1+\frac{2B\sqrt{\xi^2+\alpha^2}}{A-B\sqrt{\xi^2+\alpha^2}}\right)\frac{e^{-\sqrt{\xi^2+\alpha^2}(y'+y)}}{\sqrt{\xi^2+\alpha^2}}e^{i(x'-x)\xi}d\xi,$$

and using the fact that (see [29])

$$\frac{1}{4\pi}\int_{-\infty}^{\infty}\frac{e^{-\sqrt{\xi^2+\alpha^2}|y'-y|}}{\sqrt{\xi^2+\alpha^2}}e^{i(x'-x)\xi}d\xi = \frac{i}{4}H_0^{(1)}(i\alpha R),$$

where $R = \sqrt{(x'-x)^2+(y'-y)^2}$, as well as the fact that

$$K_0(kR) = \frac{\pi i}{2}H_0^{(1)}(ikR),$$

we have

$$\frac{1}{4\pi}\int_{-\infty}^{\infty}\frac{e^{-\sqrt{\xi^2+\alpha^2}|y'-y|}}{\sqrt{\xi^2+\alpha^2}}e^{i(x'-x)\xi}d\xi = \frac{1}{2\pi}K_0(\alpha R).$$

Similarly, from [28], we have,

$$\frac{1}{4\pi}\int_{-\infty}^{\infty}\frac{e^{-\sqrt{\xi^2+\alpha^2}(y'+y)}}{\sqrt{\xi^2+\alpha^2}}e^{i(x'-x)\xi}d\xi = \frac{1}{2\pi}K_0(\alpha R^*),$$

where $R^* = \sqrt{(x'-x)^2+(y'+y)^2}$. This results in the Green's function becoming

$$G(\boldsymbol{r}|\boldsymbol{r'}) = \frac{1}{2\pi}K_0(\alpha R) - \frac{1}{2\pi}K_0(\alpha R^*) - \frac{2B}{4\pi}\int_{-\infty}^{\infty}\frac{e^{-\sqrt{\xi^2+\alpha^2}(y'+y)}}{(A-B\sqrt{\xi^2+\alpha^2})}e^{i(x'-x)\xi}d\xi. \quad (3.3.6)$$

It is important to observe at this point, that this expression makes sense physically, in that if the surface was a PEC, then $B = 0$, causing the third term in (3.3.6) to vanish. This is consistent with an assumed Dirichlet boundary condition on the surface, and is confirmed in [104]. Furthermore, we note that the first two terms in (3.3.6) correspond to the "classical" wave behavior, whereas the third term in (3.3.6) incorporates the surface wave behavior expected with an impedance-type surface.

The only question remaining is if it is possible to reduce the integral expression in (3.3.6), which represents the surface wave behavior, into a simpler expression using residue analysis. In order to facilitate evaluating this integral using residue theory, the third term in (3.3.6) will be rewritten as

$$-\frac{2B}{4\pi}\int_{-\infty}^{\infty}\frac{e^{-\sqrt{\xi^2+\alpha^2}(y'+y)}}{(A-B\sqrt{\xi^2+\alpha^2})}e^{i(x'-x)\xi}d\xi =$$
$$-\frac{2B}{4\pi}\int_{-\infty}^{\infty}\frac{\left(-\frac{\frac{A}{B}+\sqrt{\xi^2+\alpha^2}}{B}\right)e^{-\sqrt{\xi^2+\alpha^2}(y'+y)}e^{i(x'-x)\xi}}{\left(\xi+\sqrt{(\frac{A}{B})^2-\alpha^2}\right)\left(\xi-\sqrt{(\frac{A}{B})^2-\alpha^2}\right)}d\xi.$$

If ξ is treated as a complex variable, then the integrand has branch points at $\xi = \pm i\alpha$ and poles at $\xi = \pm\sqrt{\left(\frac{A}{B}\right)^2-\alpha^2}$, and it can be shown the contribution due to the poles is represented by

$$i\left[-\frac{A}{B}\frac{e^{-\frac{A}{B}(y'+y)}e^{i|x-x'|\sqrt{(\frac{A}{B})^2-\alpha^2}}}{\sqrt{(\frac{A}{B})^2-\alpha^2}}\right].$$

Hein makes the observation that this expression "describes the asymptotic behavior of the surface waves, which are linked to the presence of the poles" [42]. He adds

that in order to express the proper physical results (that is, an outgoing progressive surface wave, and not a standing surface wave), the above expression becomes:

$$i\left[-\frac{A}{B}\frac{e^{-\frac{A}{B}(y'+y)}}{\sqrt{(\frac{A}{B})^2-\alpha^2}}\cos\left(|x-x'|\sqrt{\left(\frac{A}{B}\right)^2-\alpha^2}\right)\right].$$

As for the fourth term of the Green's function regarding the contributions of the branch cuts, we note that Politis et al. in [82], Durán et al. in [28], and Hein in [42] all reconcile this term in different ways, and it is worth citing each result. For example, Politis derives an explicit integral expression for the branch cuts and further provides a series expansion of this term in polar coordinates [82]. He states this expression is "more convenient for numerical purposes"; for our case it would be expressed as follows:

$$-\frac{1}{\pi}\int_{\alpha}^{\infty}\frac{e^{\xi|x-x'|}}{(\frac{A}{B})^2-\alpha^2+\xi^2}\times \\ \left(\sqrt{\xi^2-\alpha^2}\cos\left(\sqrt{\xi^2-\alpha^2}(y'+y)\right)+\frac{A}{B}\sin\left(\sqrt{\xi^2-\alpha^2}(y'+y)\right)\right)d\xi.$$

Durán in [28], however, reconciles this remaining term in the Green's function by using an inverse fast Fourier transform (IFFT) during the numerical implementation to get the spatial result. Applying this to our result yields the expression:

$$\frac{B}{2\pi}\int_{-\infty}^{\infty}\frac{e^{-\sqrt{\xi^2+\alpha^2}(y'+y)}}{(A-B\sqrt{\xi^2+\alpha^2})}e^{i(x'-x)\xi}d\xi.$$

Hein states that this term can be reduced to be better suited for numerical integration [42]. Applying his technique to our case yields:

$$\frac{\alpha}{2\pi}e^{-\frac{A}{B}(y'+y)}\int_{-\infty}^{y'+y}K_1(\alpha\sqrt{(x'-x)^2+\xi^2})\frac{\xi e^{\frac{A}{B}\xi}}{\sqrt{(x'-x)^2+\xi^2}}d\xi.$$

Therefore, Hein's recent development with this portion of the Green's function is most suitable to apply for both analytical and numerical methods, so we will consider our final Green's function expression in the spatial domain for the problem to be the following:

$$\begin{aligned} G(\boldsymbol{r}|\boldsymbol{r'}) &= \frac{1}{2\pi}K_0(\alpha R) - \frac{1}{2\pi}K_0(\alpha R^*) \\ &\quad - i\Big[- \frac{A}{B}\frac{e^{-\frac{A}{B}(y'+y)}}{\sqrt{(\frac{A}{B})^2-\alpha^2}}\cos\Big(|x-x'|\sqrt{\Big(\frac{A}{B}\Big)^2-\alpha^2}\Big)\Big] \\ &\quad + \frac{\alpha}{2\pi}e^{-\frac{A}{B}(y'+y)}\int_{-\infty}^{y'+y} K_1(\alpha\sqrt{(x'-x)^2+\xi^2})\frac{\xi e^{\frac{A}{B}\xi}}{\sqrt{(x'-x)^2+\xi^2}}d\xi. \end{aligned} \tag{3.3.7}$$

3.4 Steklov-Poincaré Operator Analysis

Recall the integral representation of the solution in the exterior domain (the annular sector depicted in Figure 7) is

$$\begin{aligned} u(\boldsymbol{r}) &= \iint_{\mathcal{U}_R} f(\boldsymbol{r'})G(\boldsymbol{r}|\boldsymbol{r'})dS' - \frac{1}{A}\int_{\Gamma_{\text{ext}}} h(\boldsymbol{r'})\frac{\partial G(\boldsymbol{r}|\boldsymbol{r'})}{\partial y'}dx' \\ &\quad + \int_{\mathcal{B}_R}\big(G(\boldsymbol{r}|\boldsymbol{r'})\frac{\partial u(\boldsymbol{r'})}{\partial \boldsymbol{n}_{\boldsymbol{r'}}} - u(\boldsymbol{r'})\frac{\partial G(\boldsymbol{r}|\boldsymbol{r'})}{\partial \boldsymbol{n}_{\boldsymbol{r'}}}\big)d\theta' \ ; \boldsymbol{r} \in \mathcal{U}_R. \end{aligned} \tag{3.4.1}$$

At this point, we wish to implement an integral equation method along the artificial boundary, $\mathcal{B}_R$, to couple the solution along the artificial boundary. We will henceforth name the DtN operator as the Steklov-Poincarè operator. This is because we will be using integral operator theory to obtain an expression for this operator. It is expressed in terms of integral equations and not series expressions, and the literature is consistent in this regard.

First, let us define formally the map $\mathcal{T}_R : H^{1/2}(\mathcal{B}_R) \to H^{-1/2}(\mathcal{B}_R)$, where $u \in H^{1/2}(\mathcal{B}_R)$ is a radiating solution to the modified Helmholtz equation mapped to its normal derivative $\dfrac{\partial u}{\partial n} \in H^{-1/2}(\mathcal{B}_R)$. Throughout the literature, the idea of mapping a

solution to its normal derivative has several other names, such as the capacity operator [77] or the Calderon operator [75]. With a Robin boundary condition enforced at the ground plane for this particular problem geometry, it does not appear that an exact series representation is possible as it was with the PEC or PMC case. Therefore, using the integral representation of the solution, we can express the mapping of the integral representation of the exact solution in the exterior domain to its normal derivative as restricted to $\mathcal{B}_R$ as the Steklov-Poincaré operator [54].

Givoli further describes this type of mapping as an exact nonlocal absorbing boundary condition. The term "nonlocal" refers to the fact that we are using a boundary integral operator over the entire artificial semicircle $\mathcal{B}_R$ [32]. The boundary conditions are nonreflecting as well in that we would expect no spurious reflections [54]. In fact, this type of artificial boundary condition was the result of many years of trying to reduce or eliminate spurious reflections [32]. This technique of truncating the domain and using a boundary integral on the artificial boundary is referred to as a hybrid FE/BI method, and is considered a "mainstream method" for analysis in the computational electromagnetic community [107]. In addition, Givoli makes an interesting observation worth mentioning in the context of our research. He states that in the area of acoustics, "the DtN condition can be perceived as a nonlocal *impedance boundary condition*, relating the normal velocity $(\frac{\partial u}{\partial r})$ and the pressure (u) on the boundary" [32]. He further states that this mapping can be difficult to express in "closed analytic form," especially in cases of "special geometries" and the "time-dependent case" [32].

From (3.4.1), we shift $\boldsymbol{r}$ onto the artificial boundary $\mathcal{B}_R$, to obtain

$$\frac{1}{2}u(\boldsymbol{r}) = \overbrace{\iint_{\mathcal{U}_R} f(\boldsymbol{r'})G(\boldsymbol{r}|\boldsymbol{r'})dS'}^{\text{Newton potential}} - \frac{1}{A}\int_{\Gamma_{\text{ext}}} h(\boldsymbol{r'})\frac{\partial G(\boldsymbol{r}|\boldsymbol{r'})}{\partial y'}dx' + \int_{\mathcal{B}_R}\Big(\underbrace{G(\boldsymbol{r}|\boldsymbol{r'})\frac{\partial u(\boldsymbol{r'})}{\partial \boldsymbol{n}_{\boldsymbol{r'}}}}_{\text{Single-layer potential}} - \underbrace{u(\boldsymbol{r'})\frac{\partial G(\boldsymbol{r}|\boldsymbol{r'})}{\partial \boldsymbol{n}_{\boldsymbol{r'}}}}_{\text{Double-layer potential}}\Big)d\theta' \,;\boldsymbol{r}\in\mathcal{B}_R. \tag{3.4.2}$$

At this point, it is worth discussing how to treat the inhomogeneities incorporated with the Newton potential and the term accounting for the effects of the impedance plane. There are several possibilities on how to treat these terms, which result from the time discretization of the PDE. In our case, it is divided into two portions, the domain integral $\mathcal{U}_R$ as well as the boundary integral Γ_{ext}. While using this technique will require further discretization of the domain and a portion of the boundary, it is only done "for purposes of numerical integration" [22]. This computation will ultimately be considered as the known forcing terms or right-hand side of the variational formulation. As we will develop, the other terms in (3.4.2) will help constitute the Steklov-Poincarè operator expression.

Taking a normal derivative $\dfrac{\partial}{\partial n}$ of (3.4.2) along $\mathcal{B}_R$ yields the hypersingular boundary integral equation:

$$\frac{1}{2}\frac{\partial u(\boldsymbol{r})}{\partial \boldsymbol{n}_{\boldsymbol{r}}} = \overbrace{\frac{\partial}{\partial n}\Big(\iint_{\mathcal{U}_R} f(\boldsymbol{r'})G(\boldsymbol{r}|\boldsymbol{r'})dS' - \frac{1}{A}\int_{\Gamma_{\text{ext}}} h(\boldsymbol{r'})\frac{\partial G(\boldsymbol{r}|\boldsymbol{r'})}{\partial y'}dx'\Big)}^{\text{Normal Derivative of Newton potential}} + \int_{\mathcal{B}_R}\Big(\underbrace{\frac{\partial G(\boldsymbol{r}|\boldsymbol{r'})}{\partial \boldsymbol{n}_{\boldsymbol{r}}}\frac{\partial u(\boldsymbol{r'})}{\partial \boldsymbol{n}_{\boldsymbol{r'}}}}_{\text{Adjoint Double-layer potential}} - \underbrace{u(\boldsymbol{r'})\frac{\partial}{\partial \boldsymbol{n}_{\boldsymbol{r}}}\frac{\partial G(\boldsymbol{r}|\boldsymbol{r'})}{\partial \boldsymbol{n}_{\boldsymbol{r'}}}}_{\text{Hypersingular operator}}\Big)d\theta' \,;\boldsymbol{r}\in\mathcal{B}_R. \tag{3.4.3}$$

We define $\varphi(\boldsymbol{r'}) = \dfrac{\partial u(\boldsymbol{r'})}{\partial \boldsymbol{n}_{\boldsymbol{r'}}}$ as in Hsiao et al. in [48], so all of the boundary integral

operators for $\boldsymbol{r} \in \mathcal{B}_R$ are expressed as follows:

$$(S\varphi)(\boldsymbol{r}) = \int_{\mathcal{B}_R} G(\boldsymbol{r}|\boldsymbol{r'})\varphi(\boldsymbol{r'})d\theta', \qquad \text{(Single-layer potential operator)} \tag{3.4.4}$$

$$(Du)(\boldsymbol{r}) = \int_{\mathcal{B}_R} u(\boldsymbol{r'})\frac{\partial G(\boldsymbol{r}|\boldsymbol{r'})}{\partial \boldsymbol{n}_{\boldsymbol{r'}}}d\theta', \qquad \text{(Double-layer potential operator)} \tag{3.4.5}$$

$$(A\varphi)(\boldsymbol{r}) = \int_{\mathcal{B}_R} \frac{\partial G(\boldsymbol{r}|\boldsymbol{r'})}{\partial \boldsymbol{n}_{\boldsymbol{r}}}\varphi(\boldsymbol{r'})d\theta', \qquad \text{(Adjoint Double-layer potential operator)} \tag{3.4.6}$$

$$(Hu)(\boldsymbol{r}) = -\int_{\mathcal{B}_R} u(\boldsymbol{r'})\frac{\partial}{\partial \boldsymbol{n}_{\boldsymbol{r}}}\frac{\partial G(\boldsymbol{r}|\boldsymbol{r'})}{\partial \boldsymbol{n}_{\boldsymbol{r'}}}d\theta'. \qquad \text{(Hypersingular operator)} \tag{3.4.7}$$

The mapping properties are respectively defined as follows:

$$S : H^{-1/2}(\mathcal{B}_R) \to H^{1/2}(\mathcal{B}_R),$$
$$D : H^{1/2}(\mathcal{B}_R) \to H^{1/2}(\mathcal{B}_R),$$
$$A : H^{-1/2}(\mathcal{B}_R) \to H^{-1/2}(\mathcal{B}_R),$$
$$H : H^{1/2}(\mathcal{B}_R) \to H^{-1/2}(\mathcal{B}_R).$$

Because we are dealing with an operator of the form $-\Delta + \alpha^2$ (the modified Helmholtz operator in Equation (3.2.1)), Costabel states that this identical form is the "mathematically simplest case" of a formally positive second order elliptic partial differential operator [23]. Also, if a fundamental solution exists for use in the integral representation expression, as we earlier demonstrated with the development of the Green's function for the impedance half-plane, then the mapping properties are well-established for the preceding boundary integral operators. In particular, the operators are bounded [21].

If we further define the Newton potential and the impedance plane term to be

$$(Nf)(\boldsymbol{r}) = \iint_{\mathcal{U}_R} f(\boldsymbol{r'})G(\boldsymbol{r}|\boldsymbol{r'})dS' \ ; \ \boldsymbol{r} \in \mathcal{B}_R, \tag{3.4.8}$$

$$(Ph)(\boldsymbol{r}) = -\frac{1}{A}\int_{\Gamma_{\text{ext}}} h(\boldsymbol{r'})\frac{\partial G(\boldsymbol{r}|\boldsymbol{r'})}{\partial y'}dx' \ ; \ \boldsymbol{r} \in \mathcal{B}_R, \tag{3.4.9}$$

and note that their mapping properties are

$$N : L^2(\mathcal{U}_R) \to H^{1/2}(\mathcal{B}_R),$$
$$P : L^2(\mathcal{U}_R) \to H^{1/2}(\mathcal{B}_R),$$

then N and P are bounded operators as well (See Steinbach in [97]).

Therefore, denoting I as the identity operator, we can rewrite (3.4.2) in operator notation as

$$\frac{1}{2}(Iu)(\boldsymbol{r}) = (S\varphi)(\boldsymbol{r}) - (Du)(\boldsymbol{r}) + (Nf)(\boldsymbol{r}) + (Ph)(\boldsymbol{r}) \ ; \ \boldsymbol{r} \in \mathcal{B}_R \implies$$
$$(S\varphi)(\boldsymbol{r}) = (\frac{1}{2}I + D)u(\boldsymbol{r}) - [(Nf)(\boldsymbol{r}) + (Ph)(\boldsymbol{r})] \ ; \ \boldsymbol{r} \in \mathcal{B}_R.$$

Assuming the Single-layer potential operator, S, is linear and invertible (because it is $H^{-1/2}(\mathcal{B}_R)$-elliptic ; see Proposition 3.4.1) yields

$$S^{-1}(S\varphi)(\boldsymbol{r}) = S^{-1}(\frac{1}{2}I + D)u(\boldsymbol{r}) - S^{-1}[(Nf)(\boldsymbol{r}) + (Ph)(\boldsymbol{r})] \ ; \boldsymbol{r} \in \mathcal{B}_R \implies$$
$$\varphi(\boldsymbol{r}) = S^{-1}(\frac{1}{2}I + D)u(\boldsymbol{r}) - S^{-1}[(Nf)(\boldsymbol{r}) + (Ph)(\boldsymbol{r})] \ ; \boldsymbol{r} \in \mathcal{B}_R. \tag{3.4.10}$$

Here, as in [48], we define $\mathcal{T}_R$ as a Steklov-Poincarè operator as follows:

$$(\mathcal{T}_R u)(\boldsymbol{r}) = S^{-1}(\frac{1}{2}I + D)u(\boldsymbol{r}),$$

where we have $\mathcal{T}_R : H^{1/2}(\mathcal{B}_R) \to H^{-1/2}(\mathcal{B}_R)$.

We further define the normal derivatives of the Newton potential and the impedance plane terms to be

$$(N'f)(\boldsymbol{r}) = \frac{\partial}{\partial r}\bigg(\iint_{\mathcal{U}_R} f(\boldsymbol{r'})G(\boldsymbol{r}|\boldsymbol{r'})dS' \bigg) \; ; \; \boldsymbol{r} \in \mathcal{B}_R, \tag{3.4.11}$$

$$(P'h)(\boldsymbol{r}) = \frac{\partial}{\partial r}\bigg(-\frac{1}{A}\int_{\Gamma_{\text{ext}}} h(\boldsymbol{r'})\frac{\partial G(\boldsymbol{r}|\boldsymbol{r'})}{\partial y'}dx' \bigg) \; ; \; \boldsymbol{r} \in \mathcal{B}_R, \tag{3.4.12}$$

and observe that their mapping properties are

$$N' : L^2(\mathcal{U}_R) \to H^{-1/2}(\mathcal{B}_R),$$
$$P' : L^2(\mathcal{U}_R) \to H^{-1/2}(\mathcal{B}_R).$$

Then the hypersingular boundary integral equation in (3.4.3) can be cast as

$$\begin{aligned}
\frac{1}{2}(I\varphi)(\boldsymbol{r}) &= (A\varphi)(\boldsymbol{r}) + (Hu)(\boldsymbol{r}) + (N'f)(\boldsymbol{r}) + (P'h)(\boldsymbol{r}) \\
(\frac{1}{2}I - A)\varphi(\boldsymbol{r}) &= (Hu)(\boldsymbol{r}) + (N'f)(\boldsymbol{r}) + (P'h)(\boldsymbol{r}) \\
(\frac{1}{2}I - A)\varphi(\boldsymbol{r}) - (I\varphi)(\boldsymbol{r}) &= (Hu)(\boldsymbol{r}) - (I\varphi) + (N'f)(\boldsymbol{r}) + (P'h)(\boldsymbol{r}) \\
(-\frac{1}{2}I\varphi)(\boldsymbol{r}) - (A\varphi)(\boldsymbol{r}) &= (Hu)(\boldsymbol{r}) - (I\varphi) + (N'f)(\boldsymbol{r}) + (P'h)(\boldsymbol{r}) \\
\varphi(\boldsymbol{r}) &= (\frac{1}{2}I + A)\varphi(\boldsymbol{r}) + (Hu)(\boldsymbol{r}) + (N'f)(\boldsymbol{r}) + (P'h)(\boldsymbol{r}).
\end{aligned}$$

Substituting the expression for $\varphi(\boldsymbol{r})$ in (3.4.10) into the above equation yields

$$\begin{aligned}\varphi(\boldsymbol{r}) &= (\frac{1}{2}I + A)\Big[S^{-1}(\frac{1}{2}I + D)u(\boldsymbol{r}) - S^{-1}[(Nf)(\boldsymbol{r}) + (Ph)(\boldsymbol{r})]\Big] + (Hu)(\boldsymbol{r}) \\ &\quad + [(N'f)(\boldsymbol{r}) + (P'h)(\boldsymbol{r})] \\ \varphi(\boldsymbol{r}) &= \underbrace{\Big[(\frac{1}{2}I + A)S^{-1}(\frac{1}{2}I + D) + H\Big]}_{\text{Symmetric form of Steklov-Poincarè operator}} u(\boldsymbol{r}) \\ &\quad - (\frac{1}{2}I + A)S^{-1}[(Nf)(\boldsymbol{r}) + (Ph)(\boldsymbol{r})] + [(N'f)(\boldsymbol{r}) + (P'h)(\boldsymbol{r})]\,; \boldsymbol{r} \in \mathcal{B}_R. \quad (3.4.13)\end{aligned}$$

The above expression (3.4.13) gives an alternative symmetric form of the Steklov-Poincarè operator as identified above [68]. Therefore, we have two expressions mapping $u(\boldsymbol{r})$ to $\varphi(\boldsymbol{r})$ for $\boldsymbol{r} \in \mathcal{B}_R$:

$$\begin{aligned}&\varphi(\boldsymbol{r}) = S^{-1}(\frac{1}{2}I + D)u(\boldsymbol{r}) - S^{-1}[(Nf)(\boldsymbol{r}) + (Ph)(\boldsymbol{r})]\,; \boldsymbol{r} \in \mathcal{B}_R, \quad \text{and} \\ &\varphi(\boldsymbol{r}) = \Big[(\frac{1}{2}I + A)S^{-1}(\frac{1}{2}I + D) + H\Big]u(\boldsymbol{r}) - (\frac{1}{2}I + A)S^{-1}[(Nf)(\boldsymbol{r}) + (Ph)(\boldsymbol{r})] \\ &\qquad + [(N'f)(\boldsymbol{r}) + (P'h)(\boldsymbol{r})]\,; \boldsymbol{r} \in \mathcal{B}_R.\end{aligned}$$

from which we can deduce that the Steklov-Poincarè operator, $\mathcal{T}_R$, may be expressed as

$$\mathcal{T}_R = S^{-1}(\frac{1}{2}I + D) = (\frac{1}{2}I + A)S^{-1}(\frac{1}{2}I + D) + H. \quad (3.4.14)$$

This is a result that is also established in the literature (see, for example, Steinbach and Wendland in [98]).

It is important to note here that we are interested in yet another symmetric representation of the Steklov-Poincarè operator, $\mathcal{T}_R$, as

$$\mathcal{T}_R = S^{-1}(\frac{1}{2}I + D) = S^{-1}(\frac{1}{2}I + D)SS^{-1} = S^{-1}ZS^{-1}, \quad (3.4.15)$$

where $Z = (\frac{1}{2}I + D)S$. According to Hsiao , this alternative symmetric representation is important "when coupling boundary elements with a symmetric finite element scheme, one can introduce a modified hybrid discretization scheme" [48]. It also avoids the use of the hypersingular operator. This certainly applies to our problem, and we will discuss this further when we develop the finite element approximation.

Before we prove the main theorems in this section, we present several well-known propositions for boundary integral operators. The following propositions are established in several sources, but here we cite Steinbach and Wendland in [98] for their development:

Proposition 3.4.1 *The single-layer potential operator, S, is $H^{-1/2}(\mathcal{B}_R)$-elliptic, i.e.,*

$$\langle Sw, w\rangle_{L_2(\mathcal{B}_R)} \geq c_1^S \|w\|^2_{H^{-1/2}(\mathcal{B}_R)}, \forall w \in H^{-1/2}(\mathcal{B}_R). \tag{3.4.16}$$

In addition, according to [98], since the single-layer potential operator, S, is bounded, we can use the equivalent norm of the Sobolev space $H^{-1/2}(\mathcal{B}_R)$ induced by S :

$$\|w\|_S = \sqrt{\langle Sw, w\rangle_{L_2(\mathcal{B}_R)}} \qquad \forall w \in H^{-1/2}(\mathcal{B}_R),$$

as well as the equivalent norm of the Sobolev space $H^{1/2}(\mathcal{B}_R)$ induced by S^{-1} :

$$\|v\|_{S^{-1}} = \sqrt{\langle S^{-1}v, v\rangle_{L_2(\mathcal{B}_R)}} \qquad \forall v \in H^{1/2}(\mathcal{B}_R).$$

Proposition 3.4.2 *The hypersingular operator, H, is $H^{1/2}(\mathcal{B}_R)$-elliptic, i.e.,*

$$\langle Hw, w\rangle_{L_2(\mathcal{B}_R)} \geq c_1^H \|w\|^2_{H^{1/2}(\mathcal{B}_R)}, \forall w \in H^{1/2}(\mathcal{B}_R). \tag{3.4.17}$$

Proposition 3.4.3 *The double-layer potential operator D can be symmetrized as fol-*

lows:

$$DS = SA \qquad HD = AH \qquad SH = \frac{1}{4}I - D^2 \qquad HS = \frac{1}{4}I - A^2. \tag{3.4.18}$$

Proposition 3.4.4 *The inverse of the single-layer potential operator is bounded, i.e.,*

$$c_1^S \langle S^{-1}w, w\rangle_{L_2(\mathcal{B}_R)} \leq \|w\|^2_{H^{1/2}(\mathcal{B}_R)} \qquad \forall w \in H^{1/2}(\mathcal{B}_R). \tag{3.4.19}$$

Proposition 3.4.5 *The Steklov-Poincarè operator, $\mathcal{T}_R$, is $H^{1/2}(\mathcal{B}_R)$-elliptic, i.e.,*

$$\langle \mathcal{T}_R w, w\rangle_{L_2(\mathcal{B}_R)} \geq c_1^H \|w\|^2_{H^{1/2}(\mathcal{B}_R)}, \forall w \in H^{1/2}(\mathcal{B}_R). \tag{3.4.20}$$

Proposition 3.4.6 *The operator S is self-adjoint, and there exists the self-adjoint square root $S^{1/2}$ satisfying $S = S^{1/2}S^{1/2}$ and $\left\|S^{-1/2}w\right\|_{L_2(\mathcal{B}_R)} = \|w\|_{S^{-1}}$.*

The following theorem is also proved in [98], and due to its importance in proving Theorem 3.4.8, we present it here with an expansion of the details and reasoning:

Theorem 3.4.7 *For all $w \in H^{1/2}(\mathcal{B}_R)$, the following estimate holds:*

$$\left\|(\frac{1}{2}I + D)w\right\|_{S^{-1}} \leq c_K \|w\|_{S^{-1}}, \tag{3.4.21}$$

where $c_K = \frac{1}{2} + \sqrt{\frac{1}{4} - c_1^H \cdot c_1^S} > 0.$

Proof :

We first note that

$$\begin{aligned}\left\|\left(\frac{1}{2}I + D\right)w\right\|_{S^{-1}}^2 &= \langle S^{-1}\left(\frac{1}{2}I + D\right)w, \left(\frac{1}{2}I + D\right)w\rangle_{L_2(\mathcal{B}_R)} \quad \text{(Def'n of norm)} \\ &= \langle\left(\frac{1}{2}I + A\right)S^{-1}\left(\frac{1}{2}I + D\right)w, w\rangle_{L_2(\mathcal{B}_R)} \quad \text{(Symmetry in Eq ref)} \\ &= \langle \mathcal{T}_R w, w\rangle_{L_2(\mathcal{B}_R)} - \langle Hw, w\rangle_{L_2(\mathcal{B}_R)}. \end{aligned} \tag{3.4.22}$$

Now we further establish the properties of the inner products as in [98],

$$\begin{aligned}\langle \mathcal{T}_R w, w\rangle_{L_2(\mathcal{B}_R)} &= \langle S^{-1/2}S\mathcal{T}_R w, S^{-1/2}w\rangle_{L_2(\mathcal{B}_R)} \\ &\leq \left\|S^{-1/2}S\mathcal{T}_R w\right\|_{L_2(\mathcal{B}_R)} \left\|S^{-1/2}w\right\|_{L_2(\mathcal{B}_R)} \\ &= \|S\mathcal{T}_R w\|_{S^{-1}} \|w\|_{S^{-1}} \\ &= \left\|\left(\frac{1}{2}I + D\right)w\right\|_{S^{-1}} \|w\|_{S^{-1}}. \\ \langle Hw, w\rangle_{L_2(\mathcal{B}_R)} &\geq c_1^H \|w\|_{H^{1/2}(\mathcal{B}_R)}^2 \\ &\geq c_1^H c_1^S \langle S^{-1}w, w\rangle_{L_2(\mathcal{B}_R)} \\ &= c_1^H c_1^S \|w\|_{S^{-1}}^2. \end{aligned}$$

Then we can rewrite (3.4.22) as

$$\begin{aligned}\left\|\left(\frac{1}{2}I + D\right)w\right\|_{S^{-1}}^2 &= \langle \mathcal{T}_R w, w\rangle_{L_2(\mathcal{B}_R)} - \langle Hw, w\rangle_{L_2(\mathcal{B}_R)} \\ &\leq \left\|\left(\frac{1}{2}I + D\right)w\right\|_{S^{-1}} \|w\|_{S^{-1}} - c_1^H c_1^S \|w\|_{S^{-1}}^2. \end{aligned} \tag{3.4.23}$$

If we let $a = \left\| \left(\frac{1}{2}I + D\right)w \right\|_{S^{-1}} > 0$ and $b = \|w\|_{S^{-1}} > 0$, then we have

$$\begin{aligned}
a^2 &\leq ab - c_1^H c_1^S b^2 \\
\frac{a^2}{b^2} &\leq \frac{a}{b} - c_1^H c_1^S \\
\left(\frac{a}{b}\right)^2 - \frac{a}{b} &\leq -c_1^H c_1^S \\
\left(\frac{a}{b}\right)^2 - \frac{a}{b} + \frac{1}{4} &\leq \frac{1}{4} - c_1^H c_1^S \\
\left(\frac{a}{b} - \frac{1}{2}\right)^2 &\leq \frac{1}{4} - c_1^H c_1^S \\
\frac{1}{2} - \sqrt{\frac{1}{4} - c_1^H c_1^S} \leq \frac{a}{b} &\leq \frac{1}{2} + \sqrt{\frac{1}{4} - c_1^H c_1^S}.
\end{aligned}$$

Therefore we have

$$\frac{\left\| \left(\frac{1}{2}I + D\right)w \right\|_{S^{-1}}}{\|w\|_{S^{-1}}} \leq \frac{1}{2} + \sqrt{\frac{1}{4} - c_1^H c_1^S} = c_K. \square$$

Before we frame the variational problem in the next chapter, we prove the following theorem, similar to Cakoni and Colton's Theorem 5.20 in [10]:

Theorem 3.4.8 *The Steklov-Poincarè operator, $\mathcal{T}_R$, is a bounded, linear operator from $H^{1/2}(\mathcal{B}_R) \to H^{-1/2}(\mathcal{B}_R)$. Also, the principal part of $\mathcal{T}_R$, referred to as $\mathcal{T}_{R,P}$, satisfies the coercivity estimate*

$$-\langle \mathcal{T}_{R,P} u, u \rangle \geq C \|u\|^2_{H^{1/2}(\mathcal{B}_R)}$$

for some $C > 0$, such that the difference $\mathcal{T}_R - \mathcal{T}_{R,P}$ is a compact operator from $H^{1/2}(\mathcal{B}_R) \to H^{-1/2}(\mathcal{B}_R)$.

Proof :

To prove boundedness of the Steklov-Poincarè operator, $\mathcal{T}_R$, we use the equivalent

norms of the Sobolev spaces defined earlier, as well as Proposition 3.4.6., which yields

$$\begin{aligned}
\|\mathcal{T}_R w\|_S &= \sqrt{\langle S\mathcal{T}_R w, \mathcal{T}_R w\rangle_{L_2(\mathcal{B}_R)}} \\
&= \sqrt{\langle SS^{-1}\big(\frac{1}{2}I + D\big)w, S^{-1}\big(\frac{1}{2}I + D\big)w\rangle_{L_2(\mathcal{B}_R)}} \\
&= \sqrt{\langle S^{-1/2}\big(\frac{1}{2}I + D\big)w, S^{-1/2}\big(\frac{1}{2}I + D\big)w\rangle_{L_2(\mathcal{B}_R)}} \\
&\leq \sqrt{\left\|\big(\frac{1}{2}I + D\big)w\right\|^2_{S^{-1}}} \\
&= \left\|\big(\frac{1}{2}I + D\big)w\right\|_{S^{-1}} \leq c_K \|w\|_{S^{-1}} .
\end{aligned} \tag{3.4.24}$$

Linearity follows directly from the expression in (3.4.14).

At this point, having shown boundedness and linearity, we define the principal part of $\mathcal{T}_R$ to be $\mathcal{T}_{R,P}$, which corresponds to the Laplacian portion of the operator. Ideally, for our problem, this would be the case where $\alpha^2 = 0$ in (3.3.1). However, because we have defined $\alpha^2 = \dfrac{1}{(\delta t)^2\beta}$, we note that this does not correspond to a physical situation, but is only studied in order to help frame the variational formulation problem. According to Durán et al. in [29], the principal part of this operator can be associated with the Green's function for the Laplace equation with a Neumann boundary condition enforced at the ground plane (i.e., referring again to (3.3.1), $\alpha^2 = 0$ implies $A = 0$ and that the normal derivative of the Green's function must be equal to zero at the ground plane). The Green's function, as shown in Durán in [29], is

$$G(\boldsymbol{r}|\boldsymbol{r'}) = \frac{1}{2\pi}\log R + \frac{1}{2\pi}\log R^*.$$

In fact, this idea is supported by Khoromskij and Wittum in [60], where they seek a simpler, alternate expression for the Steklov-Poincarè operator previously derived in (3.4.14). They derive an explicit integral representation for the approximation of the Steklov-Poincarè operator whose principal part is the related Green's function.

Furthermore, this explicit representation is in hypersingular form. This idea is also explored in [57] and [59].

Durán goes on to state the following:

> That Green's function has been obtained by a principle of symmetry with respect to the x_1-axis (i.e. $x-$axis). Thus, the continuity and coercivity properties of its associated integral operator (i.e. the principal part of the operator) on S^+ (i.e. the half-circle, or our semicircle $\mathcal{B}_R$) are reduced to the whole circle S. [29]

This makes sense in the context of the Laplacian in that it is radially symmetric [73]. Thus, we can study the properties of the case where $\alpha^2 = 0$ for a disk, denoted $\mathcal{B}_{\text{DISK}}$, which is comparable to our operator $\mathcal{T}_{R,P}$ extended to the whole circle. We note that if u is a radiating solution outside a disk $\mathcal{B}_{\text{DISK}}$ of radius R, then we can separate variables and obtain

$$u(r,\theta) = \sum_{-\infty}^{\infty} a_n r^{-n} e^{in\theta}, \qquad r \geq R \quad \text{and} \quad 0 \leq \theta \leq 2\pi.$$

As in Cakoni and Colton in [10], we can state that for data on the disk

$$u|_{\partial\mathcal{B}_{\text{DISK}}} = \sum_{-\infty}^{\infty} b_n e^{in\theta};$$

with coefficients $b_n = a_n R^{-n}$, the mapping of $T_{R,P} : u \to \dfrac{\partial u}{\partial n}$ yields

$$T_{R,P} u = -\sum_{-\infty}^{\infty} \frac{n}{R} b_n e^{in\theta}.$$

Then it follows as in Cakoni and Colton that for a disk $\mathcal{B}_{\text{DISK}}$,

$$-\int_{\partial\mathcal{B}_{\text{DISK}}} T_{R,P} w \bar{w} ds \geq C \left\| w \right\|^2_{H^{1/2}(\partial\mathcal{B}_{\text{DISK}})}.$$

Then through an extension argument we can establish

$$-\int_{\partial\mathcal{B}_R} T_{R,P} w \bar{w} ds \geq C \left\| w \right\|^2_{H^{1/2}(\partial\mathcal{B}_R)}.$$

It can then be shown from several sources (see, for example, [29] or [10]) that $\mathcal{T}_R - \mathcal{T}_{R,P}$ is a compact operator from $H^{1/2}(\mathcal{B}_R) \to H^{-1/2}(\mathcal{B}_R)$. These properties are also more explicitly stated and proved in Kirsch in [61], as well as in Hettlich in [43]. $\square$

As a result, this theorem will help us prove the well-posedness in the next chapter. Even though we do not have an explicit series representation for the operator, we used an important idea in that the principal part of the Steklov-Poincarè operator satisfies a coercivity estimate. This will be discussed again during the variational formulation chapter.

3.5 Green's Function Analysis: Derivative and Singularity Evaluation

Having both the integral representation of the solution in the exterior domain in (3.2.10), as well as the Green's function in (3.3.7), we are ready to establish the existence of the normal derivatives, which will be required for numerical implementation. Singularities will also need to be addressed during the boundary integral matrix construction.

The normal derivative of the first two terms of the Green function as expressed in (3.3.7) is given by:

$$\begin{aligned}\frac{\partial}{\partial \boldsymbol{n}_{\boldsymbol{r'}}}\Big[\frac{1}{2\pi}K_0(\alpha R) - \frac{1}{2\pi}K_0(\alpha R^*)\Big] &= -\frac{\alpha}{2\pi}K_1(\alpha R)\frac{(x'-x, y'-y)}{\sqrt{(x'-x)^2+(y'-y)^2}} \cdot \hat{n}_{\boldsymbol{r'}} \\ &\quad + \frac{\alpha}{2\pi}K_1(\alpha R^*)\frac{(x'-x, y'+y)}{\sqrt{(x'-x)^2+(y'+y)^2}} \cdot \hat{n}_{\boldsymbol{r'}}\end{aligned}$$

where $\hat{n}_{\boldsymbol{r'}} = \dfrac{\boldsymbol{r'}}{\|\boldsymbol{r'}\|}$, which is the outward unit normal vector to the boundary at the

point $\boldsymbol{r'}$. At this point, we address how to evaluate a singularity for the normal derivative evaluated at these first two terms of the Green's function. Specifically, we will be interested in evaluating the normal derivative as R and R^* both approach zero. We will derive the case for $R \to 0$ and R^* can be derived analogously.

We first note that

$$\cos\theta = -\frac{(x'-x, y'-y)}{\sqrt{(x'-x)^2+(y'-y)^2}} \cdot \hat{n}_{\boldsymbol{r'}}$$

where θ is the angle between $-\hat{n}_{\boldsymbol{r'}}$ and $\boldsymbol{r} - \boldsymbol{r'}$, and this is a common vector calculus result that can be derived from the law of cosines. We also use the fact that for small arguments, $K_0(x) \approx -\log(x)$, so it follows that $K_1(x) \approx \frac{1}{x}$. It is also noted in Wiersig in [110] that $\cos\theta = \frac{1}{2}\chi\,|\boldsymbol{r} - \boldsymbol{r'}|$, where χ is the curvature of the curve at the boundary.

Therefore, taking the limit as $R \to 0$, we have

$$\begin{aligned}
\lim_{R\to 0}\Big(-\frac{\alpha}{2\pi}\Big)K_1(\alpha R)\frac{(x'-x, y'-y)}{\sqrt{(x'-x)^2+(y'-y)^2}} \cdot \hat{n}_{\boldsymbol{r'}} & \\
&= \lim_{R\to 0}\Big(-\frac{\alpha}{2\pi}\Big)\Big(\frac{1}{\alpha R}\Big)\Big(-\frac{1}{2}\chi\,|\boldsymbol{r}-\boldsymbol{r'}|\Big) \\
&= \lim_{R\to 0}\Big(-\frac{\alpha}{2\pi}\Big)\Big(\frac{1}{\alpha R}\Big)\Big(-\frac{1}{2}\chi R\Big) \\
&= \lim_{R\to 0}\frac{1}{4\pi}\chi.
\end{aligned}$$

However, the curvature χ is finite, and furthermore is 0 for straight line segments, which we will be using for the boundary element method, so we can conclude that

$$\lim_{R\to 0}\Big(-\frac{\alpha}{2\pi}\Big)K_1(\alpha R)\frac{(x'-x, y'-y)}{\sqrt{(x'-x)^2+(y'-y)^2}} \cdot \hat{n}_{\boldsymbol{r'}} = 0.$$

which we will need to evaluate the expression at a singularity. As previously stated,

this will also apply evaluating the case when $R^* \to 0$.

Also, the previous result, although not explicitly proven as we have done, is used in such works by Schneider and Salon in [91] and [93] and [90], and Koopmann and Benner in [63]. They implement these results in the boundary integral formulation phase in dealing with singularities of modified bessel functions of the second kind.

The derivatives of the third term of the Green's function expression in (3.3.7) can be expressed as follows:

$$\frac{\partial G_3}{\partial y} = \frac{\partial G_3}{\partial y'} = i\Big[\left(\frac{A}{B}\right)^2 \frac{e^{-\frac{A}{B}(y'+y)}}{\sqrt{(\frac{A}{B})^2 - \alpha^2}} \cos\Big(|x-x'|\sqrt{\left(\frac{A}{B}\right)^2 - \alpha^2}\Big)\Big].$$

$$\frac{\partial G_3}{\partial x'} = i\Big[\frac{A}{B} e^{-\frac{A}{B}(y'+y)} \sin\Big(|x-x'|\sqrt{\left(\frac{A}{B}\right)^2 - \alpha^2}\Big)\Big].$$

$$\frac{\partial G_3}{\partial x} = -\frac{\partial G_3}{\partial x'}.$$

The derivatives of the fourth term of the Green's function expression in (3.3.7) can be expressed as follows for y and y':

$$\frac{\partial G_4}{\partial y} = \frac{\partial G_4}{\partial y'} = -\frac{A}{B}\frac{\alpha}{2\pi} e^{-\frac{A}{B}(y'+y)} \int_{-\infty}^{y'+y} K_1(\alpha\sqrt{(x'-x)^2+\xi^2}) \frac{\xi e^{\frac{A}{B}\xi}}{\sqrt{(x'-x)^2+\xi^2}} d\xi$$
$$+ \frac{\alpha}{2\pi} K_1(\alpha\sqrt{(x'-x)^2+(y'+y)^2}) \frac{y'+y}{\sqrt{(x'-x)^2+(y'+y)^2}}.$$

The derivatives of the fourth term of the Green's function expression in (3.3.7) can be expressed as follows for x and x':

$$\frac{\partial G_4}{\partial x} = \frac{\alpha}{\pi} e^{-\frac{A}{B}(y'+y)} \int_{-\infty}^{y'+y} \Bigg[K_1(\alpha\sqrt{(x'-x)^2+\xi^2}) \frac{\xi e^{\frac{A}{B}\xi}(x'-x)}{\Big((x'-x)^2+\xi^2\Big)^{3/2}} -$$
$$\alpha K_1'(\alpha\sqrt{(x'-x)^2+\xi^2}) \frac{\xi e^{\frac{A}{B}\xi}(x'-x)}{\Big((x'-x)^2+\xi^2\Big)} \Bigg] d\xi,$$

$$\frac{\partial G_4}{\partial x'} = \frac{\alpha}{\pi} e^{-\frac{A}{B}(y'+y)} \int_{-\infty}^{y'+y} \Bigg[- K_1(\alpha\sqrt{(x'-x)^2+\xi^2}) \frac{\xi e^{\frac{A}{B}\xi}(x'-x)}{\Big((x'-x)^2+\xi^2\Big)^{3/2}} + \\ \alpha K_1'(\alpha\sqrt{(x'-x)^2+\xi^2}) \frac{\xi e^{\frac{A}{B}\xi}(x'-x)}{\Big((x'-x)^2+\xi^2\Big)} \Bigg] d\xi.$$

Once again, in dealing with the singularities for these expressions in the boundary integral formulation phase, we can refer to the works cited previously, or Ramesh and Lean in [86].

At this point, we can discuss an alternate expression for the fourth term of the Green's function for more effective computation. This is done in order to "isolate the poles" and "adequately treat the slow decrease at infinity" when $y' + y = 0$, which would occur when on the impedance plane (Γ_{ext}) [42]. For the case when $\left|\frac{A}{B}\right| > |\alpha|$, we can apply Hein's technique to our case and get:

$$G_4(\boldsymbol{r}|\boldsymbol{r'}) = \frac{1}{\pi} \int_0^\infty \Big(\frac{e^{-\sqrt{\xi^2+\alpha^2}(y'+y)}}{(\frac{A}{B} - \sqrt{\xi^2+\alpha^2})} - \frac{\frac{A}{B}}{\sqrt{(\frac{A}{B})^2-\alpha^2}} \cdot \frac{e^{-\frac{A}{B}\xi(y'+y)/\sqrt{(\frac{A}{B})^2-\alpha^2}}}{\sqrt{(\frac{A}{B})^2-\alpha^2}-\xi} \Big) \times \\ \cos(\xi(x'-x)) d\xi + \frac{\frac{A}{B}}{2\pi\sqrt{(\frac{A}{B})^2-\alpha^2}} e^{-\frac{A}{B}(y'+y)} \times \\ \Bigg\{ e^{i(x-x')\sqrt{(\frac{A}{B})^2-\alpha^2}} \mathrm{Ei}\Big[\frac{A}{B}(y'+y) - i\sqrt{\big(\frac{A}{B}\big)^2-\alpha^2}(x-x')\Big] \\ + e^{-i(x-x')\sqrt{(\frac{A}{B})^2-\alpha^2}} \mathrm{Ei}\Big[\frac{A}{B}(y'+y) + i\sqrt{\big(\frac{A}{B}\big)^2-\alpha^2}(x-x')\Big] \Bigg\},$$

where Ei denotes the exponential integral function.

It follows that the derivative with respect to x' of the preceding term is

$$\frac{\partial G_4}{\partial x'} = -\frac{1}{\pi}\int_0^\infty \Big(\frac{e^{-\sqrt{\xi^2+\alpha^2}(y'+y)}}{(\frac{A}{B}-\sqrt{\xi^2+\alpha^2})} - \frac{\frac{A}{B}}{\sqrt{(\frac{A}{B})^2-\alpha^2}}\cdot\frac{e^{-\frac{A}{B}\xi(y'+y)/\sqrt{(\frac{A}{B})^2-\alpha^2}}}{\sqrt{(\frac{A}{B})^2-\alpha^2}-\xi}\Big)\times$$
$$\sin(\xi(x'-x))d\xi + \frac{\frac{A}{B}}{2\pi\sqrt{(\frac{A}{B})^2-\alpha^2}}e^{-\frac{A}{B}(y'+y)}\times$$
$$\Big\{ie^{i(x-x')\sqrt{(\frac{A}{B})^2-\alpha^2}}\mathrm{Ei}\Big[\frac{A}{B}(y'+y) - i\sqrt{\big(\frac{A}{B}\big)^2-\alpha^2}(x-x')\Big]$$
$$- ie^{-i(x-x')\sqrt{\left(\frac{A}{B}\right)^2-\alpha^2}}\mathrm{Ei}\Big[\frac{A}{B}(y'+y) + i\sqrt{\big(\frac{A}{B}\big)^2-\alpha^2}(x-x')\Big]\Big\},$$

and with respect to x is

$$\frac{\partial G_4}{\partial x} = \frac{1}{\pi}\int_0^\infty \Big(\frac{e^{-\sqrt{\xi^2+\alpha^2}(y'+y)}}{(\frac{A}{B}-\sqrt{\xi^2+\alpha^2})} - \frac{\frac{A}{B}}{\sqrt{(\frac{A}{B})^2-\alpha^2}}\cdot\frac{e^{-\frac{A}{B}\xi(y'+y)/\sqrt{(\frac{A}{B})^2-\alpha^2}}}{\sqrt{(\frac{A}{B})^2-\alpha^2}-\xi}\Big)\times$$
$$\sin(\xi(x'-x))d\xi + \frac{\frac{A}{B}}{2\pi\sqrt{(\frac{A}{B})^2-\alpha^2}}e^{-\frac{A}{B}(y'+y)}\times$$
$$\Big\{ - ie^{i(x-x')\sqrt{(\frac{A}{B})^2-\alpha^2}}\mathrm{Ei}\Big[\frac{A}{B}(y'+y) - i\sqrt{\big(\frac{A}{B}\big)^2-\alpha^2}(x-x')\Big]$$
$$+ ie^{-i(x-x')\sqrt{(\frac{A}{B})^2-\alpha^2}}\mathrm{Ei}\Big[\frac{A}{B}(y'+y) + i\sqrt{\big(\frac{A}{B}\big)^2-\alpha^2}(x-x')\Big]\Big\}.$$

These are obviously complicated terms to analyze and implement, and we leave the computations with respect to the y' and y variable to the numerical phase.

In summary, the normal derivatives of the Green's function can be evaluated at any point, provided the gradient can be calculated, by observing that

$$\frac{\partial G}{\partial \boldsymbol{n}_{\boldsymbol{r'}}} = \Big(\frac{\partial G}{\partial x'}, \frac{\partial G}{\partial y'}\Big)\cdot\hat{n}_{\boldsymbol{r'}},$$
$$\frac{\partial G}{\partial \boldsymbol{n}_{\boldsymbol{r}}} = \Big(\frac{\partial G}{\partial x}, \frac{\partial G}{\partial y}\Big)\cdot\hat{n}_{\boldsymbol{r}}.$$

Furthermore, we mention that the hypersingular operator will require the computation of $\frac{\partial}{\partial \boldsymbol{n_r}} \frac{\partial G(\boldsymbol{r}|\boldsymbol{r'})}{\partial \boldsymbol{n_{r'}}}$. This will require the values of $\frac{\partial^2 G}{\partial x \partial x'}$, $\frac{\partial^2 G}{\partial y \partial x'}$, $\frac{\partial^2 G}{\partial x \partial y'}$, and $\frac{\partial^2 G}{\partial y \partial y'}$ to be computed. These can also be computed during the computational phase, but care is needed in evaluating the singularities and ensuring the proper expression is obtained.

IV. Variational Formulation

4.1 Recasting the Boundary Value Problem

Since the ultimate goal of the previous mathematical formulation was to lay the foundation to establish existence and uniqueness, in this section we find a weak solution of the variational form. We first note that on the artificial boundary, $\mathcal{B}_R$, the normal derivative of the total electric field satisfies the continuity condition:

$$\left.\frac{\partial u}{\partial n}\right|_{r=R} = \left.\frac{\partial u^i}{\partial n}\right|_{r=R} + \left.\frac{\partial u^s}{\partial n}\right|_{r=R}. \tag{4.1.1}$$

Recall the expression derived previously in (3.4.10):

$$\varphi(\boldsymbol{r}) = S^{-1}(\frac{1}{2}I + D)u(\boldsymbol{r}) - S^{-1}[(Nf)(\boldsymbol{r}) + (Ph)(\boldsymbol{r})]; \quad \boldsymbol{r} \in \mathcal{B}_R,$$

where the Newton Potential and impedance plane terms are

$$(Nf)(\boldsymbol{r}) = \iint_{\mathcal{U}_R} f(\boldsymbol{r'})G(\boldsymbol{r}|\boldsymbol{r'})dS'; \quad \boldsymbol{r} \in \mathcal{B}_R, \tag{4.1.2}$$

$$(Ph)(\boldsymbol{r}) = -\frac{1}{A}\int_{\Gamma_{\text{ext}}} h(\boldsymbol{r'})\frac{\partial G(\boldsymbol{r}|\boldsymbol{r'})}{\partial y'}dx'; \quad \boldsymbol{r} \in \mathcal{B}_R, \tag{4.1.3}$$

where $f(\boldsymbol{r}) = \alpha^2\tilde{u}^{s,n+1}$ and $h(\boldsymbol{r}_s) = \delta t\gamma\alpha^2\tilde{u}^{s,n+1} - \tilde{\dot{u}}^{s,n+1}$. This allows us to write

$$(N\tilde{u}^{s,n+1})(\boldsymbol{r}) = \alpha^2 \iint_{\mathcal{U}_R} \tilde{u}^{s,n+1}G(\boldsymbol{r}|\boldsymbol{r'})dS'; \quad \boldsymbol{r} \in \mathcal{B}_R, \tag{4.1.4}$$

$$(P\tilde{u}^{s,n+1})(\boldsymbol{r}) = -\frac{1}{A}\int_{\Gamma_{\text{ext}}} \left[\delta t\gamma\alpha^2\tilde{u}^{s,n+1} - \tilde{\dot{u}}^{s,n+1}\right]\frac{\partial G(\boldsymbol{r}|\boldsymbol{r'})}{\partial y'}dx'; \quad \boldsymbol{r} \in \mathcal{B}_R. \tag{4.1.5}$$

Then we can define

$$(\Phi_R \tilde{u}^{s,n+1})(\boldsymbol{r}) = (N\tilde{u}^{s,n+1})(\boldsymbol{r}) + (P\tilde{u}^{s,n+1})(\boldsymbol{r}),$$

and note that since the Newton Potential and impedance plane terms are bounded, then Φ_R is bounded. We can also define

$$(\Psi_R \tilde{u}^{s,n+1})(\boldsymbol{r}) = S^{-1}(\Phi\tilde{u}^{s,n+1})(\boldsymbol{r}),$$

and note that since S^{-1} is bounded (see Proposition 3.4.4.), then Ψ_R is bounded. Now (3.4.10) becomes

$$\varphi(\boldsymbol{r}) = \frac{\partial u(\boldsymbol{r})}{\partial \boldsymbol{n}_{\boldsymbol{r}}} = (\mathcal{T}_R u)(\boldsymbol{r}) - (\Psi_R \tilde{u}^{s,n+1})(\boldsymbol{r}); \quad \boldsymbol{r} \in \mathcal{B}_R.$$

Applying this to the continuity property in (4.1.1) yields

$$\left.\frac{\partial u}{\partial n}\right|_{r=R} = \left.\frac{\partial u^i}{\partial n}\right|_{r=R} + (\mathcal{T}_R(u-u^i)) - (\Psi_R \tilde{u}^{s,n+1}); \quad \boldsymbol{r} \in \mathcal{B}_R. \tag{4.1.6}$$

This is the transparent boundary condition on $\mathcal{B}_R$, so we may now rewrite (3.1.5) as

$$\begin{cases} -\Delta u^{n+1} + \alpha^2 \varepsilon_r u^{n+1} = \alpha^2 \varepsilon_r \tilde{u}^{n+1} \text{ in } \Omega_R, \\ \delta t \gamma \alpha^2 u^{n+1} + \dfrac{\eta}{\mu}\dfrac{\partial u^{n+1}}{\partial n} = \delta t \gamma \alpha^2 \tilde{u}^{n+1} - \tilde{u}^{n+1} \text{ on } S, \\ \dfrac{\partial u^{n+1}}{\partial n} - \mathcal{T}_R u^{n+1} = \dfrac{\partial u^i}{\partial n} - (\Psi_R \tilde{u}^{s,n+1}) - \mathcal{T}_R(u^i) \text{ on } \mathcal{B}_R. \end{cases} \tag{4.1.7}$$

Now we seek to solve (4.1.7) through a variational method.

4.2 Variational Formulation

Instead of enforcing the boundary conditions on the test function space V as in [105], we choose to define the subspace V simply as $H^1(\Omega_R)$, which has the H^1-norm, i.e.,

$$\|u\|_V = \|u\|_{H^1(\Omega_R)}.$$

The variational formulation of (4.1.7) will be to find $u \in V$ such that

$$b_{TM}(u, v) = F(v) \qquad \forall v \in V. \tag{4.2.1}$$

Note that because we are enforcing Robin boundary conditions on the surface S, these boundary conditions are considered natural and do not need to be incorporated into the solution space V. That is, the boundary conditions "appear naturally" and are automatically incorporated into the boundary integral expressions and are satisfied by weak solutions [46]. We first must construct the sesquilinear form $b_{TM}(u, v)$ as well as the conjugate linear functional $F(v)$. To do this, we multiply (4.1.7) by a test function $v \in V$ to obtain (we suppress the $n+1$ superscript):

$$-\int_{\Omega_R} \Delta u \bar{v} dxdy + \alpha^2 \int_{\Omega_R} \varepsilon_r u \bar{v} dxdy = \alpha^2 \int_{\Omega_R} \varepsilon_r \tilde{u} \bar{v} dxdy \tag{4.2.2}$$

$$\delta t \gamma \alpha^2 \int_S u \bar{v} d\ell + \frac{\eta}{\mu} \int_S \frac{\partial u}{\partial n} \bar{v} d\ell = \delta t \gamma \alpha^2 \int_S \tilde{u} \bar{v} d\ell - \int_S \tilde{\dot{u}} \bar{v} d\ell \tag{4.2.3}$$

$$\int_{\mathcal{B}_R} \frac{\partial u}{\partial n} \bar{v} d\ell - \int_{\mathcal{B}_R} \mathcal{T}_R u \bar{v} d\ell = \int_{\mathcal{B}_R} \frac{\partial u^i}{\partial n} \bar{v} d\ell - \int_{\mathcal{B}_R} \Psi_R \tilde{u}^s \bar{v} d\ell - \int_{\mathcal{B}_R} \mathcal{T}_R(u^i) \bar{v} d\ell \tag{4.2.4}$$

Noting Green's identity:

$$\int_{\Omega_R} \nabla u \cdot \nabla \bar{v} dxdy = \int_{\mathcal{B}_R \cup S} \frac{\partial u}{\partial n} \bar{v} d\ell - \int_{\Omega_R} \Delta u \bar{v} dxdy,$$

we can rewrite (4.2.2) as

$$\int_{\Omega_R} \nabla u \cdot \nabla \bar{v} dxdy - \int_{\mathcal{B}_R \cup S} \frac{\partial u}{\partial n} \bar{v} d\ell + \alpha^2 \int_{\Omega_R} \varepsilon_r u \bar{v} dxdy = \alpha^2 \int_{\Omega_R} \varepsilon_r \tilde{u} \bar{v} dxdy, \text{ or } \quad (4.2.5)$$

$$\int_{\Omega_R} \nabla u \cdot \nabla \bar{v} dxdy - \Big(\int_{\mathcal{B}_R} \frac{\partial u}{\partial n} \bar{v} d\ell + \int_S \frac{\partial u}{\partial n} \bar{v} d\ell \Big) + \alpha^2 \int_{\Omega_R} \varepsilon_r u \bar{v} dxdy$$
$$= \alpha^2 \int_{\Omega_R} \varepsilon_r \tilde{u} \bar{v} dxdy. \quad (4.2.6)$$

Now substituting the known values from (4.2.3) and (4.2.4):

$$\int_S \frac{\partial u}{\partial n} \bar{v} d\ell = \frac{\mu}{\eta} \left[\delta t \gamma \alpha^2 \int_S \tilde{u} \bar{v} d\ell - \int_S \tilde{\dot{u}} \bar{v} d\ell - \delta t \gamma \alpha^2 \int_S u \bar{v} d\ell \right], \text{ and}$$
$$\int_{\mathcal{B}_R} \frac{\partial u}{\partial n} \bar{v} d\ell = \int_{\mathcal{B}_R} \mathcal{T}_R u \bar{v} d\ell + \int_{\mathcal{B}_R} \frac{\partial u^i}{\partial n} \bar{v} d\ell - \int_{\mathcal{B}_R} \Psi_R \tilde{u}^s \bar{v} d\ell - \int_{\mathcal{B}_R} \mathcal{T}_R(u^i) \bar{v} d\ell$$

and letting

$$J = \left. \frac{\partial u^i}{\partial n} \right|_{r=R} - \mathcal{T}_R u^i,$$

we obtain for (4.2.2):

$$\int_{\Omega_R} \nabla u \cdot \nabla \bar{v} dxdy - \left[\int_{\mathcal{B}_R} \mathcal{T}_R u \bar{v} d\ell + \int_{\mathcal{B}_R} J \bar{v} d\ell - \int_{\mathcal{B}_R} \Psi_R \tilde{u}^s \bar{v} d\ell \right.$$
$$\left. + \frac{\mu}{\eta} \delta t \gamma \alpha^2 \int_S \tilde{u} \bar{v} d\ell - \frac{\mu}{\eta} \int_S \tilde{\dot{u}} \bar{v} d\ell - \frac{\mu}{\eta} \delta t \gamma \alpha^2 \int_S u \bar{v} d\ell \right]$$
$$+ \alpha^2 \int_{\Omega_R} \varepsilon_r u \bar{v} dxdy = \alpha^2 \int_{\Omega_R} \varepsilon_r \tilde{u} \bar{v} dxdy. \quad (4.2.7)$$

Observing that for $\eta \neq 0$, gathering appropriate terms yields

$$\int_{\Omega_R} \nabla u \cdot \nabla \bar{v} dxdy - \int_{\mathcal{B}_R} \mathcal{T}_R u \bar{v} d\ell + \frac{\mu}{\eta} \delta t \gamma \alpha^2 \int_S u \bar{v} d\ell + \alpha^2 \int_{\Omega_R} \varepsilon_r u \bar{v} dxdy$$
$$= \int_{\mathcal{B}_R} J \bar{v} d\ell - \int_{\mathcal{B}_R} \Psi_R \tilde{u}^s \bar{v} d\ell + \frac{\mu}{\eta} \delta t \gamma \alpha^2 \int_S \tilde{u} \bar{v} d\ell - \frac{\mu}{\eta} \int_S \tilde{\dot{u}} \bar{v} d\ell + \alpha^2 \int_{\Omega_R} \varepsilon_r \tilde{u} \bar{v} dxdy.$$

So now we define the sesquilinear form

$$b_{TM}(u,v) = \int_{\Omega_R} \nabla u \cdot \nabla \bar{v} dxdy - \int_{\mathcal{B}_R} \mathcal{T}_R u \bar{v} d\ell + \frac{\mu}{\eta} \delta t \gamma \alpha^2 \int_S u \bar{v} d\ell + \alpha^2 \int_{\Omega_R} \varepsilon_r u \bar{v} dxdy, \tag{4.2.8}$$

as well as the bounded conjugate linear functional term

$$F(v) = \int_{\mathcal{B}_R} J \bar{v} d\ell - \int_{\mathcal{B}_R} \Psi_R \tilde{u}^s \bar{v} d\ell + \frac{\mu}{\eta} \delta t \gamma \alpha^2 \int_S \tilde{u} \bar{v} d\ell - \frac{\mu}{\eta} \int_S \tilde{\dot{u}} \bar{v} d\ell + \alpha^2 \int_{\Omega_R} \varepsilon_r \tilde{u} \bar{v} dxdy, \tag{4.2.9}$$

and we follow [10] to rewrite $b_{TM}(u,v) = b_{TM1}(u,v) + b_{TM2}(u,v)$, where

$$\begin{aligned} b_{TM1}(u,v) &= \int_{\Omega_R} \Big(\nabla u \cdot \nabla \bar{v} + u \bar{v} \Big) dxdy - \int_{\mathcal{B}_R} \mathcal{T}_{R,P} u \bar{v} d\ell \\ b_{TM2}(u,v) &= \big(-1 \big) \int_{\Omega_R} u \bar{v} dxdy - \int_{\mathcal{B}_R} \big(\mathcal{T}_R - \mathcal{T}_{R,P} \big) u \bar{v} d\ell \qquad (4.2.10) \\ &\quad + \frac{\mu}{\eta} \delta t \gamma \alpha^2 \int_S u \bar{v} d\ell + \alpha^2 \int_{\Omega_R} \varepsilon_r u \bar{v} dxdy. \qquad (4.2.11) \end{aligned}$$

Now the problem becomes finding $u \in V$ such that

$$b_{TM1}(u,v) + b_{TM2}(u,v) = F(v) \qquad \forall v \in V. \tag{4.2.12}$$

The motivation for splitting up the sesquilinear form $b_{TM}(u,v)$ (as well as splitting up the Steklov-Poincarè operator, $\mathcal{T}_R$) is that the entire term itself is not strictly coercive, but a portion of it (i.e. $b_{TM1}(u,v)$) can be shown to be. We will also need to show that $b_{TM2}(u,v)$ is a compact operator. This is similar to the idea discussed by Kress in [64] of decomposing an integral operator into a compact operator and a operator with a bounded inverse. He notes that this idea goes as far back as 1919, and he notes its use in the context of nonsmooth boundaries with edges and corners. However, we will also see that this decomposition allows us to show that $b_{TM}(u,v)$ satisfies a Gårding's inequality. This is a class of problems where the sesquilinear

term can be written as the sum of a coercive term and a compact perturbation [25].

At this point, we present the well-known Lax-Milgram Lemma from Cakoni and Colton in [10], which will be used to prove the well-posedness of the established problem:

Theorem 4.2.1 (Lax-Milgram Lemma) *Assume that b is a bilinear functional mapping $V \times V \to \mathbb{C}$ for which there exist constants $D_1, D_2 > 0$ such that*

$$|b(u,v)| \leq D_1 \|u\|_V \|v\|_V \qquad \forall u, v \in V \tag{4.2.13}$$

and

$$b(u,u) \geq D_2 \|u\|_V^2 \qquad \forall u \in V. \tag{4.2.14}$$

Then, for every bounded conjugate linear functional $F : V \to \mathbb{C}$ there exists a unique element $u \in V$ such that

$$b(u,v) = F(v) \qquad \forall v \in V. \tag{4.2.15}$$

Furthermore, $\|u\|_V \leq D_3 \|F\|_{V'}$, for $D_3 > 0$, a constant independent of F.

We will also require use of the following theorem established in Cakoni and Colton in [10]:

Theorem 4.2.2 (Trace Theorem) *Let $D \subset \mathbb{R}^2$ be a simply connected bounded domain with ∂D in class C^2. Then there exists a positive constant D_4 such that*

$$\|u\|_{H^{1/2}(\partial D)} \leq D_4 \|u\|_{H^1(D)} \qquad \forall u \in H^1(D).$$

Not only does the trace theorem state the trace operator can be "extended as a continuous mapping from $H^1(D) \to H^{1/2}(\partial D)$", but also "this extension has a continuous right inverse" [10]. That means that for any $f \in H^{1/2}(\partial D)$, there exists a $u \in H^1(D)$

such that the trace of u is f, and $\|u\|_{H^1(D)} \leq D_5 \|f\|_{H^{1/2}(\partial D)}$, where $D_5 > 0$ is a constant independent of f [10]. This will be extremely important when proving the coercivity and continuity properties of the sesquilinear term.

We are now ready to prove our main theorem.

Theorem 4.2.3 *The variational problem* (4.2.1) *is well-posed: a solution $u \in V$ exists, is unique, and there exists a $C > 0$, such that*

$$\|u\| \leq C\Big[\left\|u^i\right\| + \|\tilde{u}^s\| + \|\tilde{u}\| + \left\|\tilde{\tilde{u}}\right\| + \|\varepsilon_r \tilde{u}\| \Big].$$

Proof:

We first must show that $b_{TM1}(u, v)$ is strictly coercive, i.e. (4.2.14):

$$\begin{aligned} b_{TM1}(u,u) &= \int_{\Omega_R} \Big(\nabla u \cdot \nabla \bar{u} + u\bar{u} \Big) dxdy - \int_{\mathcal{B}_R} \mathcal{T}_{R,P} u \bar{u} d\ell \\ &\geq \|u\|^2_{H^1(\Omega_R)} + D_6 \|u\|^2_{H^{1/2}(\mathcal{B}_R)} \\ &\geq \|u\|^2_{H^1(\Omega_R)} + D_7 \|u\|^2_{H^1(\Omega_R)} \\ &\geq (1 + D_7) \|u\|^2_{H^1(\Omega_R)} . \end{aligned}$$

We also show that $b_{TM1}(u,v)$ is bounded, or continuous, i.e. (4.2.13):

$$\begin{aligned}
|b_{TM1}(u,v)| &= \left| \int_{\Omega_R} \Big(\nabla u \cdot \nabla \bar{v} + u\bar{v} \Big) dxdy - \int_{\mathcal{B}_R} \mathcal{T}_{R,P} u \bar{v} d\ell \right| \\
&\leq \left| \int_{\Omega_R} \Big(\nabla u \cdot \nabla \bar{v} + u\bar{v} \Big) dxdy \right| + \left| \int_{\mathcal{B}_R} \mathcal{T}_{R,P} u \bar{v} d\ell \right| \\
&\leq \int_{\Omega_R} |\nabla u \cdot \nabla \bar{v}| \, dxdy + \int_{\Omega_R} |u\bar{v}| \, dxdy + \left| \int_{\mathcal{B}_R} \mathcal{T}_{R,P} u \bar{v} d\ell \right| \\
&\leq \|\nabla u\|_{L^2} \|\nabla v\|_{L^2} + \|u\|_{L^2} \|v\|_{L^2} + D_8 \|u\|_{H^{1/2}(\mathcal{B}_R)} \|v\|_{H^{1/2}(\mathcal{B}_R)} \\
&\leq \|u\|_{H^1(\Omega_R)} \|v\|_{H^1(\Omega_R)} + D_9 \|u\|_{H^1(\Omega_R)} \|v\|_{H^1(\Omega_R)} \\
&= (1 + D_9) \|u\|_{H^1(\Omega_R)} \|v\|_{H^1(\Omega_R)} .
\end{aligned}$$

Thus, as in Cakoni and Colton in [10], we may apply the Lax-Milgram Lemma and state there exists a bijective bounded linear operator $B_1 : V \to V$ with bounded inverse such that

$$b_{TM1}(u,v) = \langle B_1 u, v \rangle \qquad \forall v \in V.$$

For $b_{TM2}(u,v)$, we split up the individual terms and show that each is a compact operator, and deduce that a linear combination of these operators is compact as well. We introduce the bounded linear operator $B_2 : V \to V$:

$$\begin{aligned}
b_{TM2}(u,v) &= \langle B_2 u, v \rangle \\
&= \big(-1 \big) \langle u, v \rangle_{L^2(\Omega_R)} - \langle \big(\mathcal{T}_R - \mathcal{T}_{R,P} \big) u, v \rangle + \big(\frac{\mu}{\eta} \delta t \gamma \alpha^2 \big) \langle u, v \rangle_{L^2(\Omega_R)} \\
&\quad + \alpha^2 \langle \varepsilon_r u, v \rangle_{L^2(\Omega_R)} \qquad \forall v \in V.
\end{aligned}$$

Cakoni and Colton in [10] prove that the portion of the operator representing $\langle u, v \rangle_{L^2(\Omega_R)}$ is compact, based on a lemma stating the injection or imbedding of $H^1(\Omega_R)$ into $L^2(\Omega_R)$ is compact. It was established earlier in Theorem 3.4.8 that $\mathcal{T}_R - \mathcal{T}_{R,P}$ is a compact operator.

Following Monk in [75], we define the space $L^2_{\varepsilon_r}(\Omega_R)$ with inner product as

$$\langle u, v\rangle_{L^2_{\tilde{\varepsilon}_r}(\Omega_R)} = \langle \varepsilon_r u, v\rangle \qquad \forall u, v \in L^2_{\varepsilon_r}(\Omega_R).$$

Then the norm on $L^2_{\varepsilon_r}(\Omega_R)$ is equivalent to the standard $L^2(\Omega_R)$ norm. This establishes that the term $\alpha^2\langle \varepsilon_r u, v\rangle_{L^2(\Omega_R)}$ is compact. Therefore, we can deduce that the operator B_2, a linear combination of compact operators, is compact. We establish that $F(v)$ is bounded:

$$\begin{aligned}
|F(v)| &= \left| \int_{\mathcal{B}_R} J\bar{v}d\ell - \int_{\mathcal{B}_R} \Psi_R \tilde{u}^s \bar{v}d\ell + \frac{\mu}{\eta}\delta t\gamma\alpha^2 \int_S \tilde{u}\bar{v}d\ell - \frac{\mu}{\eta}\int_S \tilde{\dot{u}}\bar{v}d\ell + \alpha^2 \int_{\Omega_R} \varepsilon_r \tilde{u}\bar{v}dxdy \right| \\
&\leq \left| \int_{\mathcal{B}_R} J\bar{v}d\ell \right| + \left| \int_{\mathcal{B}_R} \Psi_R \tilde{u}^s \bar{v}d\ell \right| + \left| \frac{\mu}{\eta}\delta t\gamma\alpha^2 \int_S \tilde{u}\bar{v}d\ell \right| + \left| \frac{\mu}{\eta}\int_S \tilde{\dot{u}}\bar{v}d\ell \right| \\
&+ \left| \alpha^2 \int_{\Omega_R} \varepsilon_r \tilde{u}\bar{v}dxdy \right| \\
&\leq \|J\| \|v\| + \|\Psi_R \tilde{u}^s\| \|v\| + C_3 \|\tilde{u}\| \|v\| + C_4 \left\|\tilde{\dot{u}}\right\| \|v\| + C_5 \|\varepsilon_r \tilde{u}\| \|v\| \\
&\leq \left\| \frac{\partial u^i}{\partial n} - \mathcal{T}_R u^i \right\| \|v\| + \|\Psi_R \tilde{u}^s\| \|v\| + C_3 \|\tilde{u}\| \|v\| + C_4 \left\|\tilde{\dot{u}}\right\| \|v\| + C_5 \|\varepsilon_r \tilde{u}\| \|v\| \\
&\leq \left\| \frac{\partial u^i}{\partial n} \right\| \|v\| + \left\|\mathcal{T}_R u^i\right\| \|v\| + C_2 \|\tilde{u}^s\| \|v\| + C_3 \|\tilde{u}\| \|v\| + C_4 \left\|\tilde{\dot{u}}\right\| \|v\| \\
&+ C_5 \|\varepsilon_r \tilde{u}\| \|v\| \\
&\leq C_1 \left\|u^i\right\| \|v\| + C_2 \|\tilde{u}^s\| \|v\| + C_3 \|\tilde{u}\| \|v\| + C_4 \left\|\tilde{\dot{u}}\right\| \|v\| + C_5 \|\varepsilon_r \tilde{u}\| \|v\| \\
&= \left[C_1 \left\|u^i\right\| + C_2 \|\tilde{u}^s\| + C_3 \|\tilde{u}\| + C_4 \left\|\tilde{\dot{u}}\right\| + C_5 \|\varepsilon_r \tilde{u}\| \right] \|v\| .
\end{aligned}$$

If we set $\tilde{C} = \max\{C_1, C_2, C_3, C_4, C_5\}$, then we have

$$\begin{aligned}
|F(v)| &\leq \left[\tilde{C} \left\|u^i\right\| + \tilde{C} \|\tilde{u}^s\| + \tilde{C} \|\tilde{u}\| + \tilde{C} \left\|\tilde{\dot{u}}\right\| + \tilde{C} \|\varepsilon_r \tilde{u}\| \right] \|v\| \\
&= \tilde{C} \left[\left\|u^i\right\| + \|\tilde{u}^s\| + \|\tilde{u}\| + \left\|\tilde{\dot{u}}\right\| + \|\varepsilon_r \tilde{u}\| \right] \|v\| .
\end{aligned}$$

Since

$$|F(v)| \leq \tilde{C}\Big[\left\|u^i\right\| + \|\tilde{u}^s\| + \|\tilde{u}\| + \left\|\tilde{\tilde{u}}\right\| + \|\varepsilon_r\tilde{u}\|\Big]\|v\|,$$

$\|F\| \leq \tilde{C}\Big[\|u^i\| + \|\tilde{u}^s\| + \|\tilde{u}\| + \left\|\tilde{\tilde{u}}\right\| + \|\varepsilon_r\tilde{u}\|\Big]$. We also can let $w \in V$ be the unique element such that

$$F(v) = \langle w, v\rangle$$

which is true due to the Riesz representation theorem.

At this point, we can recast (4.2.12) as finding $u \in V$ such that

$$B_1u + B_2u = (B_1 + B_2)u = w. \tag{4.2.16}$$

Here, we cite McLean in [73], Theorem 2.33, which states in the context of our problem that if $B = B_1 + B_2$, where B_1 has a bounded inverse and B_2 is compact, then B is "Fredholm with zero index, and hence the Fredholm alternative holds" for the equation $Bu = w$. As a result, we may state uniqueness implies existence.

Thus, in proving uniqueness, $b_{TM}(u,u) = 0$ implies

$$\begin{aligned} b_{TM}(u,u) &= \int_{\Omega_R} \nabla u \cdot \nabla\bar{u}dxdy - \int_{\mathcal{B}_R} \mathcal{T}_R u\bar{u}d\ell + \frac{\mu}{\eta}\delta t\gamma\alpha^2\int_S u\bar{u}d\ell \\ &\quad + \alpha^2\int_{\Omega_R}\varepsilon_r u\bar{u}dxdy = 0 \\ &= \int_{\Omega_R} |\nabla u|^2 + \alpha^2\varepsilon_r|u|^2\,dxdy - \int_{\mathcal{B}_R}\mathcal{T}_R u\bar{u}d\ell + \frac{\mu}{\eta}\delta t\gamma\alpha^2\int_S |u|^2\,d\ell = 0 \\ \int_{\mathcal{B}_R}\mathcal{T}_R u\bar{u}d\ell &= \int_{\Omega_R}|\nabla u|^2 + \alpha^2\varepsilon_r|u|^2\,dxdy + \frac{\mu}{\eta}\delta t\gamma\alpha^2\int_S |u|^2\,d\ell. \end{aligned} \tag{4.2.17}$$

We further assume for the cavity filling material $\Re(\varepsilon_r) > 0$ and $\Im(\varepsilon_r) \leq 0$, whereas for the surface S, we assume $\mu = 1$ and a real-valued η where $\Im(\eta) = 0$ on S.

This implies that the imaginary part of the right-hand side of (4.2.17) is less than

or equal to zero, which, in turn, implies

$$\Im\Big(\int_{\mathcal{B}_R} \mathcal{T}_R u\bar{u}d\ell\Big) \leq 0.$$

Here, we apply Theorem 3.2 presented in Ihlenburg in [54]. The idea of this theorem is also presented in several different sources (see, for example, Theorem 3.6 in Cakoni and Colton in [10], Theorem 5.5 from Angell and Kirsch in [6], or Theorem 2.12 from Colton and Kress in [19]). This theorem states that a solution of the variational formulation is unique if $\Im\langle Gu, u\rangle < 0$ holds for all $u \in H^{1/2}(\Gamma_a)$, $u \neq 0$, where $Gu = \dfrac{\partial u}{\partial n}$ on Γ_a, where Γ_a is an artificial boundary enclosing the desired domain. Thus, since

$$\Im\Big(\int_{\mathcal{B}_R} \mathcal{T}_R u\bar{u}d\ell\Big) \leq 0,$$

then $u \equiv 0$.

The application, though, is in the context of the exterior boundary value problem (i.e., $u \equiv 0$ outside of Ω_R). Because we are dealing with an elliptic operator in the form of the modified Helmholtz operator, the solution is analytic. Ihlenburg further mentions that the analytic continuation principle (or unique continuation principle in Cakoni and Colton) can be applied to state $u \equiv 0$ in the interior (i.e. Ω_R). Therefore, $b_{TM}(u, u) = 0$ implies $u = 0$, so the solution is unique, which by the Fredholm alternative implies existence.

Finally, the Fredholm alternative also implies the boundedness of the inverse of $(B_1 + B_2)$, which for constants $D_0, C > 0$ yields

$$\begin{aligned}\|u\| \leq D_0 \|F\| &\leq D_0\Big[\tilde{C}\Big[\,\big\|u^i\big\| + \|\tilde{u}^s\| + \|\tilde{u}\| + \big\|\tilde{\dot{u}}\big\| + \|\varepsilon_r\tilde{u}\|\,\Big]\Big] \\ &= C\Big[\,\big\|u^i\big\| + \|\tilde{u}^s\| + \|\tilde{u}\| + \big\|\tilde{\dot{u}}\big\| + \|\varepsilon_r\tilde{u}\|\,\Big].\end{aligned}$$

This completes the proof.□

Thus, we have established well-posedness of the solution: existence, uniqueness, and an estimate which bounds the solution. From this estimate, a continuous dependence on the initial (or forcing) data can be determined.

V. Finite Element Analysis

5.1 Construction of the Discrete Problem

Now we transition to constructing the discrete problem from the variational formulation in (4.2.1), which will provide the foundation to solve numerically. Consider the following statement from Rjasanow and Steinbach in their book *The Fast Solution of Boundary Integral Equations*:

> When boundary integral equations are approximated and solved numerically , the study of stability and convergence is the most important issue. The most popular methods are the Galerkin methods which perfectly fit to the variational formulation of the boundary integral equations. [89]

Not only does Ihlenburg in his book *Finite Element Analysis of Acoustic Scattering* add this is an area of ongoing research, but he also describes exactly the coupling approach we intend to use:

> In practice, one is not necessarily interested in computing the far-field results directly from the discrete model. Rather, one may use the coupled finite-infinite element discretization to obtain an approximate solution of the near field problem in (the bounded domain). In the second step, one then computes the far-field pattern from the Helmholtz integral equation, using the numerical solution on a "collection surface" in the near field. If such an approach is taken, the discretization with infinite elements is effectively used for "mapping" numerically the far-field behavior onto the near field. [54]

Applying this to our problem, we previously derived an expression for the fields exterior to the cavity in (3.2.10), and also obtained a variational formulation for the near fields in the cavity in the bounded domain (see (4.2.1), (4.2.8), and (4.2.9)). Once the solution is obtained from the bounded problem, it is applied to obtain the

desired expression of the far-field. Clearly, the "collection surface" described above corresponds to our semicircular artificial boundary, $\mathcal{B}_R$.

The finite element method is one of the "most powerful methods for approximating solutions to PDEs" [35]. It is based on the fundamental concept of writing the boundary value problem in weak or variational form, as in (4.2.1), and using the Galerkin method to solve the equation on a finite dimensional subspace V_h of the solution space V, resulting in a linear, finite system of equations. A basis of piecewise polynomials is chosen for the finite dimensional subspace so that the matrix of the linear system is sparse. We will consider three aspects of constructing V_h: the triangulation of the domain, working with functions $v_h \in V_h$ that are "piecewise polynomials", and creating a basis in the space V_h whose functions have small supports that are easy to describe [18].

For the first aspect, we assume the bounded domain Ω_R is covered by a family of quasiuniform triangular subsets. We define $\tau_h = \{K\}$ as the partition (or triangulation or mesh) of Ω_R where each $K \in \tau_h$ represents a triangle (i.e. each finite element). These finite elements form an exact partition of Ω_R; that is, $\Omega_R = \bigcup_{K\in\tau_h} K$ [7].

For an arbitrary triangle K, we denote

$$h_K = \text{diam}(K) = \max\{\|\mathbf{x} - \mathbf{y}\| \mid \mathbf{x}, \mathbf{y} \in K\},$$

which corresponds to the length of the longest side. We further define the mesh size, h, of the partition τ_h, as

$$h = \max_{K\in\tau_h} h_K,$$

and s_K as the diameter of the largest circle inscribed in K [7]. A family of triangulations is *regular* if there exists a constant c_0 such that $h_K/s_K \leq c_0$ for all K and $h \to 0$ [7]. We further note from Atkinson and Han in [7] that a family of triangulations

$\{\tau_h\}$ is quasiuniform if each triangulation τ_h is regular, and there exists a constant c_0 such that

$$\min_{K\in\tau_h} h_K / \max_{K\in\tau_h} h_K \geq c_0.$$

For the second and third aspects in constructing V_h, following [104], we have the finite-dimensional subspace V_h of the test space V:

$$V_h = \{v_h \in H^1(\Omega_R) : v_h|_K \in P_1, K \in \tau_h\},$$

where $\{\phi_j^h(x)\}_{j=1}^N$ is a linear nodal basis of V_h. Each $v_h \in V_h$ is expressed as

$$v_h = \sum_{j=1}^{N} v_j \phi_j^h(x).$$

(That is, each v_h can be written as a linear combination of the basis vectors.) According to Ciarlet in [18], $v_h \in V_h$ is the key to all convergence results, and helps yield simple computations of coefficients. We also note V_h is closed in V and $V_h \to V$ as $h \to 0$.

Therefore, having constructed V_h, the fully discrete problem is to find $u_h^n \in V_h, n = 1, 2, \ldots, N$, such that

$$b_{TM}(u_h^n, v_h) = F^n(v_h) \quad \forall v_h \in V_h, \tag{5.1.1}$$

where $b_{TM}(u_h^n, v_h)$ and $F^n(v_h)$ are defined as in (4.2.8) and (4.2.9), respectively. The bilinear form $b_{TM}(u_h^n, v_h)$ can be written as the sum of a positive definite (coercive) operator and a compact operator, as seen previously for (4.2.12). According to Pomp in [83] and Hildebrandt and Wienholtz in [44], this is equivalent to satisfying a Gårding's inequality; thus, the discrete problem (5.1.1) has a unique solution and Céa's lemma

applies:

$$\|u^n - u_h^n\|_V \leq C \inf_{v_h \in V_h} \|u^n - v_h\|_V . \tag{5.1.2}$$

Furthermore, "for a mesh width $h_0 > 0$ and a constant $C > 0$ such that for all $h < h_0$, the condition of uniform V_h ellipticity applies":

$$|b_{TM}(v_h, v_h)| \geq C \|v_h\|^2 \quad \forall v_h \in V_h,$$

which means the linear system has a unique solution due to the Lax-Milgram lemma, for all $h < h_0$ [44].

This is considered the h-version of the finite element method (and why we write V_h), where we achieve convergence by refining the mesh ($h \to 0$). Another option is to increase the polynomial degree, referred to as the p-version of FEM. It is also possible to combine these methods through an hp-version. Nevertheless, the choice of method depends on the knowledge of regularity of the problem [7]. In addition, since $V_h \subset V$ for each h, this approximation is conforming [75].

5.2 Error Analysis

Recall Céa's lemma, (5.1.2), which simply shows that to estimate the finite solution error (or discretization error) $\|u^n - u_h^n\|_V$, we only need to estimate the approximation error $\|u^n - v_h\|_V$. The infimum portion of Céa's lemma "characterizes the exact solution in the subspace that is spanned by the FE shape functions. If the infimum is reached on an element $v_h \in V_h$, then this element is the best approximation of u^n in the subspace V_h" [54]. We further note that Céa's lemma is a quasioptimal error estimate because up to constant C, the discretization error is bounded by the approximation error. An optimal estimate would be $C = 1$ [75].

It is clear the Galerkin method is tied directly to the H^1 or energy norm, so we

would expect the best approximation to the solution to be measured in this norm [36]. H^1 error norm is "relevant for exterior problems if one is interested in the far-field response" [54]. Recall that we are computing the scattered field from a boundary integral equation in the exterior of the cavity, where we will use the finite element data on the artificial boundary (or collecting surface), $\mathcal{B}_R$. Ihlenburg adds that "since this integral equation involves u and its normal derivative, the H^1 error norm is appropriate for error control in the near field. The situation is different for interior problems. Here, the L^2 error norm may be more appropriate for error control" [54].

However, the L^2 space is not always well-suited for approximating functions in regions which are rapidly oscillating with small amplitudes. Small details may be lost, so H^1 incorporates not only the difference in the functions but also in the gradients [38]. Therefore, in the context of the solution to the interior problem, our goal is to quantify the finite solution error $\|u^n - u_h^n\|$ in both the L^2 and H^1 norms.

In general, there are two types of error estimation: *a priori* and *a posteriori*. An *a priori* estimate is the "error to be expected in a computation to be done," whereas *a posteriori* estimates are "generated in the course of computation" [87]. More specifically, according to Ihlenburg, *a priori* error estimation is descibed as follows :

> The error function is estimated in a suitable functional norm *without quantitative input from the computed solution.* The estimates are based on the approximation properties of the subspace where the numerical solution is sought and on the stability properties of the differential operator or variational form. The estimates are generally global; i.e., the error function is estimated in an integral norm computed over the whole solution domain. [54]

He adds that *a posteriori* error estimation can be described as follows:

> The error function is estimated *employing the computed solution of the discrete model* as data for the estimates. In practice, the estimates are usually part of an adaptive mesh refinement methodology. For mesh refinement, one needs local information on the error. *A posteriori* error estimation should therefore be given in a norm that is defined on a single element or on a patch of adjacent elements. [54]

Furthermore, the *a priori* error bounds are asymptotic, not absolute. That is, "the bounds will not tell how small the error is when the solution is approximated on a particular mesh. Instead, the bounds show how the error decreases as the mesh is refined" [36]. Accordingly, local mesh adaptation is not used. This is in contrast to *a posteriori* error bounds, which are expressed in terms of residuals of approximate solution, not in terms of powers of a mesh size or constants depending on the exact solution. [87]. Therefore, we are providing only *a priori* error estimates.

Up to now, we have not determined the symmetry of the sesquilinear term $b_{TM}(u, v)$. It has not been a factor for the existence and uniqueness proofs, so in order to establish the error bounds for the L^2 and H^1 norms, we will follow [92] and assume the more general case that $b_{TM}(u, v)$ is nonsymmetric, but is still bounded as before.

In addition, the following theorem, which is similar to one presented by Van and Wood in [105], will determine uniform convergence estimates:

Theorem 5.2.1 *Let $u^n \in V$ and $u_h^n \in V_h$ be the solutions to* (4.2.1) *and* (5.1.1)*, respectively, for $F^n \in V'$. Given $\epsilon > 0$, there exists an $h_0 = h_0(\epsilon)$ such that for all $0 < h < h_0$, then*

$$\|u^n - u_h^n\|_{L^2(\Omega_R)} \leq \epsilon \|u^n - u_h^n\|_V . \tag{5.2.1}$$

Furthermore, if given $\epsilon > 0$, there exists an $h_1 = h_1(\epsilon)$ such that for all $0 < h < h_1$, then

$$\|u^n - u_h^n\|_V \leq C\epsilon \|F^n\|_{L^2(\Omega_R)} \tag{5.2.2}$$

for some positive constant C independent of h. It follows that

$$\|u^n - u_h^n\|_{L^2(\Omega_R)} \leq C\epsilon^2 \|F^n\|_{L^2(\Omega_R)}. \tag{5.2.3}$$

Also we will use the following Lemmas, the first of which is proven in both [92] and [105], and the second is proven in [92]:

Lemma 5.2.2 *Let $D = \{f : f \in L^2(\Omega_R), \|f\|_{L^2(\Omega_R)} = 1\}$ be the unit sphere in $L^2(\Omega_R)$. For $f \in D$, let W be the set of solutions $w \in V$ to the auxiliary / adjoint bilinear form*

$$b_{TM}(w, v) = \langle f, v \rangle \qquad \forall v \in V.$$

Then W is compact in V.

Lemma 5.2.3 *Let V be a fixed compact subset of $H^1(\Omega_R)$. Then given any $\epsilon > 0$, there exists an $h_0 = h_0(\epsilon, V)$ such that for each $u \in V$ and each $0 < h < h_0$, there exists a $v_h \in V_h$ satisfying*

$$\|u - v_h\|_V \leq \epsilon.$$

Proof of Theorem 5.2.1:

We use an Aubin-Nitsche duality argument, assuming $b_{TM}(u, v)$ is nonsymmetric, and follow the reasoning in [92] and [105]. Let $b_{TM}^*(\cdot, \cdot)$ be the adjoint bilinear form to $b_{TM}(\cdot, \cdot)$ defined by

$$b_{TM}^*(u, v) = b_{TM}(v, u) \quad \forall u, v \in V.$$

We know

$$b_{TM}^*(w^*, v) = \langle g, v \rangle \quad \forall v \in V$$

has a unique solution for all $g \in L^2(\Omega_R)$, and

$$\|w^*\|_V \leq c \|g\|_{L^2(\Omega_R)}.$$

If we view $u^n - u_h^n$ as a linear functional in $L^2(\Omega_R)$, then

$$\|u^n - u_h^n\|_{L^2(\Omega_R)} = \sup_{\|g\|_{L^2(\Omega_R)}=1} \langle u^n - u_h^n, g \rangle.$$

Then, for $v_h \in V_h$, we have

$$\begin{aligned}
\langle g, u^n - u_h^n \rangle &= \langle u^n - u_h^n, g \rangle \\
&= b_{TM}^*(w^*, u^n - u_h^n) \\
&= b_{TM}^*(w^* - v_h, u^n - u_h^n) + b_{TM}^*(v_h, u^n - u_h^n) \\
&= b_{TM}(u^n - u_h^n, w^* - v_h) + b_{TM}(u^n - u_h^n, v_h) \\
&= b_{TM}(u^n - u_h^n, w^* - v_h) \\
&\leq c \|u^n - u_h^n\|_V \|w^* - v_h\|_V .
\end{aligned}$$

By using an approximation property argument from Strang and Fix in [99], we can choose v_h such that $\|w^* - v_h\|_V \leq \epsilon \|w^*\|_V$. Therefore,

$$\begin{aligned}
\langle u^n - u_h^n, g \rangle &\leq c \|u^n - u_h^n\|_V \epsilon \|w^*\|_V \\
&\leq c_1 \|u^n - u_h^n\|_V \epsilon c_2 \|g\|_{L^2(\Omega_R)} \\
\sup_{\|g\|_{L^2(\Omega_R)}=1} \langle u^n - u_h^n, g \rangle &\leq \sup_{\|g\|_{L^2(\Omega_R)}=1} c_1 \|u^n - u_h^n\|_V \epsilon c_2 \|g\|_{L^2(\Omega_R)} \\
\|u^n - u_h^n\|_{L^2(\Omega_R)} &\leq C\epsilon \|u^n - u_h^n\|_V .
\end{aligned}$$

which shows (5.2.1). To show the second estimate (5.2.2), as in [92] and [105], we set

$$\hat{F}^n = \frac{F^n}{\|F^n\|_{L^2(\Omega_R)}}, \qquad \hat{u}^n = \frac{u^n}{\|F^n\|_{L^2(\Omega_R)}}, \qquad \hat{u}_h^n = \frac{u_h^n}{\|F^n\|_{L^2(\Omega_R)}}.$$

Then we have the corresponding variational problems

$$b_{TM}(\hat{u}^n, v) = \hat{F}^n(v) \quad \forall v \in V,$$
$$b_{TM}(\hat{u}_h^n, v_h) = \hat{F}^n(v_h) \quad \forall v_h \in V_h,$$

for which we apply Céa's lemma,

$$\|\hat{u}^n - \hat{u}_h^n\|_V \leq C \inf_{v_h \in V_h} \|\hat{u}^n - v_h\|_V .$$

From Lemma 5.2.2, the set of solutions for $b_{TM}(\hat{u}^n, v) = \hat{F}^n(v), \quad \left\|\hat{F}^n\right\|_{L^2(\Omega_R)} = 1,$ is compact in V, thus we can apply the density argument in Lemma 5.2.3 to get

$$\inf_{v_h \in V_h} \|\hat{u}^n - v_h\|_V \leq \epsilon$$

for $0 < h < h_0(\epsilon, \hat{u}^n)$. Thus we conclude that

$$\|\hat{u}^n - \hat{u}_h^n\|_V \leq C\epsilon.$$

Since $\|\hat{u}^n - \hat{u}_h^n\|_V = \dfrac{\|u^n - u_h^n\|_V}{\|F^n\|_{L^2(\Omega_R)}}$, then

$$\|u^n - u_h^n\|_V \leq C\epsilon \|F^n\|_{L^2(\Omega_R)} .\square$$

In summary, we are generating *a priori* error estimates, and are simply applying previously established theory to confirm the error bounds for our problem.

5.3 Stability Analysis

For stability analysis, we initially follow Van and Wood in [105] precisely and express the Newmark scheme in a three-step formulation. We start with the discretized PDE:

$$\begin{aligned}-\Delta u^{n+2} + \alpha^2 \varepsilon_r u^{n+2} &= \alpha^2 \varepsilon_r \tilde{u}^{n+2} \\ &= \alpha^2 \varepsilon_r \Big[u^{n+1} + \delta t \dot{u}^{n+1} + \frac{(\delta t)^2}{2}(1-2\beta)\ddot{u}^{n+1} \Big].\end{aligned}$$

Using (3.1.7) to remove $\dot{u}^{n+1}$ and (3.1.4) to remove $\tilde{\ddot{u}}^{n+1}$, we obtain

$$\begin{aligned}&-\Delta u^{n+2} + \alpha^2 \varepsilon_r u^{n+2} \\ &\qquad = \alpha^2 \varepsilon_r \Big[u^{n+1} + \delta t \dot{u}^{n} + (\delta t)^2(1-\gamma)\ddot{u}^{n} + (\delta t)^2 \gamma \ddot{u}^{n+1} + \frac{(\delta t)^2}{2}(1-2\beta)\ddot{u}^{n+1} \Big].\end{aligned}$$

Using (3.1.3) to remove $\dot{u}^n$, followed by using (3.1.6) to remove $\ddot{u}^{n+1}$ and $\ddot{u}^{n+1}$ separately, and finally applying (3.1.5) to remove $\tilde{u}^{n+1}$ and $\tilde{u}^n$ separately, we obtain

$$\beta \Delta u^{n+2} + (\frac{1}{2} - 2\beta + \gamma)\Delta u^{n+1} + (\frac{1}{2} + \beta - \gamma)\Delta u^n = \beta \alpha^2 \varepsilon_r (u^{n+2} - 2u^{n+1} + u^n).$$

Therefore, the final variational form of this equation, fully discretized in both space and time, using $u_h^n \in V_h$, is

$$\begin{aligned}&\frac{1}{(\delta t)^2}\Big(\varepsilon_r(u_h^{n+2} - 2u_h^{n+1} + u_h^n), v_h\Big) \\ &+ a\Big(\beta \Delta u_h^{n+2} + (\frac{1}{2} - 2\beta + \gamma)\Delta u_h^{n+1} + (\frac{1}{2} + \beta - \gamma)\Delta u_h^n, v_h\Big) \\ &= \beta G^{n+2}(v_h) + (\frac{1}{2} - 2\beta + \gamma)G^{n+1}(v_h) + (\frac{1}{2} + \beta - \gamma)G^n(v_h) \quad \forall v_h \in V_h.\end{aligned} \tag{5.3.1}$$

This is an expected result in the literature, as seen in Van and Wood in [105], Quarteroni and Valli in [85], and Allaire in [4]. We further define for our problem

$$a(u_h^n, v_h) = \int_{\Omega_R} \nabla u_h^n \cdot \nabla v_h dxdy - \int_{\mathcal{B}_R} \mathcal{T}_R u_h^n v_h d\ell + \frac{\mu}{\eta} \delta t \gamma \alpha^2 \int_S u_h^n v_h d\ell$$

and

$$G^n(v) = \int_{\mathcal{B}_R} J^n v_h d\ell - \int_{\mathcal{B}_R} \Psi_R \tilde{u}^{s,n} v_h d\ell + \frac{\mu}{\eta} \delta t \gamma \alpha^2 \int_S \tilde{u}^n v_h d\ell - \frac{\mu}{\eta} \int_S \tilde{u}^n v d\ell.$$

We note that $a(u_h^n, v_h)$ is symmetric, but not strictly coercive. Therefore, as in the previous section, we rewrite $a(u_h^n, v_h) = a_1(u_h^n, v_h) + a_2(u_h^n, v_h)$ as the sum of a coercive term,

$$a_1(u_h^n, v_h) = \int_{\Omega_R} \nabla u_h^n \cdot \nabla v_h dxdy - \int_{\mathcal{B}_R} \mathcal{T}_{R,P} u_h^n v_h d\ell$$

and a compact term,

$$a_2(u_h^n, v_h) = -\int_{\mathcal{B}_R} \big(\mathcal{T}_R - \mathcal{T}_{R,P}\big) u_h^n v_h d\ell + \frac{\mu}{\eta} \delta t \gamma \alpha^2 \int_S u_h^n v_h d\ell.$$

Therefore, as cited earlier in Pomp in [83], as well as Lemma 22.38 in Zeidler in [117], $a(u_h^n, v_h)$ satisfies a Gårding's inequality. That is, there exists two positive constants $\kappa > 0$ (Zeidler says $\kappa \in \mathbb{R}$) and $\nu > 0$ such that

$$a(u, u) + \kappa \|u\|_{L^2}^2 > \nu \|u\|_V^2 \quad \forall u \in V. \tag{5.3.2}$$

Therefore, the term $a(u_h^n, v_h)$ is symmetric and satisfies a Gårding's inequality. Therefore, according to Allaire in [4], the eigenvalue problem

$$a(w_h, v_h) = \lambda_h \langle w_h, v_h \rangle \quad \forall v_h \in V_h$$

has a finite number of eigenvalues satisfying

$$-\kappa \leq \lambda_{h,1} \leq \lambda_{h,2} \leq \cdots \leq \lambda_{h,M} < \infty,$$

where dim $V_h = M$ for corresponding orthonormal eigenvectors $w_{h,1}, w_{h,2}, \cdots, w_{h,M}$. As in [105], writing $w_i = w_{h,i}$ and $\lambda_i = \lambda_{h,i}$, and replacing w_i for v_h in (5.3.1), we have

$$a(u_h^n, w_i) = a(w_i, u_h^n) = \lambda_i \langle w_i, u_h^n \rangle = \lambda_i \langle u_h^n, w_i \rangle.$$

This is also equivalent to, in referring to (5.3.2), as

$$a(u_h^n, w_i) + \kappa \langle u_h^n, w_i \rangle = \lambda_i \langle u_h^n, w_i \rangle + \kappa \langle u_h^n, w_i \rangle = (\lambda_i + \kappa) \langle u_h^n, w_i \rangle$$

and

$$\begin{aligned} &\frac{1}{(\delta t)^2} \Big(\varepsilon_r (u_h^{n+2} - 2u_h^{n+1} + u_h^n), w_i \Big) \\ &+ (\lambda_i + \kappa) \Big(\beta \Delta u_h^{n+2} + (\frac{1}{2} - 2\beta + \gamma) \Delta u_h^{n+1} + (\frac{1}{2} + \beta - \gamma) \Delta u_h^n, w_i \Big) \\ &= \beta G^{n+2}(w_i) + (\frac{1}{2} - 2\beta + \gamma) G^{n+1}(w_i) + (\frac{1}{2} + \beta - \gamma) G^n(w_i) \\ &\equiv G^*. \end{aligned} \tag{5.3.3}$$

Without loss of generality, we further assume $\varepsilon_r = 1$ and $G^* = 0$, and from [105], we have the eigenvalue equation: find λ_h and $u_h \in V_h$ such that

$$a(u_h, v_h) + \kappa \langle u_h, v_h \rangle = (\lambda_h + \kappa) \langle u_h, v_h \rangle_{L^2_{\varepsilon_r}(\Omega_R)} \quad \forall v_h \in V_h. \tag{5.3.4}$$

Now we have that $a(\cdot, \cdot) + \kappa(\cdot, \cdot)$ is coercive, so we have $\lambda_i + \kappa > 0$, where the

corresponding orthonormal eigenvectors satisfy

$$(w_i, w_j)_{L^2_{\tilde{\varepsilon}_r}(\Omega_R)} = \delta_{ij}$$

Hence, by replacing $u_h^n = \sum_{i=1}^{M} u_i^n w_{h,i}$ into (5.3.3), we get for $i = 1, 2, ..., M$,

$$\begin{aligned} &\frac{1}{(\delta t)^2}\Big(u_i^{n+2} - 2u_i^{n+1} + u_i^n\Big) \\ &+ (\lambda_i + \kappa)\Big(\beta \Delta u_i^{n+2} + (\frac{1}{2} - 2\beta + \gamma)\Delta u_i^{n+1} + (\frac{1}{2} + \beta - \gamma)\Delta u_i^n\Big) = 0. \end{aligned} \tag{5.3.5}$$

We rewrite this three-level scheme as

$$\begin{aligned} u_i^{n+2} &= \frac{2 - (\lambda_i + \kappa)(\delta t)^2(\frac{1}{2} - 2\beta + \gamma)}{1 + (\lambda_i + \kappa)(\delta t)^2\beta} u_i^{n+1} - \frac{1 + (\lambda_i + \kappa)(\delta t)^2(\frac{1}{2} + \beta - \gamma)}{1 + (\lambda_i + \kappa)(\delta t)^2\beta} u_i^n \\ &\equiv b_{11} u_i^{n+1} - b_{12} u_i^n. \end{aligned}$$

Thus, (5.3.5) can be written in matrix form as

$$\begin{bmatrix} u_i^{n+2} \\ u_i^{n+1} \end{bmatrix} = \begin{bmatrix} b_{11} & -b_{12} \\ 1 & 0 \end{bmatrix} \begin{bmatrix} u_i^{n+1} \\ u_i^n \end{bmatrix} \equiv B_i \begin{bmatrix} u_i^{n+1} \\ u_i^n \end{bmatrix},$$

where B_i denotes the iteration matrix, and for stability, the Von Neumann necessary condition is $\rho(B_i) \leq 1$ where the spectral radius $\rho(B_i)$ denotes the maximum modulus

of the eigenvalues of B_i. Therefore, we consider the characteristic equation of B_i:

$$\begin{aligned}\det(\zeta I - B_i) &= \det\left\{\begin{bmatrix}\zeta & 0\\ 0 & \zeta\end{bmatrix} - \begin{bmatrix}b_{11} & -b_{12}\\ 1 & 0\end{bmatrix}\right\} = 0\\ &= \det\left\{\begin{bmatrix}\zeta - b_{11} & b_{12}\\ -1 & \zeta\end{bmatrix}\right\} = 0\\ &= \zeta^2 - \zeta b_{11} + b_{12} = 0.\end{aligned}$$

and calculate the roots of this equation which are the eigenvalues of the matrix B_i. The roots are

$$\zeta_{1,2} = \frac{b_{11} \pm \sqrt{b_{11}^2 - 4b_{12}}}{2}.$$

In order to analyze when $|\zeta_1|, |\zeta_2| \leq 1$, we must calculate the discriminant, Δ:

$$\begin{aligned}\Delta &= b_{11}^2 - 4b_{12}\\ &= \left[\frac{2 - (\lambda_i + \kappa)(\delta t)^2(\frac{1}{2} - 2\beta + \gamma)}{1 + (\lambda_i + \kappa)(\delta t)^2\beta}\right]^2 - 4\left[\frac{1 + (\lambda_i + \kappa)(\delta t)^2(\frac{1}{2} + \beta - \gamma)}{1 + (\lambda_i + \kappa)(\delta t)^2\beta}\right]\\ &= \frac{-4(\lambda_i + \kappa)(\delta t)^2 + (\lambda_i + \kappa)^2(\delta t)^4[(\gamma + 0.5)^2 - 4\beta]}{[1 + (\lambda_i + \kappa)(\delta t)^2\beta]^2}.\end{aligned}$$

This expression is confirmed in Allaire in [4]. Since the denominator is always positive, in analyzing the sign of Δ, without loss of generality, we will assume henceforth that

$$\Delta = -4(\lambda_i + \kappa)(\delta t)^2 + (\lambda_i + \kappa)^2(\delta t)^4\Big[\big(\gamma + \frac{1}{2}\big)^2 - 4\beta\Big].$$

Consider, then, the following two cases: *Case 1:* $\Delta \leq 0$

This implies that the roots ζ_1, ζ_2 are complex conjugates, so we require

$$|\zeta_1| = |\zeta_2| = \left| \frac{b_{11}}{2} + \frac{\sqrt{-1}\sqrt{b_{11}^2 - 4b_{12}}}{2} \right| = \sqrt{\frac{b_{11}^2}{4} - \frac{b_{11}^2 - 4b_{12}}{4}} = \sqrt{b_{12}} \leq 1.$$

Thus, if $b_{12} \leq 1$, then

$$b_{12} = \frac{1 + (\lambda_i + \kappa)(\delta t)^2(\frac{1}{2} + \beta - \gamma)}{1 + (\lambda_i + \kappa)(\delta t)^2 \beta} \leq 1,$$

which is equivalent to $\frac{1}{2} + \beta - \gamma \leq \beta$, or $\gamma \geq \dfrac{1}{2}$. As a result, we have that for this case,

$$(\lambda_i + \kappa)(\delta t)^2 \Big[\big(\gamma + \frac{1}{2}\big)^2 - 4\beta \Big] \leq 4 \;\Rightarrow\; \gamma \geq \frac{1}{2}.$$

Case 2: $\Delta > 0$

This is

$$(\lambda_i + \kappa)(\delta t)^2 \Big[\big(\gamma + \frac{1}{2}\big)^2 - 4\beta \Big] > 4.$$

Then, without loss of generality, we assume $\zeta_1 < \zeta_2$, so we require

$$-1 \leq \zeta_1 = \frac{b_{11}}{2} - \frac{\sqrt{\Delta}}{2} < \frac{b_{11}}{2} + \frac{\sqrt{\Delta}}{2} = \zeta_2 \leq 1.$$

For $-1 \leq \zeta_1$, we have

$$-1 \leq \frac{b_{11}}{2} - \frac{\sqrt{\Delta}}{2} \Rightarrow 1 + b_{12} \geq -b_{11}.$$

Whereas for $\zeta_2 \leq 1$ we have

$$\frac{b_{11} + \sqrt{\Delta}}{2} \leq 1 \Rightarrow 1 + b_{12} \geq b_{11}.$$

These together imply that $1 + b_{12} \geq |b_{11}|$. However, we see that this results in two

inequalities that must be satisfied [105]. For $1 + b_{12} \geq -b_{11}$, we have

$$\frac{1}{(\lambda_i + \kappa)(\delta t)^2} \geq \frac{\gamma}{2} - \beta,$$

but for $1 + b_{12} \geq b_{11}$ we have

$$\frac{1}{(\lambda_i + \kappa)(\delta t)^2} \geq \frac{\gamma}{2} - \beta - \frac{1}{4}.$$

Therefore, in order to satisfy both inequalities, we can reduce this to

$$\frac{1}{(\lambda_i + \kappa)(\delta t)^2} \geq \frac{\gamma}{2} - \beta.$$

To summarize, for *Case 1* ($\Delta \leq 0$), we have

$$(\lambda_i + \kappa)(\delta t)^2\Big[\big(\gamma + \frac{1}{2}\big)^2 - 4\beta\Big] \leq 4 \quad \text{implies} \quad \gamma \geq \frac{1}{2}.$$

Whereas for *Case 2* ($\Delta > 0$) we have

$$(\lambda_i + \kappa)(\delta t)^2\Big[\big(\gamma + \frac{1}{2}\big)^2 - 4\beta\Big] > 4 \quad \text{implies} \quad (\lambda_i + \kappa)(\delta t)^2(2\gamma - 4\beta) \leq 4.$$

We further assume that $\beta \geq 0$ and $\gamma \geq \frac{1}{2}$. In fact, it is shown in Dautray and Lions that the scheme is unstable for $\gamma < \frac{1}{2}$ [24]. We first observe the property that $(\lambda_i + \kappa)(\delta t)^2 > 0$. Thus, if $\Big[\big(\gamma + \frac{1}{2}\big)^2 - 4\beta\Big] < 0$, then only Case 1 applies. If $\Big[\big(\gamma + \frac{1}{2}\big)^2 - 4\beta\Big] \geq 0$, then we have stability as long as $(2\gamma - 4\beta) \leq 0$. These statements can be combined to deduce that we have unconditional stability for $\gamma \leq 2\beta$ for arbitrary δt. However, if $\gamma > 2\beta$, then we require

$$\max_i (\lambda_i + \kappa)(\delta t)^2 \leq \frac{4}{(2\gamma - 4\beta)},$$

which is a conditional situation that depends on finding $\max_i \lambda_i$ and κ.

It can also be shown that when $\gamma = \frac{1}{2}$, a conditional stability arises dependent on finding the values of λ_i and κ. Also, Van and Wood state that $\gamma = \frac{1}{2}$ is not always the best value to use, and that in practice, a value of $\gamma > \frac{1}{2}$ "is often used to damp out the higher frequencies while preserving the more accurate lower ones" [105].

Therefore, we can summarize these results in a theorem:

Theorem 5.3.1 *The Newmark scheme for the TM variational problem is unconditionally stable for arbitrary $\delta t > 0$ satisfying*

$$2\beta \geq \gamma > \frac{1}{2}.$$

As with the error analysis section, during our stability analysis we have built upon existing theory and analysis, and refined it to apply to our problem.

VI. Numerical Simulation

6.1 Finite Element Approximation

The goal in this section is to set the framework for the numerical implementation. Starting with the triangulation and basis as described earlier, the fully discrete problem is to find $u_h^{n+1} \in V_h, n = 1, 2, \ldots, N$, such that

$$b_{TM}(u_h^{n+1}, v_h) = F^{n+1}(v_h) \quad \forall v_h \in V_h, \tag{6.1.1}$$

where $b_{TM}(u_h^{n+1}, v_h)$ and $F^{n+1}(v_h)$ are defined as in (4.2.8) and (4.2.9), respectively.

Since each $v_h \in V_h$ and $u_h^{n+1} \in V_h$ is expressed as

$$v_h = \sum_{j=1}^{N} v_j \phi_j^h.$$

and

$$u_h^{n+1} = \sum_{i=1}^{N} u_i^{n+1} \phi_i^h,$$

then

$$b_{TM}(\sum_{i=1}^{N} u_i^{n+1} \phi_i^h, \sum_{j=1}^{N} v_j \phi_j^h) = F^{n+1}(\sum_{j=1}^{N} v_j \phi_j^h).$$

Due to linearity, this yields

$$\sum_{j=1}^{N} v_j b_{TM}(\sum_{i=1}^{N} u_i^{n+1} \phi_i^h, \phi_j^h) = \sum_{j=1}^{N} v_j F^{n+1}(\phi_j^h).$$

In order for equality to hold for all v_j, it follows that

$$b_{TM}(\sum_{i=1}^{N} u_i^{n+1} \phi_i^h, \phi_j^h) = F^{n+1}(\phi_j^h) \quad \text{for } j = 1, ..., N.$$

Applying linearity again yields

$$\sum_{i=1}^{N} b_{TM}(\phi_i^h, \phi_j^h) u_i^{n+1} = F^{n+1}(\phi_j^h) \quad \text{for } j = 1, ..., N.$$

Then, referring to (4.2.8) to discretize $b_{TM}(\phi_i^h, \phi_j^h)$, we obtain the matrix equation:

$$\sum_{i=1}^{N} ([K]_{ji} + \alpha^2 [M]_{ji} + \frac{\mu}{\eta} \delta t \gamma \alpha^2 [P]_{ji} + [Q]_{ji}) u_i^{n+1} = F_j^{n+1} \quad \text{for } j = 1, ..., N. \tag{6.1.2}$$

Here we define the stiffness matrix

$$[K]_{ji} = \int_{\Omega_R} \nabla \phi_i^h \cdot \nabla \phi_j^h dx dy, \tag{6.1.3}$$

the mass matrix

$$[M]_{ji} = \int_{\Omega_R} \varepsilon_r \phi_i^h \phi_j^h dx dy, \tag{6.1.4}$$

the boundary matrix

$$[P]_{ji} = \int_S \phi_i^h \phi_j^h d\ell, \tag{6.1.5}$$

and the artificial boundary matrix

$$[Q]_{ji} = -\int_{\mathcal{B}_R} \mathcal{T}_R \phi_i^h \phi_j^h d\ell. \tag{6.1.6}$$

The right-hand side vector F_j^{n+1} is

$$\begin{aligned} F_j^{n+1} = & \int_{\mathcal{B}_R} (\frac{\partial u^{i,n+1}}{\partial n} - \mathcal{T}_R u^{i,n+1}) \phi_j^h d\ell - \int_{\mathcal{B}_R} \Psi_R \tilde{u}^{s,n+1} \phi_j^h d\ell \\ & + \frac{\mu}{\eta} \delta t \gamma \alpha^2 \int_S \tilde{u}^{n+1} \phi_j^h d\ell - \frac{\mu}{\eta} \int_S \tilde{u}^{n+1} \phi_j^h d\ell + \alpha^2 \int_{\Omega_R} \varepsilon_r \tilde{u}^{n+1} \phi_j^h dx dy. \end{aligned} \tag{6.1.7}$$

While the stiffness, mass, and boundary matrix expressions are straightforward

for the left-hand side of the equation, the artificial boundary matrix is more difficult to evaluate. Here, we refer to Steinbach's work in which he addresses "defining a computable approximation of the Steklov-Poincarè operator" [96]. The advantage of his approach is that it is a symmetric approximation that does not involve the hypersingular operator. Referring back to (3.4.15), we have

$$\mathcal{T}_R = S^{-1} Z S^{-1}$$

where $Z = (\frac{1}{2}I + D)S$ and $Z : H^{-1/2}(\mathcal{B}_R) \to H^{1/2}(\mathcal{B}_R)$. We further define for $\varphi(\boldsymbol{r'}) = \dfrac{\partial u(\boldsymbol{r'})}{\partial \boldsymbol{n}_{\boldsymbol{r'}}}$,

$$(Z\varphi)(\boldsymbol{r}) = \frac{1}{2}\int_{\mathcal{B}_R} G(\boldsymbol{r}|\boldsymbol{r'})\varphi(\boldsymbol{r'})d\theta' + \int_{\mathcal{B}_R} \frac{\partial G(\boldsymbol{r}|\boldsymbol{r'})}{\partial \boldsymbol{n}_{\boldsymbol{r'}}} \int_{\mathcal{B}_R} G(\boldsymbol{r'}|\boldsymbol{s'})\varphi(\boldsymbol{s'})d\theta'_{s'}d\theta'. \quad (6.1.8)$$

Thus, Z admits a direct Galerkin discretization.

We also need to further define X_h and Y_h, where X_h is the space of traces of finite elements $v_h \in V_h \subset V = H^1(\Omega_R)$ and Y_h is its dual space. Thus, we have the spaces of trial functions:

$$X_h = \text{span}\{\phi_k\}_{k=1}^N \subset H^{1/2}(\mathcal{B}_R),$$
$$Y_h = \text{span}\{\psi_k\}_{k=1}^N \subset H^{-1/2}(\mathcal{B}_R).$$

We see that X_h is the approximation of $u|_{\mathcal{B}_R}$, consisting of continuous piecewise linear functions, and Y_h is the approximation of $\partial_n u|_{\mathcal{B}_R}$, consisting of constant basis functions. Furthermore, the "piecewise constant boundary functions can represent the Neumann derivatives of the piecewise linear functions exactly" [45].

Therefore, in order to evaluate

$$[Q]_{ji} = -\langle \mathcal{T}_R \phi_i^h, \phi_j^h \rangle = -\langle S^{-1} Z S^{-1} \phi_i^h, \phi_j^h \rangle = -I_h^\top S_h^{-1} Z_h S_h^{-1} I_h,$$

we can define

$$[S_h]_{\tilde{l},\tilde{k}} = \langle S\psi_{\tilde{k}}^h, \psi_{\tilde{l}}^h \rangle_{L^2(\mathcal{B}_R)}, \tag{6.1.9}$$

$$[Z_h]_{\tilde{l},\tilde{k}} = \langle Z\psi_{\tilde{k}}^h, \psi_{\tilde{l}}^h \rangle_{L^2(\mathcal{B}_R)}, \tag{6.1.10}$$

$$[I_h]_{i,\tilde{l}} = \langle \phi_i^h, \psi_{\tilde{l}}^h \rangle_{L^2(\mathcal{B}_R)}. \tag{6.1.11}$$

Therefore, the artificial boundary matrix and consequently the left-hand side admits a Galerkin discretization.

We now describe how to assemble and compute the single layer potential matrix, S. The technique described can also be applied in constructing Z. We follow the technique of Van and Wood in [104] using a standard quadrature with the midpoint formula:

$$\begin{aligned}
[S_h]_{\tilde{l},\tilde{k}} &= \langle S\psi_{\tilde{k}}^h, \psi_{\tilde{l}}^h \rangle_{L^2(\mathcal{B}_R)} \\
&= \int_{\mathcal{B}_{\tilde{l}}} \psi_{\tilde{l}}^h(\boldsymbol{r}) \int_{\mathcal{B}_{\tilde{k}}} G(\boldsymbol{r}|\boldsymbol{r'}) \psi_{\tilde{k}}^h(\boldsymbol{r'}) d\boldsymbol{r'} d\boldsymbol{r}.
\end{aligned}$$

If we divide the segments on the artificial boundary as $\mathcal{B}_{\tilde{k}} = (\boldsymbol{r}_{\tilde{k}}, \boldsymbol{r}_{\tilde{k}+1})$ and $\mathcal{B}_{\tilde{l}} = (\boldsymbol{r}_{\tilde{l}}, \boldsymbol{r}_{\tilde{l}+1})$, we then further define $\xi_{\tilde{k}} = \dfrac{\boldsymbol{r}_{\tilde{k}+1} + \boldsymbol{r}_{\tilde{k}}}{2}$ and $\xi_{\tilde{l}} = \dfrac{\boldsymbol{r}_{\tilde{l}+1} + \boldsymbol{r}_{\tilde{l}}}{2}$. Now, applying the quadrature using this midpoint formula, and noting that the basis functions are

piecewise constant over the segment with a value of 1, for $\mathcal{B}_{\tilde{k}} \neq \mathcal{B}_{\tilde{l}}$ we have

$$\int_{\mathcal{B}_{\tilde{l}}} \psi_{\tilde{l}}^{h}(\boldsymbol{r}) \int_{\mathcal{B}_{\tilde{k}}} G(\boldsymbol{r}|\boldsymbol{r'}) \psi_{\tilde{k}}^{h}(\boldsymbol{r'}) d\boldsymbol{r'} d\boldsymbol{r} \approx G(\xi_{\tilde{k}}|\xi_{\tilde{l}}).$$

Now considering the case along the diagonal of the matrix S, or when $\mathcal{B}_{\tilde{k}} = \mathcal{B}_{\tilde{l}}$, or $\xi_{\tilde{k}} = \xi_{\tilde{l}}$, we will have singularities for the first two terms in the Green's function (3.3.7). We will address this as Van and Wood did in [104] and have

$$\int_{\mathcal{B}_{\tilde{l}}} \psi_{\tilde{l}}^{h}(\boldsymbol{r}) \int_{\mathcal{B}_{\tilde{k}}} K_0(\alpha|\boldsymbol{r} - \boldsymbol{r'}) \psi_{\tilde{k}}^{h}(\boldsymbol{r'}) d\boldsymbol{r'} d\boldsymbol{r} \approx \frac{2}{\alpha} \int_{0}^{\frac{\alpha\left|\mathcal{B}_{\tilde{l}}\right|}{2}} K_0(\tau) d\tau.$$

and the remaining terms of the Green's function in (3.3.7) can be evaluated as described in Section 3.5. Also, the above expression can be evaluated exactly as provided in [1] for the term

$$\int_{0}^{x} K_0(\tau) d\tau.$$

Therefore, we have S as a square, dense boundary element matrix of size $\tilde{l} \times \tilde{k}$. This matrix is invertible and each entry element will have a real and imaginary portion, if we include the third term of the Green's function in (3.3.7). The same holds for the matrices Z and I. These three matrices will ultimately determine the artificial boundary matrix, Q, as described in (6.1). Because the dimensions of Q are not the same as the stiffness, mass, and boundary matrices, we can standardize it to the other dimensions using a process described in detail by Jin in [55]. The difference between the artificial boundary matrix and the boundary matrix is that the artificial boundary matrix reflects the fact that each boundary element interacts with every other boundary element, hence the dense square matrix. The boundary matrix, however, reflects the fact that each boundary element interacts only with adjacent boundary elements.

In analyzing the right-hand side of the equation given by (6.1.7), we first note as in [104] that $\tilde{u}^{n+1} \approx \sum_{i=1}^{N} \tilde{u}_i^{n+1}\phi_i^h$, so

$$\alpha^2 \int_{\Omega_R} \varepsilon_r \tilde{u}^{n+1}\phi_j^h dxdy \approx \sum_{i=1}^{N} \tilde{u}^{n+1} \int_{\Omega_R} \varepsilon_r \phi_i^h \phi_j^h dxdy = \sum_{i=1}^{N} [M]_{ji}\tilde{u}_i^{n+1}. \tag{6.1.12}$$

Similarly, we have $\tilde{\dot{u}}^{n+1} \approx \sum_{i=1}^{N} \tilde{\dot{u}}_i^{n+1}\phi_i^h$, which implies we also have the terms

$$\frac{\mu}{\eta}\delta t\gamma\alpha^2 \int_S \tilde{u}^{n+1}\phi_j^h d\ell \approx \frac{\mu}{\eta}\delta t\gamma\alpha^2 \sum_{i=1}^{N} \tilde{u}^{n+1} \int_S \phi_i^h \phi_j^h d\ell = \frac{\mu}{\eta}\delta t\gamma\alpha^2 \sum_{i=1}^{N} [P]_{ji}\tilde{u}_i^{n+1}. \tag{6.1.13}$$

and

$$-\frac{\mu}{\eta} \int_S \tilde{\dot{u}}^{n+1}\phi_j^h d\ell \approx \sum_{i=1}^{N} \tilde{\dot{u}}_i^{n+1} \int_S \phi_i^h \phi_j^h d\ell = -\frac{\mu}{\eta} \sum_{i=1}^{N} [P]_{ji}\tilde{\dot{u}}_i^{n+1} \tag{6.1.14}$$

Likewise, we can discretize the following term as:

$$\int_{\mathcal{B}_R} (\frac{\partial u^{inc,n+1}}{\partial n})\phi_j^h d\ell = \frac{\left|\mathcal{B}_{R_j}\right|}{2} \frac{\partial u^{inc,n+1}(\xi_j, (n+1)\delta t)}{\partial n}, \tag{6.1.15}$$

where $\left|\mathcal{B}_{R_j}\right|$ is the length of the discretized segment on the artificial boundary, ξ_j is the midpoint of the discretized segment, and $(n+1)\delta t$ is the time of evaluation. These also apply in discretizing the following term as:

$$\begin{aligned}
-\int_{\mathcal{B}_R} \mathcal{T}_R u^{inc,n+1}\phi_j^h d\ell &= -\frac{\left|\mathcal{B}_{R_j}\right|}{2} \mathcal{T}_R u^{inc,n+1}(\xi_j, (n+1)\delta t) \\
&= -\frac{\left|\mathcal{B}_{R_j}\right|}{2} \big\{ S^{-1}(\frac{1}{2}I + D) u^{inc,n+1}(\xi_j, (n+1)\delta t) \big\} \\
&= -\frac{\left|\mathcal{B}_{R_j}\right|}{2} \big\{ S^{-1}\big[\frac{1}{2} u^{inc,n+1}(\xi_j, (n+1)\delta t) \\
&+ \int_{\mathcal{B}_R} u^{inc,n+1}(\boldsymbol{r'}) \frac{\partial G(\xi_j|\boldsymbol{r'})}{\partial \boldsymbol{r'}} d\boldsymbol{r'}\big] \big\} \\
&= -\sum \frac{\left|\mathcal{B}_{R_j}\right|}{2} \big\{ S^{-1}\big[\frac{1}{2} u^{inc,n+1}(\xi_j, (n+1)\delta t) \\
&+ \sum \left|\mathcal{B}_{R_k}\right| u^{inc,n+1}(\xi_k, (n+1)\delta t) \frac{\partial G(\xi_j|(\xi_k)}{\partial n'}\big] \big\}.
\end{aligned} \tag{6.1.16}$$

We further note in the previous cases that

$$\frac{\partial u^{inc,n+1}(\xi_j,(n+1)\delta t)}{\partial n} = \nabla u^{inc,n+1}\cdot\hat{n}_{\xi_j},$$
$$\frac{\partial G(\xi_j|(\xi_k)}{\partial n'} = \nabla G\cdot\hat{n}_{\xi_k},$$

for outward unit normal vectors to the boundary $\hat{n}_{\xi_j}$ and $\hat{n}_{\xi_k}$.

Furthermore, to analyze the term $\int_{\mathcal{B}_R}\Psi_R\tilde{u}^{s,n+1}(\boldsymbol{r})\phi_j^h d\ell$, we have

$$\int_{\mathcal{B}_R}\Psi_R\tilde{u}^{s,n+1}(\boldsymbol{r})\phi_j^h d\ell \approx \frac{\left|\mathcal{B}_{R_j}\right|}{2}\Psi_R\tilde{u}^{s,n+1}(\xi_j),$$

where

$$\Psi_R\tilde{u}^{s,n+1}(\xi_j) = S^{-1}\Big\{\alpha^2\iint_{\mathcal{U}_R}\tilde{u}^{s,n+1}(\boldsymbol{r'})G(\xi_j|\boldsymbol{r'})d\boldsymbol{r'} - \frac{1}{A}\int_{\Gamma_{\text{ext}}}\left[A\tilde{u}^{s,n+1}(\boldsymbol{r'})-\tilde{\tilde{u}}^{s,n+1}(\boldsymbol{r'})\right]\frac{\partial G(\xi_j|\boldsymbol{r'})}{\partial y'}dx'\Big\}. \quad (6.1.17)$$

We will separately analyze the integral term associated with the exterior domain, $\mathcal{U}_R$, and the integral term associated with the impedance plane, Γ_{ext}. The approaches are similar.

For the first integral term, we divide the exterior domain into a triangular mesh with a sufficient number of triangles (denoted M). Even though the exterior domain will not have to be very large, because the scattered field rapidly diminishes in value away from the cavity, it is still important to ensure we have a sufficient number of triangles to ensure convergence. Each triangle, denoted Δ_k, has a centroid, denoted Λ_k, and an area, denoted $|\Delta_k|$. We then fix $\boldsymbol{r'} = \Lambda_k$ and approximate this integral

term as:

$$\alpha^2 \iint_{\mathcal{U}_R} \tilde{u}^{s,n+1}(\boldsymbol{r'}) G(\xi_j|\boldsymbol{r'}) d\boldsymbol{r'} \approx \alpha^2 \sum_{k=1}^{M} |\Delta_k| \, G(\xi_j|\Lambda_k) \tilde{u}^{s,n+1}(\Lambda_k). \tag{6.1.18}$$

We note that in approximating $\tilde{u}^{s,n+1}(\Lambda_k)$ with the Newmark scheme, we have

$$\tilde{u}^{s,n+1}(\Lambda_k) = u^{s,n}(\Lambda_k) + \delta t \dot{u}^{s,n}(\Lambda_k) + \frac{(\delta t)^2}{2}(1-2\beta)\ddot{u}^{s,n}(\Lambda_k),$$

which requires precomputation of the values of the scattered field $u^{s,n}$ at Λ_k. Thus, using the integral representation in (3.2.10), we have:

$$\begin{aligned} u^{s,n}(\Lambda_k) = \alpha^2 & \iint_{\mathcal{U}_R} G(\Lambda_k|\boldsymbol{r'}) \tilde{u}^{s,n}(\boldsymbol{r'}) d\boldsymbol{r'} \\ & - \frac{1}{A} \int_{\Gamma_{\text{ext}}} \left[A\tilde{u}^{s,n+1}(\boldsymbol{r'}) - \tilde{\dot{u}}^{s,n+1}(\boldsymbol{r'}) \right] \frac{\partial G(\Lambda_k|\boldsymbol{r'})}{\partial \boldsymbol{n}_{\boldsymbol{r'}}} dr' \\ & + \int_{\mathcal{B}_R} \big(G(\Lambda_k|\boldsymbol{r'}) \frac{\partial u^n(\boldsymbol{r'})}{\partial \boldsymbol{n}_{\boldsymbol{r'}}} - u^n(\boldsymbol{r'}) \frac{\partial G(\Lambda_k|\boldsymbol{r'})}{\partial \boldsymbol{n}_{\boldsymbol{r'}}} \big) d\theta'. \end{aligned}$$

Using the previous techniques, we can estimate $u^{s,n}(\Lambda_k)$ as follows:

$$u^{s,n}(\Lambda_k) \approx \alpha^2 \sum_{\Delta_n, \Lambda_k \notin \Delta_n} |\Delta_n| \, G(\Lambda_k|\Lambda_n) \tilde{u}^{s,n}(\Lambda_n) \tag{6.1.19}$$

$$+ \alpha^2 \tilde{u}^{s,n}(\Lambda_n) \Big\{ \frac{1}{2} \Delta_{\text{Base}} \frac{1}{2\pi} \frac{2}{\alpha} \int_0^{\frac{\alpha h'}{2}} K_0(\tau) d\tau + |\Delta_k| \, G_{\text{rem}}(\Lambda_k|\Lambda_k) \Big\} \tag{6.1.20}$$

$$+ \sum_{j=1} \left| \mathcal{B}_{R_j} \right| \Big\{ G(\Lambda_k|\xi_j) \frac{\partial u^n(\xi_j)}{\partial \boldsymbol{n}_{\boldsymbol{r'}}} - u^n(\xi_j) \frac{\partial G(\Lambda_k|\xi_j)}{\partial \boldsymbol{n}_{\boldsymbol{r'}}} \Big\} \tag{6.1.21}$$

$$- \frac{1}{A} \sum_{\ell=1} |\Gamma_{\text{ext}_\ell}| \Big\{ A\tilde{u}^{s,n+1}(\xi_\ell) - \tilde{\dot{u}}^{s,n+1}(\xi_\ell) \Big\} \frac{\partial G(\Lambda_k|\xi_\ell)}{\partial y'}. \tag{6.1.22}$$

The first term in the estimation above, (6.1.19), is similar to the previous exterior discretization, but it does not include the term when $\Lambda_k = \Lambda_n$. The second term (6.1.20) addresses this singularity by evaluating the first term of the Green's function

as previously described, and then evaluating the remaining terms of the Green's function, taking into account the singular behavior. In this term, Δ_{Base} denotes the length of the base of the triangle, and h' denotes the height of the triangle. The third term, (6.1.21), is the discretization along the artificial boundary, where u^n denotes the value of the scattered field as computed in the interior. The fourth term (6.1.22) is the discretization of the impedance plane.

Once $u^{s,n}(\Lambda_k)$ is computed, we then compute:

$$\ddot{u}^{s,n}(\Lambda_k) = \alpha^2(u^{s,n}(\Lambda_k) - \tilde{u}^{s,n}(\Lambda_k)),$$
$$\dot{u}^{s,n}(\Lambda_k) = \tilde{\dot{u}}^{s,n}(\Lambda_k) + \delta t\gamma\ddot{u}^{s,n}(\Lambda_k),$$

so that $\tilde{u}^{s,n+1}(\Lambda_k)$ and $\tilde{\dot{u}}^{s,n+1}(\Lambda_k)$ can be computed as desired.

Similarly, for the second integral term in (6.1.17), we can divide Γ_{ext} into sufficient segments to obtain the approximation:

$$-\frac{1}{A}\int_{\Gamma_{\text{ext}}}\left[A\tilde{u}^{s,n+1}(\boldsymbol{r'}) - \tilde{\dot{u}}^{s,n+1}(\boldsymbol{r'})\right]\frac{\partial G(\xi_j|\boldsymbol{r'})}{\partial y'}dx' \approx$$
$$-\frac{1}{A}\sum_{\ell=1}^{L}|\Gamma_{\text{ext}_\ell}|\left[A\tilde{u}^{s,n+1}(\xi_\ell) - \tilde{\dot{u}}^{s,n+1}(\xi_\ell)\right]\frac{\partial G(\xi_j|\xi_\ell)}{\partial y'}. \tag{6.1.23}$$

Using the same approach as with the first integral expression, in order to get $\tilde{u}^{s,n+1}(\xi_\ell)$ and $\tilde{\dot{u}}^{s,n+1}(\xi_\ell)$, we again utilize (3.2.10) to get:

$$u^{s,n}(\xi_\ell) \approx \alpha^2\sum_{n=1}|\Delta_n|\,G(\xi_\ell|\Lambda_n)\tilde{u}^{s,n}(\Lambda_n) \tag{6.1.24}$$
$$+\sum_{j=1}\left|\mathcal{B}_{R_j}\right|\left\{G(\xi_\ell|\xi_j)\frac{\partial u^n(\xi_j)}{\partial \boldsymbol{n}_{\boldsymbol{r'}}} - u^n(\xi_j)\frac{\partial G(\xi_\ell|\xi_j)}{\partial \boldsymbol{n}_{\boldsymbol{r'}}}\right\} \tag{6.1.25}$$
$$-\frac{1}{A}\sum_{m=1}|\Gamma_{\text{ext}_m}|\left\{A\tilde{u}^{s,n+1}(\xi_m) - \tilde{\dot{u}}^{s,n+1}(\xi_m)\right\}\frac{\partial G(\xi_m|\xi_\ell)}{\partial y'}. \tag{6.1.26}$$

The first term in the estimation above, (6.1.24), is similar to the previous exterior dis-

cretization, and accounts for all terms (where no singularities are present). The second term, (6.1.25), is the discretization along the artificial boundary, and no singularities should exist here. The third term (6.1.26) is the discretization of the impedance plane, and a singularity will exist when $\xi_m = \xi_\ell$.

Again, once $u^{s,n}(\xi_\ell)$ is computed, we then compute:

$$\ddot{u}^{s,n}(\xi_\ell) = \alpha^2(u^{s,n}(\xi_\ell) - \tilde{u}^{s,n}(\xi_\ell)),$$
$$\dot{u}^{s,n}(\xi_\ell) = \tilde{\dot{u}}^{s,n}(\xi_\ell) + \delta t\gamma\ddot{u}^{s,n}(\xi_\ell),$$

so that $\tilde{u}^{s,n+1}(\Lambda_k)$ and $\tilde{\dot{u}}^{s,n+1}(\Lambda_k)$ can be computed from the prediction formulas as desired.

Thus, the final discretized version of the expression in (6.1.17) is

$$\Psi_R\tilde{u}^{s,n+1}(\xi_j) = S^{-1}\Big\{\alpha^2\sum_{k=1}|\Delta_k|\,G(\xi_j|\Lambda_k)\tilde{u}^{s,n+1}(\Lambda_k) - \frac{1}{A}\sum_{\ell=1}|\Gamma_{\text{ext}_\ell}|\left[A\tilde{u}^{s,n+1}(\xi_\ell) - \tilde{\dot{u}}^{s,n+1}(\xi_\ell)\right]\frac{\partial G(\xi_j|\xi_\ell)}{\partial y'}\Big\}. \quad (6.1.27)$$

We note here that S^{-1} exists as a square, dense matrix, as previously described. The two discretized integral expressions in the braces will yield a $N_{\text{seg}} \times 1$ matrix, where N_{seg} refers to the number of segments used on the artificial boundary. When multiplied by S^{-1} , an $N_{\text{seg}} \times N_{\text{seg}}$ matrix, this will result in a $N_{\text{seg}} \times 1$ matrix. Therefore, we multiply the result by the "connectivity" matrix, $[I_h]^\top$, (see (6.1.11)), resulting in the desired $N \times 1$ matrix, where N represents the number of nodes in the interior mesh. This is similar to Copeland, Langer, and Pusch's discretization technique used in [20], and also was referred to earlier in Jin in [55].

Hence, combining the discretized approximations in (6.1.12), (6.1.13), (6.1.14), (6.1.15), (6.1.16), and (6.1.27) generates an approximation for the vector F_j^{n+1} in

(6.1.7).

We can concisely summarize the time-stepping scheme as follows (this template is adapted from Van and Wood in [104]) :

1. Form the matrices K, M, P, and Q as defined in (6.1.3) , (6.1.4), (6.1.5), and (6.1.6). This constitutes the left-hand side of the matrix equation (6.1.2).

   Begin the time loop, where $n = 0, 1, 2, \ldots, N$.

2. Compute the predicted values $\tilde{u}^{s,n+1}$ (see (3.1.3)) and $\tilde{\dot{u}}^{s,n+1}$ (see (3.1.4)) in the interior Ω_R. These predicted values are based on the finite element solution computed in the previous time step (see (6.1.2)).

3. Compute the predicted values $\tilde{u}^{s,n+1}$ (see (3.1.3)) and $\tilde{\dot{u}}^{s,n+1}$ (see (3.1.4)) in the exterior $\mathcal{U}_R$. These predicted values are based on the exterior solution computed from the integral representation (the discretized version of (3.2.10)) in the previous time step.

4. Construct the right-hand side vector F_j^{n+1} as defined in (6.1.7).

5. Compute the solution of the matrix equation in (6.1.2). This will be the solution in the interior of the cavity Ω_R.

6. Using the interior solution computed in the previous step (u^{n+1}), and noting that $u^{s,n+1} = u^{n+1} - u^{\text{inc},n+1}$ along $\mathcal{B}_R$, compute the solution in the exterior domain from the integral representation (3.2.10).

7. Correct the solution computed in the interior of the cavity Ω_R by computing $\ddot{u}^{n+1}$ (see (3.1.6)) and $\dot{u}^{n+1}$ (see (3.1.7)).

8. Correct the solution computed in the exterior $\mathcal{U}_R$ by computing $\ddot{u}^{s,n+1}$ (see (3.1.6)) and $\dot{u}^{s,n+1}$ (see (3.1.7)).

6.2 Numerical Results

We will analyze numerically two separate cavity geometries: a shallow planar cavity, with dimensions 1 meter wide by 0.25 meters deep; and an overfilled cavity, with dimensions 1 meter wide by 1 meter deep, with a semicircle protrusion of 0.5 meter radius. Even though the theory presented assumes an overfilled cavity, the planar cavity results could provide a good approximation, and more importantly will provide a context for the theory presented. It will also be useful to compare the electric field depictions as well as the RCS values for both types of cavities. We previously mentioned that Wang provided numerical results for absorbing boundary conditions for curved boundaries [108]. Because our assumptions essentially approximate a first order absorbing boundary condition, this gives us a baseline to help confirm the accuracy of the depicted fields.

We started with the MATLAB code from Van and Wood in [104] as a foundation for our results, and adapted it to our boundary conditions and geometries. The idea is to depict the progression from the PEC case to the IBC case, in which we would expect to observe the attenuation of the electric field with a more absorbing boundary condition. For the planar cavity, we considered two cases: a PEC plane (Γ_{ext}) with PEC cavity walls (S), and a PEC plane with IBC cavity walls. For the overfilled cavity, we considered these two cases and added a third case: an IBC plane with IBC cavity walls. We also wanted to observe the long-term stability in these field depictions, which will validate the parameters chosen for the stability of the Newmark scheme.

We will use the following parameters for the Newmark scheme for the numerical simulations: $\gamma = 0.95$, $\beta = 0.5256$, and $\delta t = 0.0625$. This ensures that Theorem 5.3.1 is satisfied and the scheme is unconditionally stable. We assume a relative permittivity of $\varepsilon_r = 2$ for the filled media in the cavity, which satisfies the assumptions used in the

proof of Theorem 4.2.3. We assume all permeability values of μ to be 1. We assume the surface impedance values for the IBCs to be $\eta = 0.8$ if not explicitly mentioned, and we will also use $\eta = 0.2$ as a comparison for a boundary condition approaching a PEC surface. Note that $\eta = 0$ represents a strict PEC surface.

We assume an incident Gaussian pulse defined as follows:

$$u^{\text{inc}}(x, y, t) = \underbrace{A\frac{4}{T\sqrt{\pi}}}_{\text{Amplitude}} e^{-\tau^2},$$

for

$$\tau = 4\frac{(t - t_0 + x\cos\theta_{\text{inc}} + y\sin\theta_{\text{inc}})}{T}.$$

In the numerical simulations for the pulse, we set $A = 1$, $\theta_{\text{inc}} = 90°(= \pi/2)$, $T = 2$, and $t_0 = 3$. This time delay of $t_0 = 3$ means at the point $(x_0, y_0) = (0, 0)$, the Gaussian pulse will reach its maximum. There are several advantages in using the Gaussian pulse, one of which is that it is a good approximation of the pulse shape coming from certain types of lasers and other manmade systems [76]. The depicted electric fields will be the real portions plotted against time as measured in light meters, which is the amount of time for light to travel one meter in free-space.

The first set of data is for the shallow planar cavity, depicted along with the incident wave and observation point at $(0, 0)$, in Figure 8.

The first run is depicted in Figure 9. With the PEC plane and PEC cavity walls as a benchmark, we observe that the case with IBC enforced at the cavity walls exhibits more attenuated characteristics. We also observe the stability of the Newmark scheme over time.

We also want to observe the effects as $\eta \to 0$, so the subsequent run adjusts $\eta = 0.2$. We would expect the field to begin to exhibit the characteristics of a strict PEC on the plane and cavity walls. This is clearly evident in Figure 10 with the

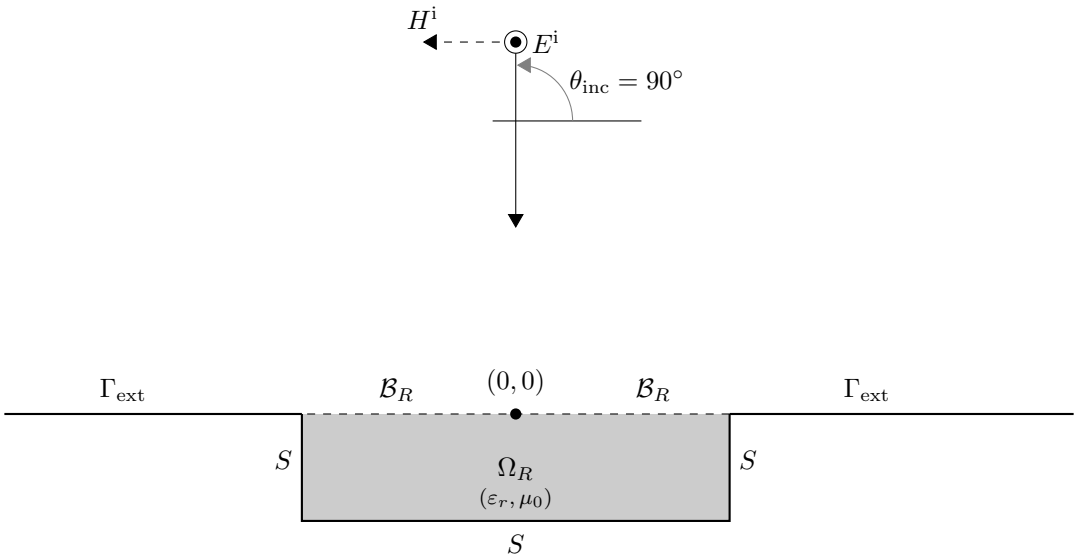

Figure 8. Shallow Planar Cavity (1 meter by 0.25 meters)

second case (PEC plane and IBC cavity walls) showing more oscillatory behavior as in the strict PEC case. Again, we observe the stability of the Newmark scheme over time.

It is essential to compute the RCS for any scattering problem, so we generated plots for two selected frequencies of 289.5 MHz and 480.45 MHz. Not only are we interested in observing the effects of the changing boundary conditions on the cavity models, but also are interested in differences between the planar and overfilled cavities as well. These plots are monostatic in that the transmitter and receiver are collocated [8]. They depict the RCS values from a normal incidence angle of 90 degrees to 170 degrees as measure from the ground plane. We again use Van and Wood's code in [104] to generate our results, in which the time domain scattered field is Fast Fourier Transformed to obtain the frequency result.

For the first RCS plot at 289.5 MHz in Figure 11, we observe the expected lobing pattern in both cases. We also observe generally lower RCS values once the IBC is introduced, particularly for values with an obervation angle less than 140 degrees.

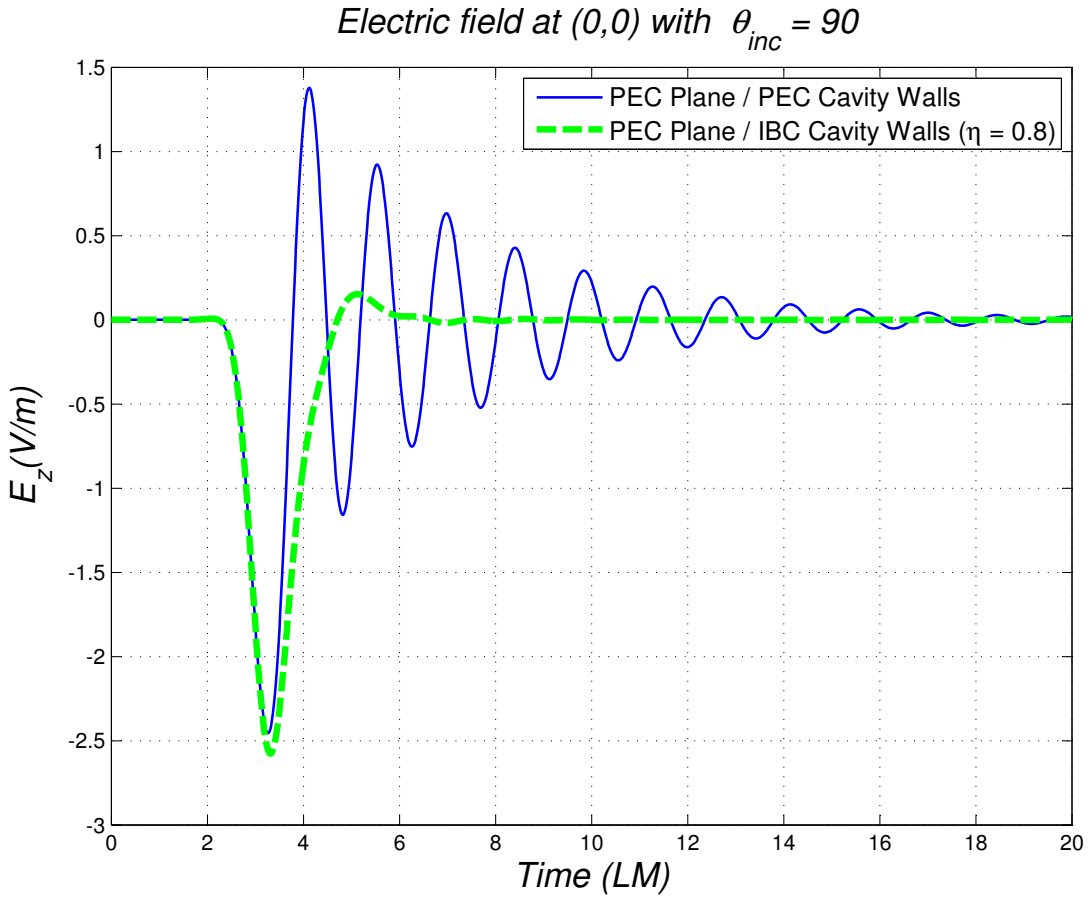

Figure 9. Shallow Cavity - TM Solution at (0,0) - Eta Point Eight

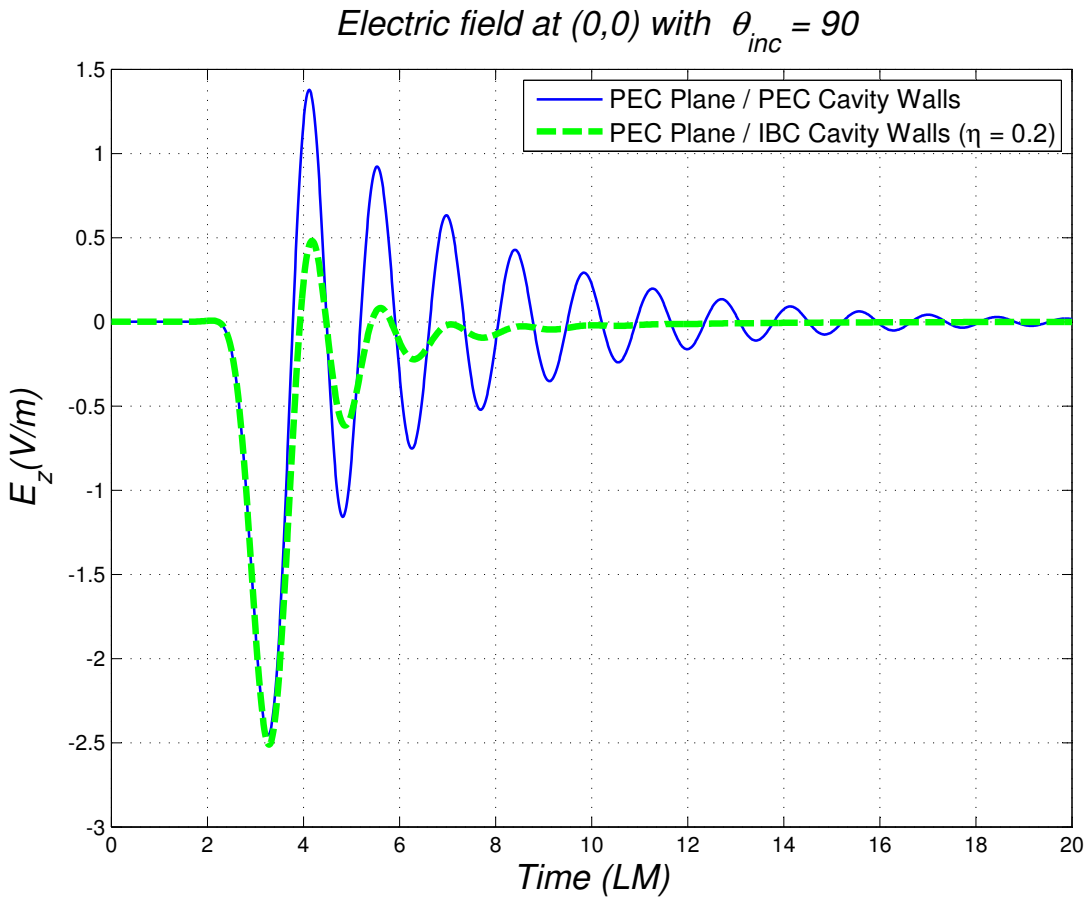

Figure 10. Shallow Cavity - TM Solution at (0,0) - Eta Point Two

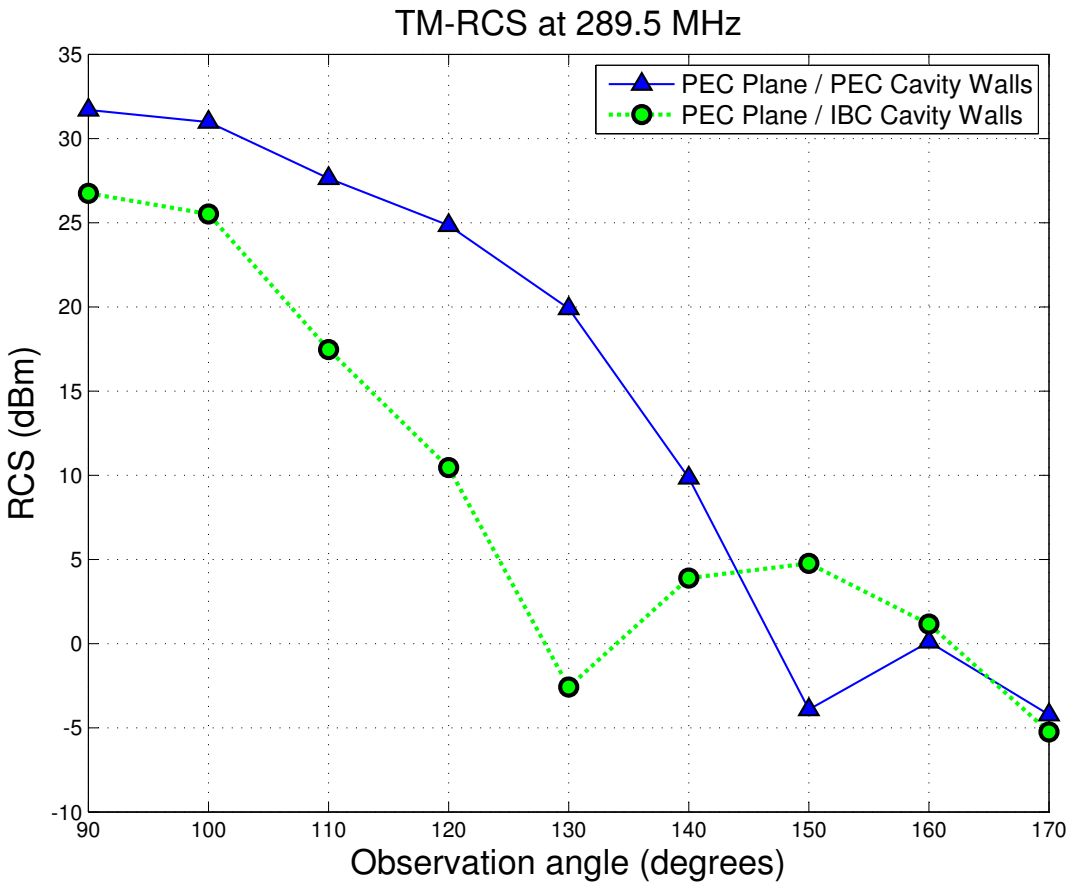

Figure 11. Radar Cross Section at 289.5 MHz

In the second RCS plot at 480.45 MHz in Figure 12, we observe much more apparent attenuation of the RCS values as the boundary condition is changed from a PEC to an IBC, as a significant gap exists between the two cases. This higher frequency also exhibits the expected lobing patterns, and the PEC plane with IBC cavity walls exhibits the lowest RCS values.

The second set of data is for the overfilled cavity model depicted along with the incident wave and observation point of $(0, 0)$ in Figure 13. We point out that the selected observation point is close to the origin in order to standardize it to the planar case and see if any differences are observed. For these results, we also include the third case of the IBC plane and IBC cavity walls. We also include the mesh discretization used for the interior domain (cavity) (Figure 14) and the exterior domain (Figure 15).

For the first result in Figure 16, we immediately notice the more oscillatory nature of the electric field. This could be due to a couple of reasons: the overfilled cavity model is physically deeper and has more material surrounding the observation point. However, we still observe the most important result; that is, as the boundary condition changes on both the plane and cavity walls from a PEC to an IBC we clearly see a progressive attenuation of the depicted fields. Also, this result is truncated at 50 LM for scaling and ease of observation. The long-term stability is evident for the PEC plane with IBC cavity walls and the IBC plane with IBC cavity walls. For the PEC plane with PEC cavity walls, the long-term stability is evident beyond 50 LM but is not depicted here as it is easier to compare the three cases in this view. The PEC case is used as a benchmark for comparison, and its stability was studied and proven by Van and Wood [104].

As with the planar case, we want to observe the effects as $\eta \to 0$, and this is shown in Figure 17. Even though the differences between Figure 16 and Figure 17 are more subtle, it still shows that as $\eta \to 0$, the fields approach the strict PEC

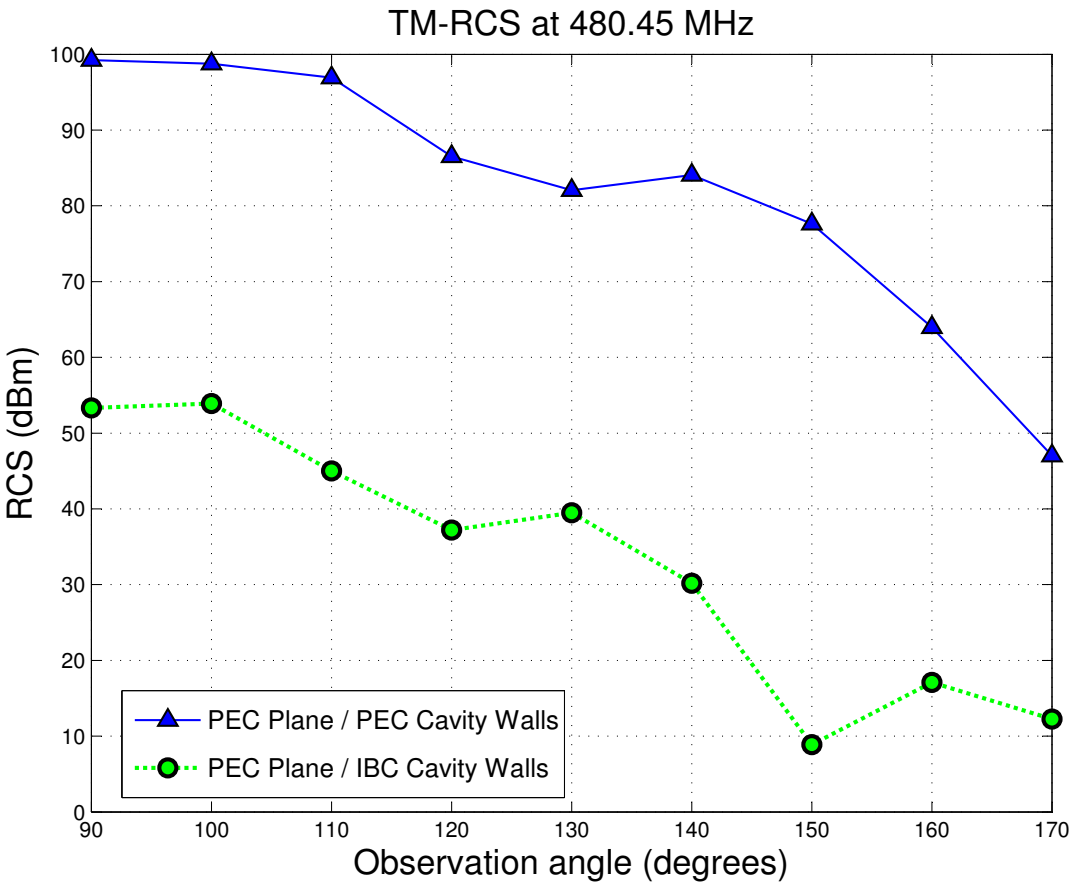

Figure 12. Radar Cross Section at 480.45 MHz

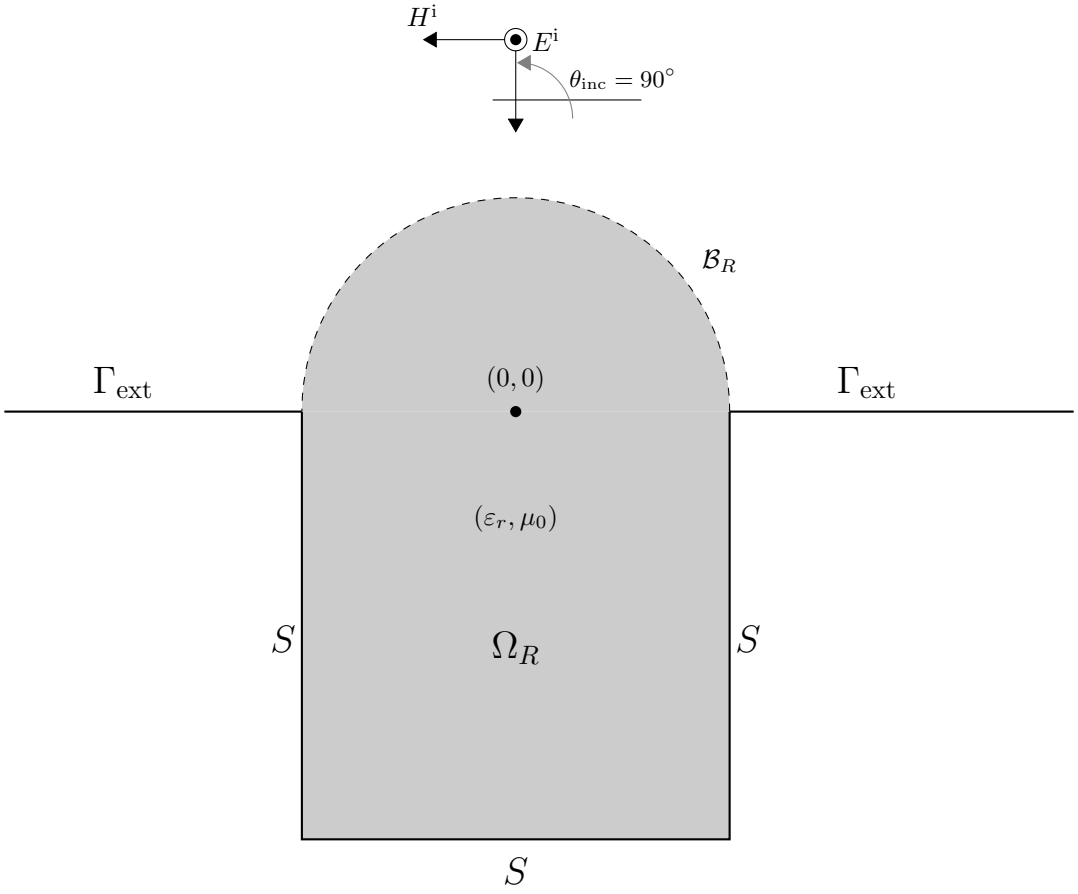

Figure 13. Overfilled Cavity (1 meter deep; 0.5 meter radius of protrusion)

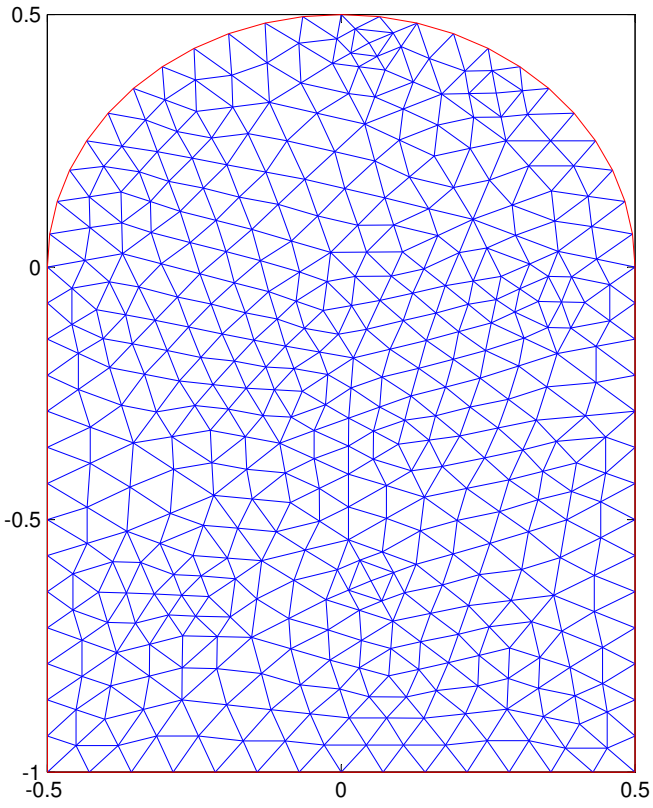

Figure 14. Interior Domain Mesh - Overfilled Cavity

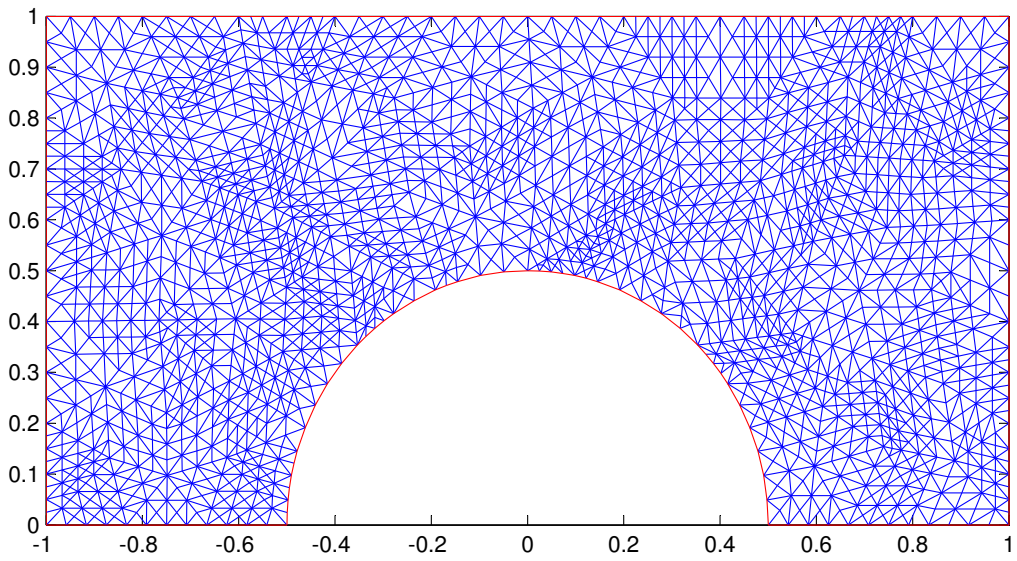

Figure 15. Exterior Domain Mesh - Overfilled Cavity

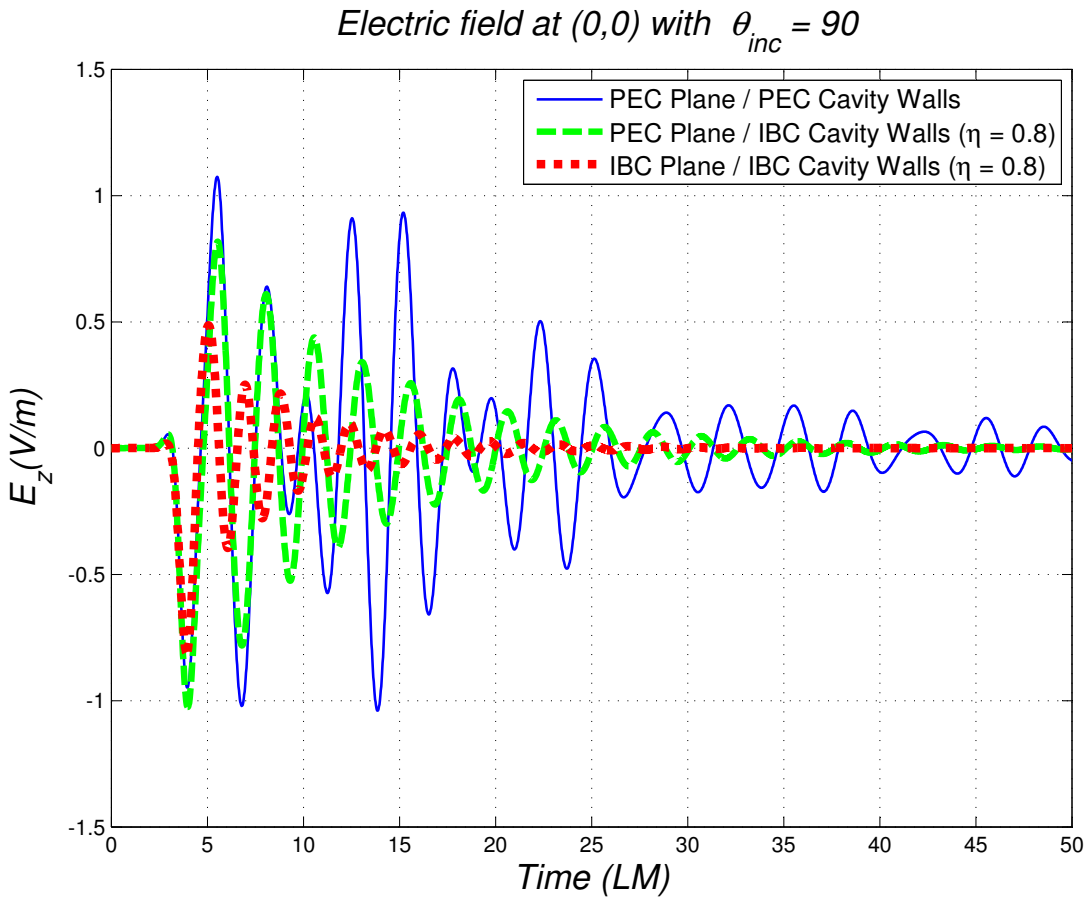

Figure 16. Overfilled Cavity - TM Solution - Eta Point Eight

behavior. This is evident in that the depiction of the field in the PEC plane with IBC cavity walls increases in magnitude to follow the strict PEC case. It is also evident in the IBC plane with IBC cavity walls case in that at approximately 10 LMs, the oscillatory nature as seen in the strict PEC case is starting to form. The stability is also observed up to 50 LM, and can be observed beyond 50 LM for the PEC plane with PEC cavity walls case.

We also observe the RCS plots for the overfilled cavity model, keeping in mind that we would expect RCS to be affected due to differences in shape and material. For the first RCS plot at 289.5 MHz in Figure 18, we note that there is little difference in RCS values for all three cases as they follow the same pattern. We do, however, start to observe the expected attenuation at observation angles beyond 130 degrees. We also note the pattern is slightly different than the planar case.

On the other hand, for the RCS plot at 480.45 MHz depicted in Figure 19, we see a much clearer separation of the three cases. We note the lobing and the clear attenuation as the IBC is introduced on both the plane and cavity walls. At this higher frequency, it is also interesting to compare the observations to the planar cavity model. We note the PEC plane and PEC cavity wall RCS values are generally lower for the overfilled cavity model than for the planar cavity model.

In summary, the results of the numerical simulation clearly agrees with the theory presented. We observed the expected attenuation of the field as the IBC was introduced on the plane and cavity walls. We also observed the changes in the RCS values as the IBC was introduced. The planar cavity model provided a good context for our theory, but ultimately the overfilled model and its corresponding numerical results indicate that our mathematical model can be numerically implemented. The long-term stability of the models was also verified.

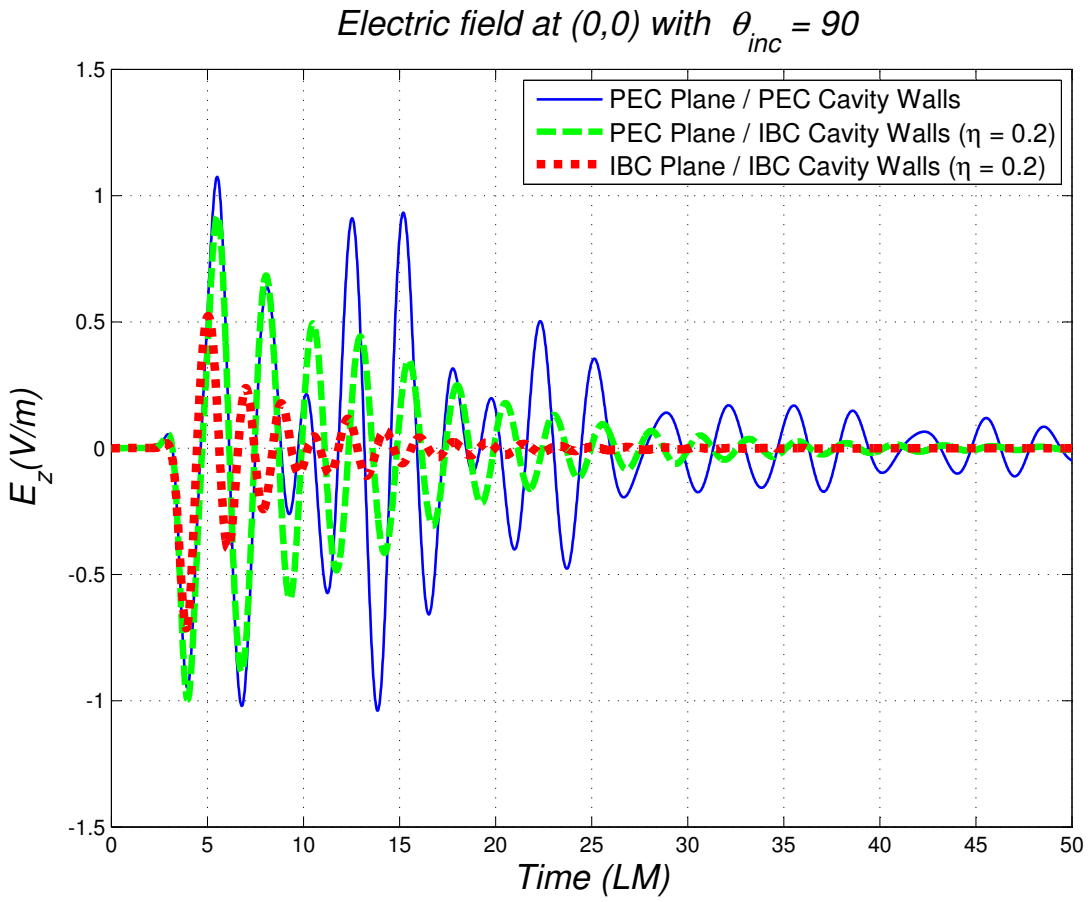

Figure 17. Overfilled Cavity - TM Solution - Eta Point Two

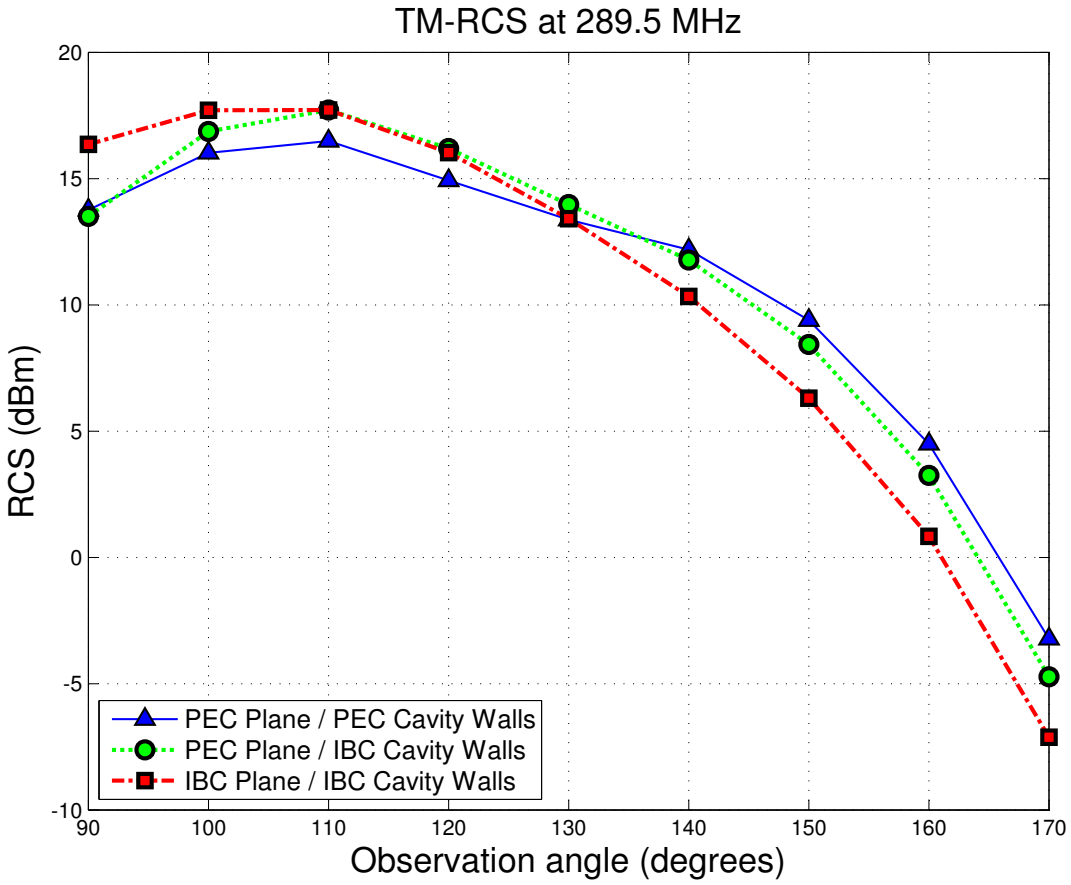

Figure 18. Overfilled Radar Cross Section at 289.5 MHz

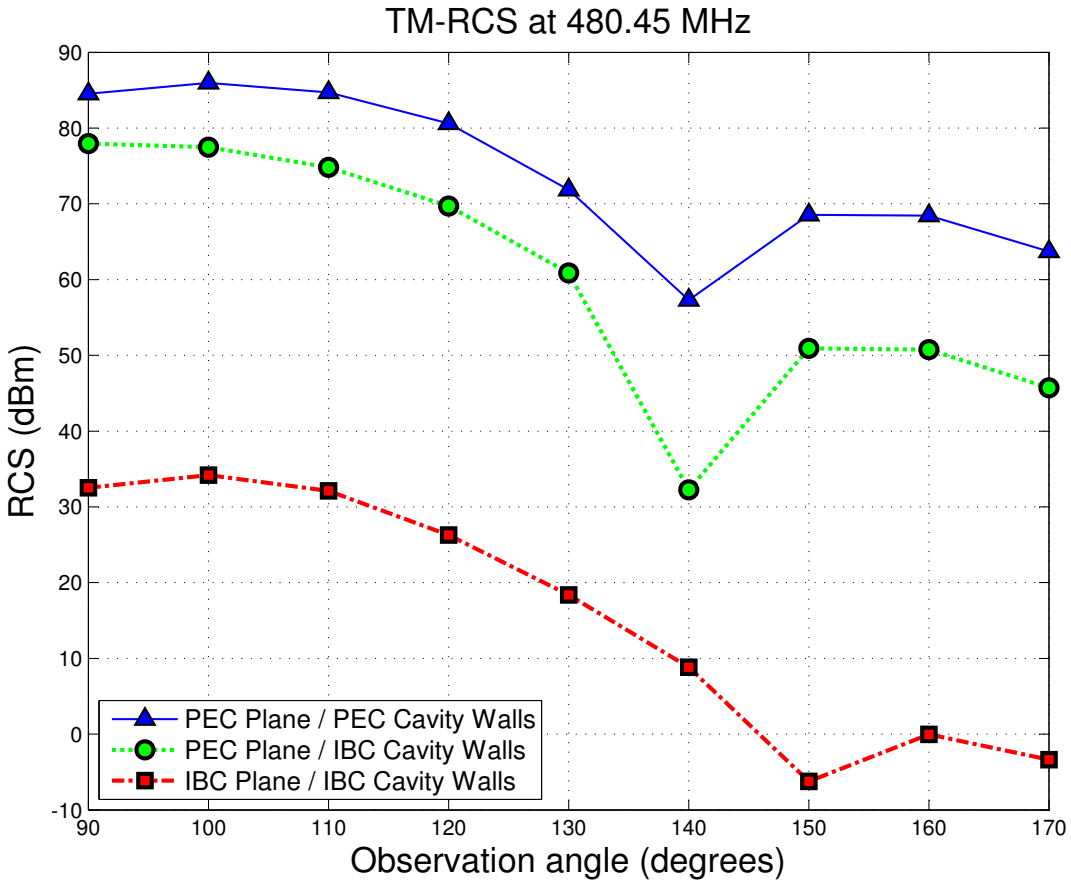

Figure 19. Overfilled Radar Cross Section at 480.45 MHz

VII. Conclusions and Future Work

7.1 Conclusions

In conclusion, given an incident electromagnetic wave impinging on an overfilled cavity in an impedance ground plane, we have determined the resulting scattered fields. Moreover, we have proven that this problem is well-posed and can be implemented through the use of the FEM. We have established a valid mathematical model for detecting scattered waves from cavities. In particular, we derived an integral representation and Green's function for the solution, and used integral operator theory in establishing well-posedness. A key step in the uniqueness and existence proofs was analyzing the properties of the Steklov-Poincarè operator. This was important because an exact series solution does not exist for IBC conditions, and using already established properties of integral operators helped facilitate this proof. One advantage of this approach was that we avoided the use of the hypersingular operator, which can be difficult to numerically evaluate, particularly at the singularities. Nevertheless, we noticed an elegant connection: the mathematical formulation sets the foundation for the variational formulation. This, in turn, is the basis for the finite element analysis, which is used for the numerical simulation. We observed that not only changing boundary conditions but changing cavity geometries had an effect on the scattered field and the RCS values.

We also have two additional contributions. In constructing the finite element approximation, we provided a method for numerical implementation that avoids use of the hypersingular operator. This approach in the literature seems limited and almost nonexistent. Though the numerical simulation involved a direct analysis and evaluation of the equations of the integral representation, this method may be more efficient when fully implemented. Also, we were able to apply and refine previous

research for parameter requirements to ensure unconditional stability for arbitrary time steps for our application of the Newmark scheme.

One of the most important observations involved the discretization of the Newton potential terms, one of which was the infinite space, $\mathcal{U}_R$, above the cavity opening (see (3.4.8)). We previously mentioned that this term results from the inhomogeneity in the PDE, and just requires proper discretization, as the finite element method is not used in this portion. During the numerical implementation, $\mathcal{U}_R$ was relatively small (2 meters wide by 1 meter long; see Figure 15), as the scattered field becomes quite small and negligible outside of this region. However, the real breakthrough in the research came when it was discovered that the solution did not converge until a sufficient number of elements were generated for this region. We believe this might be due to the fact that we were working with the constant α^2, which had an extremely large value of almost 500. As a result, when discretizing this portion of the Newton potential, even though the finite element method or adaptive mesh refinements are not used, this refinement may have helped scale the problem and avoid solution "blow up" at the appropriate steps. This is an important consideration in future applications and extensions of this work in the time domain.

7.2 Future Work

It is obvious that this research has a lot of applications and opens up many avenues for future work. Considering our general problem statement, we only investigated the TM polarization case, but the TE polarization case can be explored as well. Also, this problem can be translated into three dimensions, which would not only increase its applicability, but also be easier to work with in terms of a simpler Green's function. This was a direct scattering problem, but the IED detection application lends itself well to an inverse scattering problem. That is, given a scattered wave, determine the

properties of the scattering object. Inverse scattering theory is a popular and growing area of research.

Considering the numerical analysis of the problem, we only generated the real portion of the scattered field, but future research could also look at the imaginary portions of the field generated due to the nature of the Green's function. Also, RCS plots could be analyzed at several other frequencies. Several of the parameters could also be modified and analyzed for their effects to include: different values of ε_r (to include real and imaginary) to reflect different types of cavity material; different values of the surface impedance η; changing the angle of incidence to see its effects on the scattered field; changing the observation points along and within the artificial boundary; different overfilled cavity geometries (shallow versus deep cavities); changing the stability parameters used in the Newmark scheme to include differing time steps; and considering the effects of a Gaussian pulse versus a continuous wave. Obviously, there are many areas here that could be expanded and analyzed.

We mentioned that the IBC assumption we developed approximated a first order boundary condition, but a more robust assumption could be made involving the use of a Fourier transform. The Green's function itself for an IBC can be explored further, as Hein did thoroughly in his dissertation [42]. It was clear from the literature that there is little consistency in the Green's function expressions for an IBC. There are multiple representations for different terms, and each are quite detailed. The main difficulty seems to be in numerical implementation and the evaluation of singularities when using a boundary integral method. More standardization in this area would be very beneficial.

As mentioned during the finite element analysis, we only provided *a priori* estimates, but adaptive mesh refinement could be used to generate *a posteriori* estimates, or higher polynomial degree basis functions could even be used to help refine the so-

lution. For the finite element approximation we describe, the idea was to use it as a foundation for the numerical implementation. However, we built upon an existing code which more directly approximated the integral representations. The advantage was that this did not require inverse matrix operations, but the disadvantage was that the calculations involved hypersingular expressions with multiple derivatives, where singularities were difficult to assess. The finite element approximation we describe could be implemented as it avoids use of hypersingular expressions, and could possibly be more stable and accurate.

Finally, it is without question that this research has opened several areas for further exploration that could greatly benefit not only the academic discipline but also the military. Given the importance of radar applications and the importance of object detection and analysis in today's military, this research can be applied in many ways. Clearly, then, this work sets the foundation for extremely important topics to today's warfighter on the battlespace.

Appendix A. Derivations

Because we assume a constant surface impedance for our impedance boundary conditions in the time domain, this assumption resembles a first-order absorbing boundary condition according to Jin (see [55]) :

$$\hat{n} \times \left[\frac{1}{\mu} \nabla \times \boldsymbol{E}(\boldsymbol{r}, t) \right] + Y_c \frac{\partial}{\partial t} \big[\hat{n} \times \hat{n} \times \boldsymbol{E}(\boldsymbol{r}, t) \big] = 0 \text{ for } \boldsymbol{r} \in S \cup \Gamma_{\text{ext}} \times (0, \infty).$$

Here, $Y_c = \sqrt{\frac{\varepsilon}{\mu}}$ is defined as the intrinsic admittance of the infinite medium and $\hat{n} = \hat{y}$ as the outward unit normal to the boundary Γ_{ext}. For derivation purposes, we limit the case to the impedance plane Γ_{ext}, but note that the extension to $S \cup \Gamma_{\text{ext}}$ would require a general definition for $\hat{n}$.

For the TM case, we have $\nabla \times \boldsymbol{E}(\boldsymbol{r}, t) = \hat{x} \frac{\partial}{\partial y} E_z - \hat{y} \frac{\partial}{\partial x} E_z$, then

$$\left.\begin{aligned} \hat{n} \times \left[\frac{1}{\mu} \left(\hat{x} \frac{\partial}{\partial y} E_z - \hat{y} \frac{\partial}{\partial x} E_z \right) \right] &= \hat{z} \Big(- \frac{1}{\mu} \frac{\partial}{\partial y} E_z \Big) \\ \hat{n} \times \hat{n} \times \boldsymbol{E}(\boldsymbol{r}, t) &= \hat{z} \big(- E_z \big) \end{aligned} \right\} \Longrightarrow$$

$$\begin{aligned} \hat{z} \Big(- \frac{1}{\mu} \frac{\partial}{\partial y} E_z \Big) + Y_c \frac{\partial}{\partial t} \Big[\hat{z} \big(- E_z \big) \Big] &= 0 \\ \hat{z} \left[- \frac{1}{\mu} \frac{\partial}{\partial y} E_z + Y_c \frac{\partial}{\partial t} \big(- E_z \big) \right] &= 0 \\ - \frac{1}{\mu} \frac{\partial}{\partial y} E_z &= Y_c \frac{\partial}{\partial t} \big(E_z \big) s \\ - \frac{1}{\mu} \frac{\partial E_z}{\partial y} &= \frac{1}{\eta} \frac{\partial E_z}{\partial t}. \end{aligned}$$

Bibliography

1. Abramowitz, M. and I.A. Stegun (editors). *Handbook of Mathematical Functions with Formulas, Graphs, and Mathematical Tables*. Dover Publications, Inc., New York, 1970.

2. "Air Force Office of Scientific Research, Research Areas". World Wide Web Page. Available at *http://www.wpafb.af.mil/library/factsheets/factsheet.asp?id=9268*.

3. "Air Force Research Laboratory's Focused Long Term Challenges". World Wide Web Page. Available at *http://www.eglin.af.mil/shared/media/document/AFD-080402-005.pdf*.

4. Allaire, Grégoire. *Numerical Analysis and Optimization: An Introduction to Mathematical Modeling and Numerical Simulation*. Oxford University Press, New York, 2007.

5. Anastassiu, H.T. "A review of electromagnetic scattering analysis for inlets, cavities, and open ducts." *IEEE Antennas and Propagation Magazine*, 45(6):27–40, 2003.

6. Angell, Thomas S. and Andreas Kirsch. *Optimization Methods in Electromagnetic Radiation*. Springer-Verlag, New York, 2004.

7. Atkinson, Kendall and Weimin Han. *Theoretical Numerical Analysis: A Functional Analysis Framework*. Springer-Verlag, New York, 2001.

8. Balanis, Constantine A. *Advanced Engineering Electromagnetics*. John Wiley & Sons, Inc., Hoboken NJ, 1989.

9. Bao, Gang, Lawrence Cowsar, and Wen Masters. *Mathematical Modeling in Optical Science*. Society for Industrial and Applied Mathematics, Philadelphia PA, 2001.

10. Cakoni, Fioralba and David Colton. *Qualitative Methods in Inverse Scattering Theory*. Springer-Verlag, Berlin, 2006.

11. Chandler-Wilde, S. N. and Andrew T. Peplow. "A boundary integral equation formulation for the Helmholtz equation in a locally perturbed half-plane." *ZAMM – Journal of Applied Mathematics & Mechanics / Zeitschrift fur Angewandte Mathematik und Mechanik*, 85(2):79 – 88, 2005.

12. Chandler-Wilde, S.N. "The impedance boundary value problem for the Helmholtz equation in a half-plane." *Mathematical Methods in the Applied Sciences*, 20(10):813 – 840, 1997.

13. Chandler-Wilde, S.N. and D.C. Hothersall. "A uniformly valid far field asymptotic expansion of the Green function for two-dimensional propagation above a homogeneous impedance plane." *Journal of Sound and Vibration*, 182(5):665 – 675, 1995.

14. Chandler-Wilde, S.N., P. Monk, and M. Thomas. "The mathematics of scattering by unbounded, rough, inhomogeneous layers." *Journal of Computational and Applied Mathematics*, 204(2):549 – 559, 2007.

15. Chapko, Roman and Rainer Kress. "Rothe's method for the heat equation and boundary integral equations." *Journal of Integral Equations and Applications*, 9(1):47–69, 1997.

16. Chen, Goong and Jianxin Zhou. *Boundary Element Methods*. Academic Press, San Diego CA, 1992.

17. Chongbin, Zhao and Liu Tianyun. "Non-reflecting artificial boundaries for modelling scalar wave propagation problems in two-dimensional half space." *Computer Methods in Applied Mechanics and Engineering*, 191(41):4569 – 4585, 2002.

18. Ciarlet, Philippe G. *The Finite Element Method for Elliptic Problems*. North Holland, Amsterdam, 1978.

19. Colton, David and Rainer Kress. *Inverse Acoustic and Electromagnetic Scattering Theory*. Springer-Verlag, New York, second edition, 1998.

20. Copeland, Dylan, Ulrich Langer, and David Pusch. "From the Boundary Element Domain Decomposition Methods to Local Trefftz Finite Element Methods on Polyhedral Meshes." Michel Bercovier et al. (editors), *Domain Decomposition Methods in Science and Engineering XVIII*, 315–322. Springer-Verlag, Berlin, 2009.

21. Costabel, Martin. "Boundary integral operators on Lipschitz domains: Elementary results." *SIAM Journal on Mathematical Analysis*, 19(3):613–626, 1988.

22. Costabel, Martin. "Time-dependent Problems with the Boundary Integral Equation Method". Erwin Stein et al. (editors), *Encyclopedia of Computational Mechanics*. John Wiley & Sons, Inc., New York, 2004.

23. Costabel, Martin. "Some Historical Remarks on the Positivity of Boundary Integral Operators". Martin Schanz and Olaf Steinbach (editors), *Boundary Element Analysis – Mathematical Aspects and Applications*, 1–27. Springer-Verlag, Berlin, 2007.

24. Dautray, Robert and Jacques-Louis Lions. *Mathematical Analysis and Numerical Methods for Science and Technology: Volume 6, Evolution Problems II*. Springer-Verlag, Berlin, 1993.

25. Demkowicz, Leszek. *Computing with Hp-adaptive Finite Elements: One and two dimensional elliptic and Maxwell problems*. Chapman & Hall/CRC applied mathematics and nonlinear science series. Chapman & Hall/CRC, Boca Raton FL, 2006.

26. DuChateau, Paul and David W. Zachmann. *Schaum's Outline of Theory and Problems of Partial Differential Equations*. McGraw-Hill, New York, 1986.

27. Duffy, Dean G. *Green's Functions with Applications*. Chapman & Hall / CRC, Boca Raton FL, 2001.

28. Durán, M., R. Hein, and J.-C. Nédélec. "Computing numerically the Green's function of the half-plane Helmholtz operator with impedance boundary conditions." *Numerische Mathematik*, 107(2):295 – 314, 2007.

29. Durán, M., I. Muga, and J.-C. Nédélec. "The Helmholtz equation in a locally perturbed half-plane with passive boundary." *IMA Journal of Applied Mathematics*, 71(6):853 – 876, 2006.

30. Durán, M., I. Muga, and J.-C. Nédélec. "The Helmholtz equation in a locally perturbed half-space with non-absorbing boundary." *Archive for Rational Mechanics and Analysis*, 191(1):143 – 172, 2009.

31. Gennarelli, G., G. Pelosi, and G. Riccio. "Time domain version of the Uapo solution for the field diffracted by an anisotropic impedance half-plane." *Journal of Electromagnetic Waves & Applications*, 18(7):969 – 981, 2004.

32. Givoli, Dan. "Computational Absorbing Boundaries." Steffen Marburg and Bodo Nolte (editors), *Computational Acoustics of Noise Propagation in Fluids – Finite and Boundary Element Methods*, 145–166. Springer-Verlag, Berlin, 2008.

33. Givoli, Dan and Shmuel Vigdergauz. "Artificial boundary conditions for 2D problems in geophysics." *Computer Methods in Applied Mechanics and Engineering*, 110(1):87 – 101, 1993.

34. Glisson, A.W. "Electromagnetic scattering by arbitrarily shaped surfaces with impedance boundary conditions." *Radio Science*, 27(6):935 – 943, 1992.

35. Gockenbach, Mark S. *Partial Differential Equations: Analytical and Numerical Methods*. Society for Applied and Industrial Mathematics, Philadelphia PA, 2002.

36. Gockenbach, Mark S. *Understanding and Implementing the Finite Element Method*. Society for Applied and Industrial Mathematics, Philadelphia PA, 2006.

37. Goshin, G.G. "A boundary problem of the impedance system of a cylinder on a plane." *Izvestiya Vysshikh Uchebnykh Zavedenii, Fizika*, 11(7):154 – 156, 1968.

38. Grosso, Roberto and Thomas Ertl. "Mesh Optimization and Multilevel Finite Element Approximation." Hans-Christian Hege and Konrad Polthier (editors), *Mathematical Visualization: Algorithms, Applications, and Numerics*, 19–30. Springer-Verlag, Berlin, 1998.

39. Gustafson, Karl E. *Introduction to Partial Differential Equations and Hilbert Space Methods*. Dover Publications, Inc., Mineola NY, third edition, 1999.

40. Hamid, A.-K. and M. Hamid. "Electromagnetic scattering by a dielectric sphere partially buried in an infinite plane." *Canadian Journal of Physics*, 80(9):979 – 986, 2002.

41. Hanson, George W. and Alexander B. Yakovlev. *Operator Theory for Electromagnetics An Introduction*. Springer-Verlag, New York, 2002.

42. Hein-Hoernig, Ricardo Oliver. *Greens Functions and Integral Equations for the Laplace and Helmholtz Operators in Impedance Half-Spaces*. Ph.D. thesis, École Polytechnique, France, 2010.

43. Hettlich, F. "Frechet derivatives in inverse obstacle scattering." *Inverse Problems*, 11(2):371 – 382, 1995.

44. Hildebrandt, S. and E. Wienholtz. "Constructive proofs of representation theorems in separable Hilbert space." *Communications on Pure and Applied Mathematics*, 17(3):369–373, 1964.

45. Hofreither, Clemens, Ulrich Langer, and Clemens Pechstein. "Analysis of a non-standard finite element method based on boundary integral operators." *Electronic Transactions on Numerical Analysis*, 37:413–436, 2010.

46. Höllig, Klaus. *Finite Element Methods with B-Splines*. Society for Applied and Industrial Mathematics, Philadelphia PA, 2003.

47. Howe, Eric and Aihua Wood. "TE solutions of an integral equation method for EM scattering from a 2D cavity embedded in the ground plane." *IEEE Antennas and Wireless Propagation Letters*, 2(7):93–96, 2003.

48. Hsiao, G.C., O. Steinbach, and W.L. Wendland. "Domain decomposition methods via boundary integral equations." *Journal of Computational and Applied Mathematics*, 125(1):521–537, 2000.

49. Huang, J. and A.W. Wood. "Analysis and numerical solution of transient electromagnetic scattering from overfilled cavities." *Communications in Computational Physics*, 1(6):1043–1055, 2006.

50. Huang, J., A.W. Wood, and M.J. Havrilla. "A hybrid finite element-Laplace transform method for the analysis of transient electromagnetic scattering by

an over-filled cavity in the ground plane." *Communications in Computational Physics*, 5(1):126 – 141, 2009.

51. Huang, Junqi and Aihua Wood. "Numerical simulation of electromagnetic scattering induced by an overfilled cavity in the ground plane." *IEEE Antennas and Wireless Propagation Letters*, 4:224–228, 2005.

52. Ida, N. and S. Yuferev. "Impedance boundary conditions for transient scattering problems." *IEEE Transactions on Magnetics*, 33(2):1444–1447, 1997.

53. "IEDs: Iraq's deadly roadside bombs". World Wide Web Page, August 2006. Available at *http://news.bbc.co.uk/2/hi/middle_east/4779437.stm*.

54. Ihlenburg, Frank. *Finite Element Analysis of Acoustic Scattering*. Springer-Verlag, New York, 1998.

55. Jin, Jianming. *The Finite Element Method in Electromagnetics*. John Wiley & Sons, Inc., New York, second edition, 2002.

56. Jin, Jianming and Douglas J. Riley. *Finite Element Analysis of Antennas and Arrays*. John Wiley & Sons, Inc., Hoboken NJ, 2009.

57. Jinchao, Xu and Zhang Sheng. "Preconditioning the Poincaré-Steklov operator by using Green's function." *Mathematics of Computation*, 66(217):125 – 138, 1997.

58. Jonghoon, Bin, M.Y. Hussaini, and Lee Soogab. "Broadband impedance boundary conditions for the simulation of sound propagation in the time domain." *Journal of the Acoustical Society of America*, 125(2):664 – 675, 2009.

59. Khoromskij, Boris N. "Data-sparse elliptic operator inverse based on explicit approximation to the Green function." *Journal of Numerical Mathematics*, 11(2):135–162, 2003.

60. Khoromskij, Boris N. and Gabriel Wittum. *Numerical Solution of Elliptic Differential Equations by Reduction to the Interface*. Springer-Verlag, Berlin, 2004.

61. Kirsch, A. "The domain derivative and two applications in inverse scattering theory." *Inverse Problems*, 9(1):81 – 96, 1993.

62. Knott, E. F., J. F. Shaeffer, and M. T. Tuley. *Radar Cross Section*. Scitech Publishing, Inc., Raleigh, NC, second edition, 2004.

63. Koopmann, Gary H. and Henry Benner. "Method for computing the sound power of machines based on the Helmholtz integral." *The Journal of the Acoustical Society of America*, 71(1):78–89, 1982.

64. Kress, Rainer. *Linear Integral Equations*. Springer-Verlag, New York, second edition, 1999.

65. Kui, D. U. *Numerical Computation of Electromagnetic Scattering From Large Cavities*. Ph.D. thesis, City University of Hong Kong, 2009.

66. Kunz, Karl S. and Raymond J. Luebbers. *The Finite Difference Time Domain Method for Electromagnetics*. CRC Press, Boca Raton FL, 1993.

67. Langdon, S. and S. N. Chandler-Wilde. "A wavenumber independent boundary element method for an acoustic scattering problem." *SIAM Journal on Numerical Analysis*, 43(6):2450 – 2477, 2006.

68. Langer, Ulrich and Olaf Steinbach. "Coupled Finite and Boundary Element Domain Decomposition Methods." Martin Schanz and Olaf Steinbach (editors), *Boundary Element Analysis – Mathematical Aspects and Applications*, 61–95. Springer-Verlag, Berlin, 2007.

69. Lee, C.F., R.T. Shin, and J.A. Kong. "Time domain modeling of impedance boundary condition." *IEEE Transactions on Microwave Theory and Techniques*, 40(9):1847–1850, 1992.

70. Lines, C.D. and S.N. Chandler-Wilde. "A time domain point source method for inverse scattering by rough surfaces." *Computing*, 75(2):157 – 180, 2005.

71. Lundell, Christopher A. *Characterization and Measurement of Passive and Active Metamaterial Devices*. Master's thesis, Air Force Institute of Technology (AU), Wright-Patterson AFB OH, 2010.

72. Maloney, J.G. and G.S. Smith. "The use of surface impedance concepts in the finite-difference time-domain method." *IEEE Transactions on Antennas and Propagation*, 40(1):38–48, 1992.

73. McLean, William. *Strongly Elliptic Systems and Boundary Integral Equations*. Cambridge University Press, New York, 2000.

74. Michaels, Jim. "General: Info sharing key to fighting IEDs." *Air Force Times*, 7 January 2010.

75. Monk, Peter. *Finite Element Methods for Maxwell's Equations*. Oxford University Press, New York, 2003.

76. Mori, Andrew. *Time Domain Pulse Shaping Using a Genetic Algorithm*. Master's thesis, Stellenbosch University, Stellenbosch, South Africa, 2009.

77. Nédélec, Jean-Claude. *Acoustic and Electromagnetic Equations*. Springer-Verlag, New York, 2001.

78. Ochmann, Martin and Haike Brick. "Acoustical Radiation and Scattering above an Impedance Plane." Steffen Marburg and Bodo Nolte (editors), *Computational Acoustics of Noise Propagation in Fluids – Finite and Boundary Element Methods*, 459–494. Springer-Verlag, Berlin, 2008.

79. Oh, Kyung Suk and J.E. Schutt-Aine. "An efficient implementation of surface impedance boundary conditions for the finite-difference time-domain method." *IEEE Transactions on Antennas and Propagation*, 43(7):660–666, 1995.

80. Ozyoruk, Yusuf and Lyle N. Long. "Impedance boundary conditions for time-domain computational aeroacoustics methods." *AIAA, 35th Aerospace Sciences Meeting & Exhibit, Reno NV*. January 1997.

81. Pelosi, G. and P.Ya. Ufimtsev. "The impedance-boundary condition." *IEEE Antennas and Propagation Magazine*, 38(1):31–35, 1996.

82. Politis, Costas G., Miltiadis V. Papalexandris, and Gerassimos A. Athanassoulis. "A boundary integral equation method for oblique water-wave scattering by cylinders governed by the modified Helmholtz equation." *Applied Ocean Research*, 24(4):215 – 233, 2002.

83. Pomp, Andreas. *The Boundary-Domain Integral Method for Elliptic Systems*. Springer-Verlag, Berlin, 1998.

84. Qin, Chen, Lu Mingyu, and E. Michielssen. "Integral-equation-based analysis of transient scattering from surfaces with an impedance boundary condition." *Microwave and Optical Technology Letters*, 42(3):213 – 220, 2004.

85. Quarteroni, Alfio and Alberto Valli. *Numerical Approximation of Partial Differential Equations*. Springer-Verlag, Berlin, 1994.

86. Ramesh, P. S. and M. H. Lean. "Accurate integration of singular kernels in boundary integral formulations for Helmholtz equation." *International Journal for Numerical Methods in Engineering*, 31(6):1055–1068, 1991.

87. Rannacher, R. "Error Control in Finite Element Computations: An introduction to error estimation and mesh-size adaptation." Haydar Bulgak and Christoph Zenger (editors), *Error Control and Adaptivity in Scientific Computing*, 247–278. Kluwer Academic Publishers, Dordrecht, The Netherlands, 1999.

88. Rao, S. M. *Time Domain Electromagnetics*. Academic Press, San Diego CA, 1999.

89. Rjasanow, Sergej and Olaf Steinbach. *The Fast Solution of Boundary Integral Equations*. Springer Science + Business Media, New York, 2007.

90. Salon, S. and J. Schneider. "A hybrid finite element-boundary integral formulation of the eddy current problem." *IEEE Transactions on Magnetics*, 18(2):461 – 466, 1982.

91. Salon, S.J. and J.M. Schneider. "A comparison of boundary integral and finite element formulations on the eddy current problem." *IEEE Transactions on Power Apparatus and Systems*, PAS-100(4):1473 –1479, 1981.

92. Schatz, A.H. and Wang Junping. "Some new error estimates for Ritz-Galerkin methods with minimal regularity assumptions." *Mathematics of Computation*, 65(213):19 – 27, 1996.

93. Schneider, J. and S. Salon. "A boundary integral formulation of the eddy current problem." *IEEE Transactions on Magnetics*, 16(5):1086 – 1088, 1980.

94. Senior, T. B. A. and J. L. Volakis. *Approximate Boundary Conditions in Electromagnetics*. The Institution of Electrical Engineers, London, 1995.

95. Solin, Pavel. *Partial Differential Equations and the Finite Element Method*. John Wiley & Sons, Inc., Hoboken NJ, 2006.

96. Steinbach, Olaf. "On a hybrid boundary element method." *Numerische Mathematik*, 84(4):679 – 695, 2000.

97. Steinbach, Olaf. *Numerical Approximation Methods for Elliptic Boundary Value Problems*. Springer Science + Business Media, LLC, New York, 2008.

98. Steinbach, Olaf and W. L. Wendland. "On C. Neumann's method for second-order elliptic systems in domains with non-smooth boundaries." *Journal of Mathematical Analysis and Applications*, 262(2):733–748, 2001.

99. Strang, Gilbert and George J. Fix. *An Analysis of the Finite Element Method*. Prentice-Hall, Inc., Englewood Cliffs NJ, 1973.

100. Swearingen, M.E. and M.J. White. "Influence of scattering, atmospheric refraction, and ground effect on sound propagation through a pine forest." *Journal of the Acoustical Society of America*, 122(1):113 – 119, 2007.

101. Swearingen, Michelle E. "An analytic model for acoustic scattering from an impedance cylinder placed normal to an impedance plane." *Journal of the Acoustical Society of America*, 115(4):1383–1383, 2004.

102. Tsaur, D.-H. and K.-H. Chang. "Transverse electric scattering by a dielectric biconvex cylinder loaded with a shallow circular trough in a ground plane." *IET Microwaves, Antennas & Propagation*, 2(4):394–400, 2008.

103. Tsaur, Deng-How and Kao-Hao Chang. "TM scattering from a dielectric biconvex cylinder loading a shallow circular gap in a perfectly conducting plane". *IEEE Transactions on Antennas and Propagation*, 55(10):2928–2931, 2007.

104. Van, T and A Wood. "A time-domain finite element method for Helmholtz equations." *Journal of Computational Physics*, 183(2):486–507, 2002.

105. Van, T. and A. Wood. "Analysis of transient electromagnetic scattering from overfilled cavities." *SIAM Journal on Applied Mathematics*, 64(2):688–708, 2003.

106. Vanden Brook, Tom. "U. S. Cuts Afghan IED Toll By 37%." *USA Today*, 17 February 2011.

107. Volakis, John L., Kubilay Sertel, and Brian C. Usner. "Frequency Domain Hybrid Finite Element Methods for Electromagnetics." *Synthesis Lectures on Computational Electromagnetics*, 1(1):1–156, 2006.

108. Wang, Jian-She. "Transient scattering using finite elements with curved absorbing boundaries." *IEEE Transactions on Magnetics*, 32(3):870 –873, 1996.

109. Wassef, K.N. and A.F. Peterson. "Transient finite-element analysis using a surface admittance boundary condition to incorporate eddy-current effects." *IEEE Transactions on Magnetics*, 41(7):2236–2242, 2005.

110. Wiersig, Jan. "Boundary element method for resonances in dielectric microcavities." *Journal of Optics A: Pure and Applied Optics*, 5(1):53–60, 2003.

111. Wood, Aihua. "Analysis of electromagnetic scattering from an overfilled cavity in the ground plane." *Journal of Computational Physics*, 215(2):630 – 641, 2006.

112. Yuan, Lin and K. Grosh. "Design of ultrasonic array elements for acoustic power considerations." *IEEE Transactions on Ultrasonics, Ferroelectrics and Frequency Control*, 49(1):20 – 28, 2002.

113. Yuferev, S. and N. Ida. "Application Of Approximate Boundary Conditions To Electromagnetic Transient Scattering Problems." *Third International Conference on Computation in Electromagnetics (Conf. Publ. No. 420)*, 51–56. 1996.

114. Yuferev, S. and N. Ida. "Efficient implementation of the time domain surface impedance boundary conditions for the boundary element method." *IEEE Transactions on Magnetics*, 34(5):2763–2766, 1998.

115. Yuferev, S. and N. Ida. "Time domain surface impedance boundary conditions of high order of approximation." *IEEE Transactions on Magnetics*, 34(5):2605–2608, 1998.

116. Yuferev, S. and N. Ida. "Time domain surface impedance concept for low frequency electromagnetic problems – Part I: Derivation of high order surface impedance boundary conditions in the time domain." *IEE Proceedings – Science, Measurement and Technology*, 152(4):175–185, 2005.

117. Zeidler, Eberhard. *Nonlinear Functional Analysis and its Applications II/A: Linear Monotone Operators*. Springer-Verlag, New York, 1990.

REPORT DOCUMENTATION PAGE

Form Approved
OMB No. 0704–0188

1. REPORT DATE *(DD–MM–YYYY)*	2. REPORT TYPE	3. DATES COVERED *(From — To)*
15–09–2011	Doctoral Dissertation	Sep 2008 — Sep 2011

4. TITLE AND SUBTITLE

Analysis of Transient Electromagnetic Scattering from an Overfilled Cavity Embedded in an Impedance Ground Plane

5a. CONTRACT NUMBER

5b. GRANT NUMBER

5c. PROGRAM ELEMENT NUMBER

6. AUTHOR(S)

Robert S. Callihan, Lt Col, USAF

5d. PROJECT NUMBER

5e. TASK NUMBER

5f. WORK UNIT NUMBER

7. PERFORMING ORGANIZATION NAME(S) AND ADDRESS(ES)

Air Force Institute of Technology
Graduate School of Engineering and Management (AFIT/EN)
2950 Hobson Way
WPAFB OH 45433-7765

8. PERFORMING ORGANIZATION REPORT NUMBER

AFIT/DAM/ENC/11-01

9. SPONSORING / MONITORING AGENCY NAME(S) AND ADDRESS(ES)

Air Force Research Laboratory, Battlespace Surveillance Innovation Center
Attn: Dr. John R. Roadcap
3550 Aberdeen Ave, SE
Kirtland AFB, NM 87117
246-9101, john.roadcap@kirtland.af.mil

10. SPONSOR/MONITOR'S ACRONYM(S)

AFRL/RVBY

11. SPONSOR/MONITOR'S REPORT NUMBER(S)

12. DISTRIBUTION / AVAILABILITY STATEMENT

APPROVED FOR PUBLIC RELEASE; DISTRIBUTION UNLIMITED.

13. SUPPLEMENTARY NOTES

14. ABSTRACT

We consider the transient, or time-domain, scattering problem of a two-dimensional overfilled cavity embedded in an impedance ground plane. This problem is a significant advancement from previous work where more simplified boundary conditions were used, which can limit the number of applications. This research supports a wide range of military applications such as the study of cavity-like structures on aircraft and vehicles. More importantly, this research helps detect the biggest threat on today's battlefield: improvised explosive devices. An important step in solving the problem is introducing an artificial boundary condition on a semicircle enclosing the cavity; this couples the fields from the infinite exterior domain to those fields inside. The problem is first discretized in time using the Newmark scheme, and at each time step, we derive the variational formulation and establish well-posedness of the problem. This sets the foundation for the finite element method used in the numerical analysis. Using both a planar and overfilled cavity model, we provide numerical results through the depictions of the scattered electric field and radar cross section of the cavities.

15. SUBJECT TERMS

Overfilled Cavity, Impedance Boundary Condition, Time Domain, Finite Element Method, Green's Function

16. SECURITY CLASSIFICATION OF:			17. LIMITATION OF ABSTRACT	18. NUMBER OF PAGES	19a. NAME OF RESPONSIBLE PERSON
a. REPORT	b. ABSTRACT	c. THIS PAGE			Dr. Aihua W. Wood (ENC)
U	U	U	UU	138	19b. TELEPHONE NUMBER *(include area code)* (937) 255-3636, x4272; aihua.wood@afit.edu